UNIVERSITÀ
DEGLI STUDI
DI PADOVA

Sede Amministrativa: Università degli Studi di Padova

Dipartimento di Medicina Animale, Produzioni e Salute.

SCUOLA DI DOTTORATO DI RICERCA IN : SCIENZE VETERINARIE
INDIRIZZO: SCIENZE CLINICHE VETERINARIE
CICLO XXV

DIAGNOSTIC IMAGING IN SNAKES AND LIZARDS

Direttore della Scuola : Ch.mo Prof. Gianfranco Gabai
Coordinatore d'indirizzo: Ch.mo Prof. Maurizio Isola
Supervisore :Ch.mo Prof. Alessandro Zotti

Dottorando : Tommaso Banzato

LIST OF ABBREVIATIONS

LL: Latero-lateral

VD: ventro-dorsal

DV: dorso-ventral

CC: cranio-caudal

CT: Computed Tomography

MRI: Magnetic Resonance Imaging

ETT: Esophageal transit time

GET: Gastric emptying time

OGF: Onset of gastric filling

OLIT: Onset of large intestine transit

OSIT: Onset of small intestine transit

SITT: Small intestine transit time

CHAPTER I

DIAGNOSTIC IMAGING IN SNAKES AND LIZARDS: REVIEW OF LITERATURE

This chapter was adapted from: Banzato T, Hellebuick T, Van Calenberg A, Saunders J, Zotti A. Diagnostic imaging of Snakes and Lizards: State of the Art. Veterinary Record; 2012: *Submitted for publication*.

Abstract

Snakes and lizards are considered as "stoic" animals and often show only non-specific signs of illness. Consequently diagnostic imaging, along with clinical examination and laboratory tests, is gaining importance in making a final diagnosis and establishing a correct therapy. The large number of captive snakes and lizards species commonly kept as pets, together with the high inter- and intra-specific morphological variability innate in these animals, make the analysis of diagnostic images challenging for the veterinary practitioner. Moreover, a thorough knowledge of the anatomy, physiology and pathology of the species that are object of the clinical investigation is mandatory for the correct interpretation of diagnostic images. Despite the large amount of clinical and scientific work carried out in the last two decades, an actual standardisation of the radiographic features of snakes and lizards is far from being achieved, and therefore veterinarians often have to rely on only their clinical experience rather than on reference literature.

The aim of this paper is to review the most commonly used diagnostic imaging modalities as well as to make an updated collection of the available international references describing the normal and pathological imaging features in snakes and lizards.

Introduction

At present time some excellent references describing the anatomy, physiology [1-2] and pathology [3-4] of reptile species belonging to the suborders of ophidia and lacertilia are available, thus enabling a great increase in the demand for veterinary specialty health services for captive snakes and lizards.

Diagnostic imaging is a common means in the diagnosis and management of diseases also affecting the above reptile-pets. The use of RX and US is widespread among clinicians, while more advanced imaging tools, such as CT and MRI, are increasingly common in the veterinary clinical practice.

The most frequent fields of application for imaging techniques are in the diagnosis of these diseases: 1) skeletal (Mitchell 2002, Zotti and others 2004, Mader 2005b, Silverman 2005, Klaphake 2010)[5-9]; 2) cardio-respiratory (Snyder and others 1999, Schumacher 2003, Silverman 2005, Schillinger and others 2006, Pees 2010a)[5,10-13]; 3) gastro-intestinal (Mitchell and Diaz Figueroa 2005, Funk 2005, Silverman 2005)[5,14-15]; 4) uro-genital (Canny 1998, Hernandez-Divers and Innis 2005) disorders. Moreover, diagnostic imaging is also gaining importance among snake breeders as a tool for managing and monitoring reproduction (Canny 1998, Stahl 2002, Funk 2002, Silverman 2005, Gnudi and others 2009)[5,16-19].

Sound interpretation of the various imaging features is mandatory in such a scenario. However, this does require a thorough knowledge of the normal and pathological imaging aspects of each species studied in the clinical investigation.

At the present time, the references describing the normal imaging features of snakes and lizards are often limited to a restricted number of species and are more focused on basic imaging modalities such as RX radiography and US rather than on CT and MRI. It should be stated that, to

the best of the authors' knowledge, CT and MRI techniques can rely only upon fragmentary references or those that are difficult to locate.

The main purposes of this review are to provide the reader with: 1) a description of the different imaging techniques current in use and of usefulness, and, 2) an updated collection of the references describing the normal aspects and the pathological features for each imaging method in snakes and lizards.

Radiography

The Skeletal System

Figure 1. VD projection of the head of a Chlamydosaurus

The most commonly used radiographic projections for the examination of the head in snakes and lizards are the DV (Fig. 1) and the LL (Fig 2). Due to the small size of individual skull bones and the numerous superimpositions typical of this imaging technique, additional oblique projections may be necessary for a better characterisation of bony or soft tissues lesions. Sedation is often required both in snakes and lizards in order to obtain correct positioning of the patient. The use of a grid is recommended only in large lizards (more than 10 kg)[8].

The normal radiographic features of the head of the *Boa constrictor* and leopard gecko (*Eublepharis macularis*)[13] have been reported in literature.

The axial skeleton and the limbs (obviously only in lizards) are readily evaluated on plain radiographs. In snakes, usually, several sequential radiographs are necessary to evaluate the entire spine; it is important to study the entire spine if bony lesions are suspected because often the lesions are not apparent at the clinical examination. In lizards, if limb pathologies are suspected, the x-ray beam should be collimated on the

Figure 2. LL projection of the head of a Chlamydosaurus

affected limb. To date, no comprehensive work describing the correct radiographic positioning of the limbs of lizards is available.

Skeletal fractures are usually assessed by means of plain radiographs (Mitchell 2002, Williams 2002, Silverman 2005, Pees 2010a)[5,8,13,20]. The clinician should always be aware that, in reptiles, the fracture healing process involves a mixture of fibrous tissue and osseous callus; therefore, the clinical fracture stability usually occurs far before radiographic healing becomes evident. Life-long visualization of radiolucent fracture lines, in completely healed fractures, is not uncommon in reptiles [8].

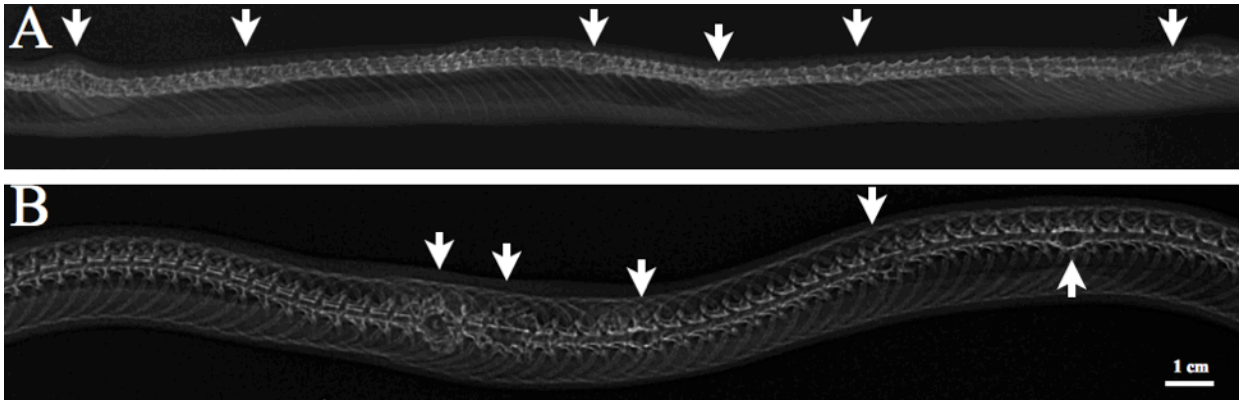

Figure 3. Vertebral abscesses in a *Lampropeltis Triangolum*. Microbiological tests retrieved a negative result. A: latero-lateral radiograph at the level of the lungs. B: dorso-ventral radiograph at the same level as A. Note the lysis of the vertebral bodies and the marked periosteal reaction. Arrows indicate the lesions.

Vertebral osteomyelitis is described in snakes as a mixture of bone lysis and exuberant periosteal reaction (Fig. 3). Osteomyelitis in lizards involving the limbs and head usually produces severe lysis but poor periosteal reaction [8,13].

Figure 4. Metabolic bone disease in a green iguana. Arrows indicate the mandibular deformities.

The radiographic signs of metabolic bone diseases in lizards include: bone loss, limb and mandibular deformities (Fig 4), and swelling of the surrounding soft tissues [6-10,13](Fig. 2).

The radiographic features of osteitis deformans (Paget's disease) have been reported in boid snakes as irregular and

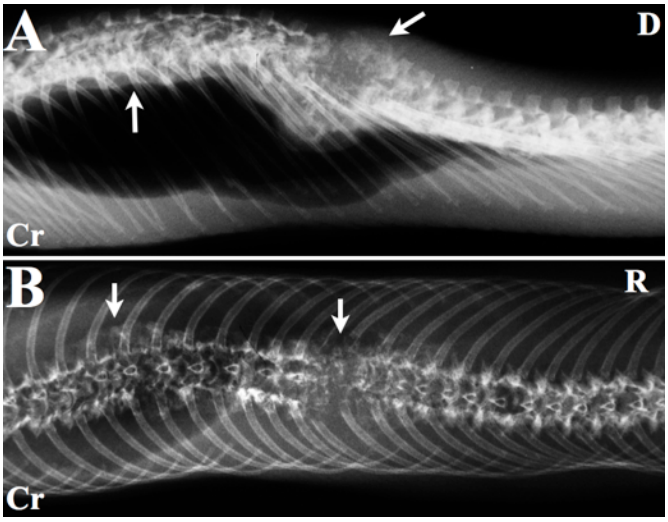

Figure 5. Pagets' disease in a boa constrictor. A: latero-lateral radiograph at the level of the lungs. B: dorso-ventral radiograph at the same level as A. Arrows indicate the lesions. Note that the cranial lesion is mostly productive whereas the caudal lesion is mostly lytic. Cr is

smoothly delineated bone proliferations surrounding the vertebral bodies and should always be differentiated from vertebral osteomyelitis or neoplasia [21](Fig. 5).

Bone tumours have been seldom described in snakes and lizards as masses with a mixed, lytic and productive radiographic appearance [22-25].

Spinal osteopathy, producing single or multiple severe deviations of the spine, is a common manifestation of many different diseases in snakes and lizards, such as: trauma, viral infection, bacterial osteomyelitis, dietary deficiency, proliferative spinal osteopathy, neoplasia, prolonged inactivity, metabolic bone disease, immune reaction, and, congenital malformation [26] (Fig. 6).

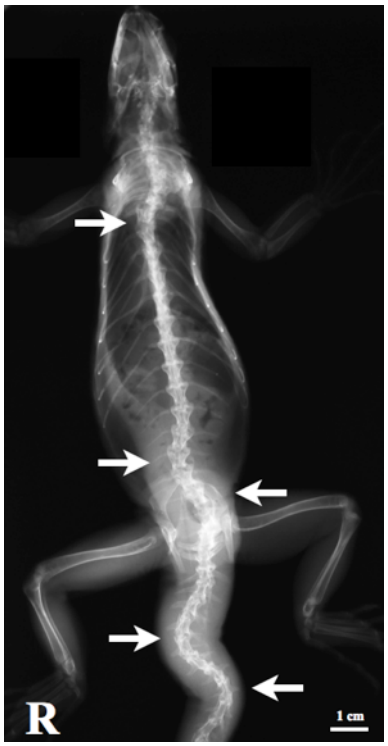

Figure 6. Dorso-ventral radiograph of a green iguana with multiple vertebral abnormalities referable to spinal osteopathy. Aetiology was not determined. R is right. Arrows indicate the abnormal vertebral segments.

The coelomic cavity

Standard radiographic examination of the coelomic cavity of snakes and lizards include LL and DV projections; to date, no remarkable differences between the right and left LL projections have been described. The lack of radiographic contrast occurring among soft tissues of the coelomic cavity, which is quite common in reptiles, prevents individual recognition of several coelomic organs [8]. On plain radiographs, only the trachea, the oesophagus (only in lizards), lungs, heart, liver and gastro-

Figure 7. Dorso-ventral radiograph of a green iguana with gastro-intestinal impaction secondary to the ingestion of large amounts of substrate (sand). Arrows indicate the dilated intestinal loops. R is right.

intestinal tract (if the intestinal loops are ingesta- or gas-filled) can be easily evaluated [8,13] in snakes and lizards. A schematic comparison between the radiographic and anatomical features of the coelomic cavity of the snake and the green iguana is reported [27].

The heart and the lungs are usually well-visible both in snakes and lizards but, due to the great anatomical and physiological differences existing between reptilian and mammalian lungs, the lung pattern classification scheme adopted in mammals is not applicable to reptiles[8]. Radiology, however, is considered as a limited diagnostic tool for lung evaluation in snakes, also because the radiographic signs of pulmonary disease become apparent only at a late stage [11]. If pneumonia is suspected, the clinician should always rely primarily on the clinical examination of the animal and then combine the results of different diagnostic tests, such as broncho-alveolar lavage, haematological screening and, radiography in order to achieve a correct diagnosis [28].

Gastro-intestinal impaction is usually radiographically evident as an abnormal accumulation of food or substrate material (usually gravel or sand) with consequent distension of the digestive system (Fig. 7). Chronic abdominal distension may be the result of a mechanical or functional ileus and it appears as an abnormal accumulation of gas in the digestive system (Fig. 8).

Upper gastro-intestinal contrast studies, using positive or double contrast techniques, have been proposed by Silverman (2005) to detect intestinal occlusions (or radiolucent foreign bodies) but, to date, the normal radiographic features and transit times are described only in the green iguana[29] and, partially, in the common tegu [30]. Global transit time in reptiles is strictly related to

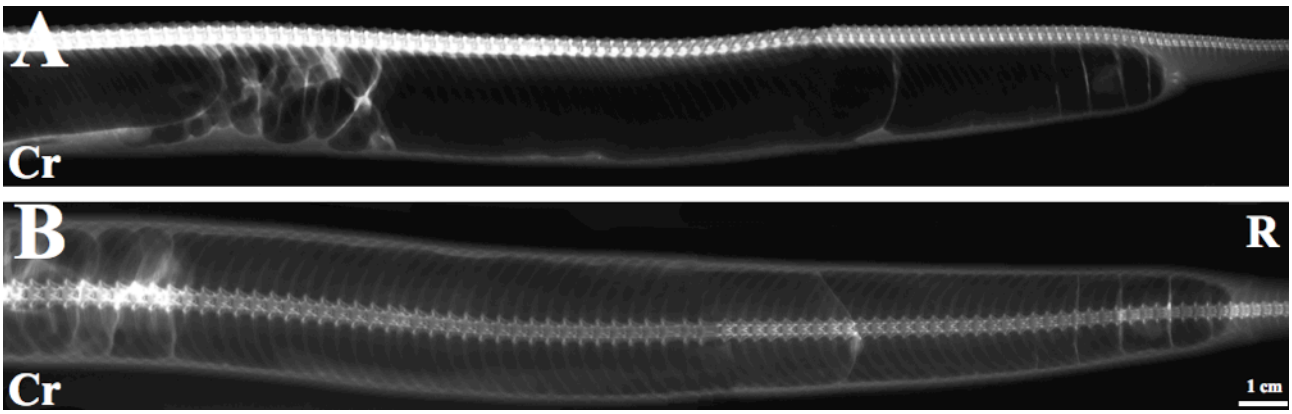

Figure 8. Chronic abdominal distension secondary to a large cloacal intramural abscess in a boa constrictor. A: latero-lateral radiograph at the level of the caudal third of the animal. B: dorso-ventral radiograph at the same level as A.

many factors such as: the species, the environmental temperature, the season, the diet, and, the type of contrast medium used [8,31]. The advantages and disadvantages of each contrast agent proposed for reptile upper gastro-intestinal studies are reported in Table 1.

The kidneys and the urinary bladder in snakes are usually not radiographically appreciable [8,16,32]. Calculi inside the urinary bladder normally occur in lizards and are often diagnosed through plain radiography [8]. In lizards the kidneys are often partially or completely embedded in the pelvic canal[2]; enlarged kidneys often protrude from the pelvic canal and may become visible as a soft tissue mass in the caudal-most portion of the coelomic cavity. Secondary signs of nephromegaly may be constipation or dystocia due to extramural compression of the cloaca[33] (Fig.9). Negative contrast procedures introducing small amounts of air into the coelomic cavity, and excretory urograms using intra-venous iodinated contrast medium, have been proposed to enhance visualisation of the kidneys in lizards[33-34].

The cloaca is usually difficult to evaluate radiographically; for this reason it is almost always impossible to detect intraluminal masses. Retrograde double contrast examination has been proposed as the standard radiographic aid for detection of intraluminal masses in the cloaca [8].

Pregnancy[8,17-18] can be radiographically assessed in most reptiles; multiple, ovoid, soft tissue radiopacities with poorly mineralised shells can usually be detected in the coelomic cavity in snakes and lizards.

Table 1. Contrast procedures reported in snakes and lizards. PO, oral administration; IV, intravenous administration.

	Contrast Medium	Radiographic technique Possible complications	Indications	References
Upper gastro-intestinal examination	Barium 25% w/v	Administer 25ml/kg PO through an oesophageal probe. Evaluate the transit at T1-2-3-6-12-24-48-72 and eventually at T96. Maximum transit time reported: ball python 72h, green iguana 144h. Reported complications include dessication of the contrast medium with consequent intestinal obstruction.	Intestinal obstruction, radiolucent foreign bodies	Smith et al, 2001; Banzato et al., 2012. Silverman, 2005
Anterograde double contrast upper gastro-intestinal examination	Barium 100% w/v + room air	Insert an oesophageal probe in the stomach; administer barium (1/4 of the gastric capacity) and then administer room air (normal gastric volume).	Intestinal obstruction, masses, foreign bodies	Silverman, 2005
Retrograde double contrast intestinal examination (large intestine)	Barium (nd), + room air	Sedation is required. Flexible catheter is inserted in the cloaca to reach the most proximal part of the colon. Barium is injected until resistance is encountered; then room air is injected.	Distal colonic obstruction	Silverman, 2005
Double contast cloacogram	Non-ionic iodinated + room air	Evacuate the cloaca by means of warm water. Inject non-ionic iodinated contrast media (50% of estimated cloacal volume); inject room air (100% to 200% estimated cloacal volume).	Cloacal radiolucent calculi - masses	Silverman, 2005
Intracoelomic negative contrast examination	Room air	Inject 5-10 ml/kg in the caudal portion of the coelomic cavity.	Masses in the caudal coelomic cavity, suspected nephromegaly.	Hernandez-Divers, 2003 Selleri and Hernandez-Divers, 2006
Descending urography	Non-ionic iodinated contrast media	Catheterise the jugular vein. Inject 800/1000 mg/kg of contrast medium. Repeat radiographs at T0-0,5-2-5-15-30-60 min. Non-ionic iodinated contrast media are reported to be sometimes nephrotoxic in mammals.	Masses in the caudal coelomic cavity, suspected nephromegaly.	Hernandez-Divers, 2003 Selleri and Hernandez-Divers, 2006
Contrast enhanced CT scans	Non-ionic iodinated contrast media	Inject 800-1000mg/kg in the caudal vein.	CT scans	Banzato et al., 2012c.

Ultrasonography

Performing ultrasonographic examinations in reptiles is not complicated but relies on high-resolution equipment[8,35]. The scaly nature of reptilian skin can lead to artefacts due the trapping of air between the scales and the coupling gel. Pees (2010b) suggests that giving thick-scaled lizards a warm bath before performing the ultrasonographic examination and using a generous amount of gel improves the image quality. Silverman (2005) proposes immerging thick-scaled patients in warm water to improve the imaging quality.

Ultrasonography is considered the imaging modality of choice for the diagnosis of ocular diseases in snakes and lizards [36]. The normal ultrasonographic features of the eye of some snake

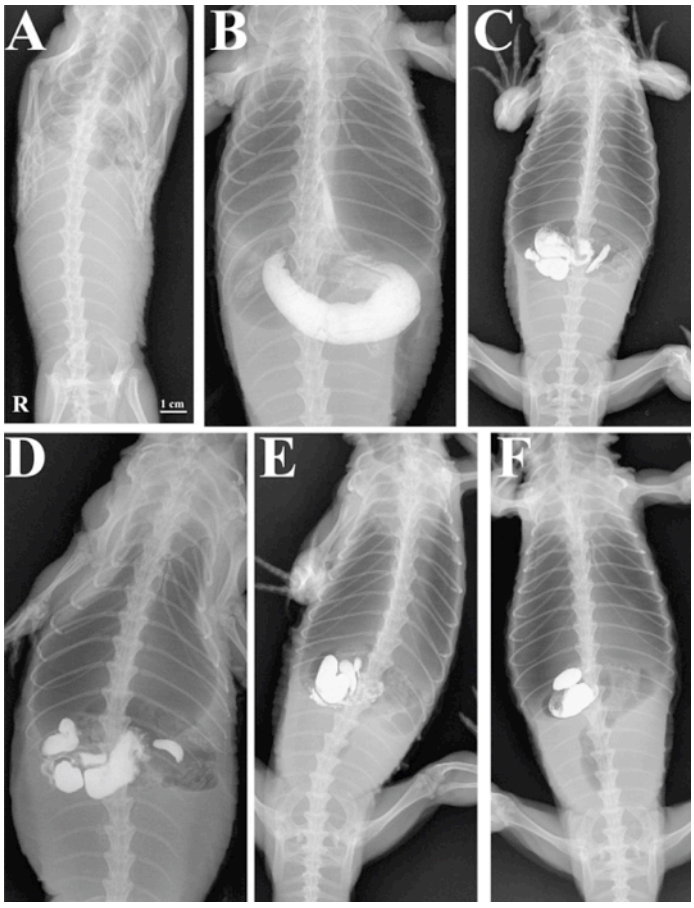

Figure 9. Upper gastrointestinal examination in a common tegu with constipation caused by bilateral nephromegaly. Radiographic times displayed are: T 0,1,6,12,24,144 hours from A to F. Note that the contrast medium at T144 was completely in the cecum but the animal was unable to defecate.

species, using high frequency (12MHz) and ultra-high frequency (50 MHz) probes, have been reported [36,37]. The ultrasonographic appearance of ocular infections, abscesses affecting the retro-bulbar space, cataract, and, ocular neoplasms have been described [36].

Ultrasonography is the reference method for the evaluation of cardiac function in snakes and lizards[8]. Although not frequent, cardiac diseases are reported both in snakes [38-44] and lizards[45]. While some papers describing the echocardiographic examination technique in snakes are currently available [10,12], to the best of our knowledge, no comprehensive description of the echocardiographic technique and pathological features exists in lizards.

The normal ultrasonographic features of the coelomic cavity of the green iguana [46], the Bosc's monitor (*Varanus exantematicus*) [47], the boa constrictor [48].

Ultrasonography is considered a high-sensibility technique for the evaluation of the coelomic organs of snakes and lizards. Nevertheless, individual coelomic organs (e.g. the spleen in snakes or the small intestine in green iguanas) may be difficult or impossible to detect in different species [46-47]. Ultrasonography has proved useful in the diagnosis of different liver diseases such as: neoplasia [14-49], hepatic lipidosis, and hepatic necrosis and abscesses [49]. The technique for ultrasound-guided liver biopsies in snakes is reported [35-50].

The normal physiological variations in the intestinal mucosa related to the time-span from feeding are well-known and should be considered when performing an ultrasonographic examination in snakes[51] (Fig. 10). In order to enhance visualization of the gastro-intestinal structures, some authors[52] suggests water administration to the patient before the examination. Dilated, immotile, intestinal loops, especially in patients that have not been fed for some time, are reported as highly suspicious for mechanical ileus [8] (Fig. 11). The ultrasonographic features of intestinal invagination are reported [52]. Likewise, abscesses or tumours, which are often the cause of obstruction, may usually be identified as masses showing a soft-tissue-like or complex-mass echogenicity. Moreover, ultrasonography may help the distinction between intra-luminal and extra-luminal masses. The evaluation of the gastrointestinal tract in lizards, particularly in herbivorous species, is often challenging due to the nearly constant presence of gas [46].

The kidneys are completely embedded in the pelvic canal in some lizard species, and thus a good acoustic window can be obtained from the dorsal wall in the region of the tail root [52]. The anatomic location of the kidneys is variable among different lizard species[53]; different coupling sites therefore have to be used in different lizard species. Echogenicity, size and perfusion of the kidneys, along with diameter of the ureters, should always be evaluated if renal failure is suspected (Fig. 12).

The presence of urate crystals (gout) in the kidneys is visible as a diffused, or localized, increase in echogenicity [35]. Urinary bladder stones are common findings in lizards and can be visualized by means of different imaging modalities (plain radiography, ultrasonography, CT) (Fig 13).

Ultrasonography is widely used both in snakes and lizards for gender determination[19,54] and for monitoring reproduction and pregnancy [17-18,55-57]. Egg retention [59-59], follicular torsion [60] (Fig. 13) and ovarian papillary cystadenocarcinomas [61], are diagnosed through ultrasonography.

Computed Tomography

The CT technique in snakes and lizards depends both on CT scanner type and technology as well as the size of the patient to be scanned. The usefulness of conventional (3rd or 4th generation) or single-slice CT scanners with reduced data-acquisition capacity and limited capability for adjusting field of view is questionable if dealing with very large or very small patients.

It is often impossible to perform a whole-body CT scan in very large patients and therefore the area to be investigated should be previously detected through other imaging modalities (e.g.: radiography or US) [62]. Likewise, use of the above devices may produce poorly detailed images in scanning very small patients. In fact, as the consequence of an inability to produce isotropic voxels, the quality of multi-planar reconstructions is often limited or non-diagnostic. Transverse orientation of the small-sized reptile pet on the CT table and the consequent latero-lateral scanning direction of the subject may provide better quality images[62]. Acquisition and reconstruction algorithms should be adapted to the region of interest; a slice thickness of 1 or 2 mm is usually adequate when considering the most common reptile-pet species [62].

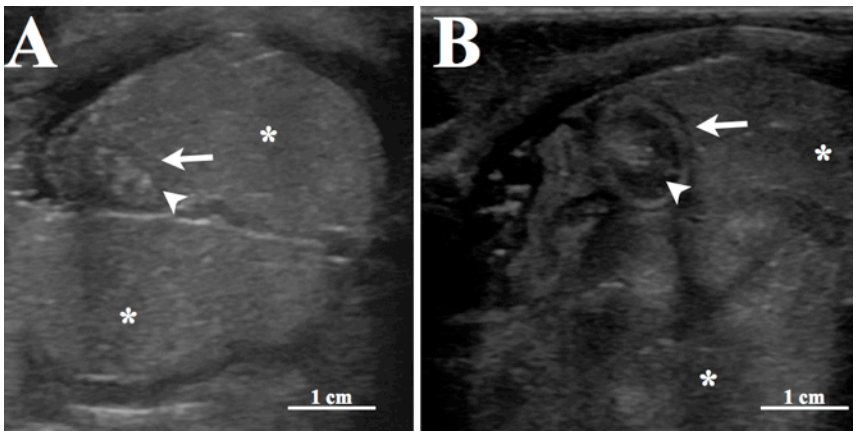

Figure 10. Transverse ultrasonographic images of the normal small intestine in a boa constrictor that had eaten 30 days (A) and 3 days (B) before the examination. Note that the mucosal layer in (A) is barely appreciable whereas in (B) the mucosa is prominent among the other layers of the intestinal wall. Arrow indicates the small intestinal wall. Arrowhead indicates the mucosal layer. * Fat bodies.

Modern multi-slice CT scanners can manage large volumes of data in a very short time while producing isotropic voxels; this enables very fast scanning of large-sized patients, thus providing high quality multi-planar and 3D reconstructions. Moreover, the scope offered by these

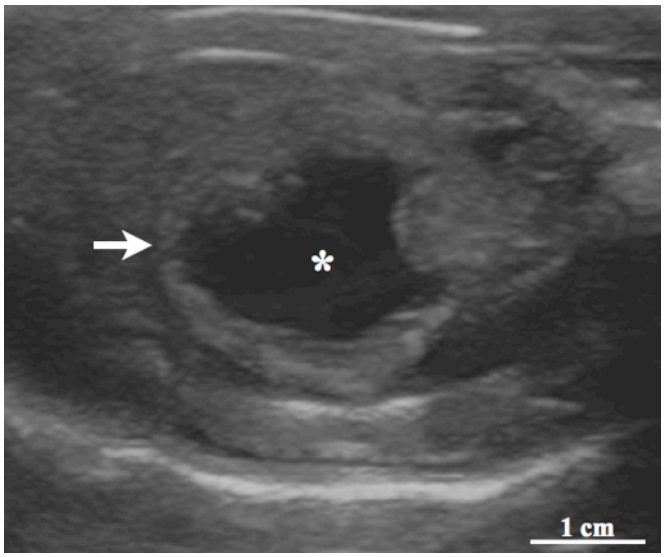

Figure 11. Transverse ultrasonographic image of a severely distended small intestinal loop in a *Python curtus* with mechanical ileus due to a foreign body (bark). Note the different appearance of the intestinal wall in comparison with Figure 8B. Arrow indicates the intestinal loop. * Intestinal lumen

new multi-slice CT scanners to freely adjust the field of view enables good image detail even in small patients. Although not usually available in veterinary clinics, mini and micro CT scanners are considered as the gold standard for tomographic studies in very small animals [63].

Sedation is often required to perform a CT examination in snakes and lizards; only very depressed patients can be imaged without sedation. Some excellent references regarding anaesthesiological protocols used in snakes and lizards are available [64-65].

The skeletal system of reptiles is less mineralised than that of equivalent-sized mammals [6], so the CT technical parameters should be consequently adjusted. However, CT is considered as a sensitive method for the diagnosis and monitoring of several skeletal diseases such as fractures [66],

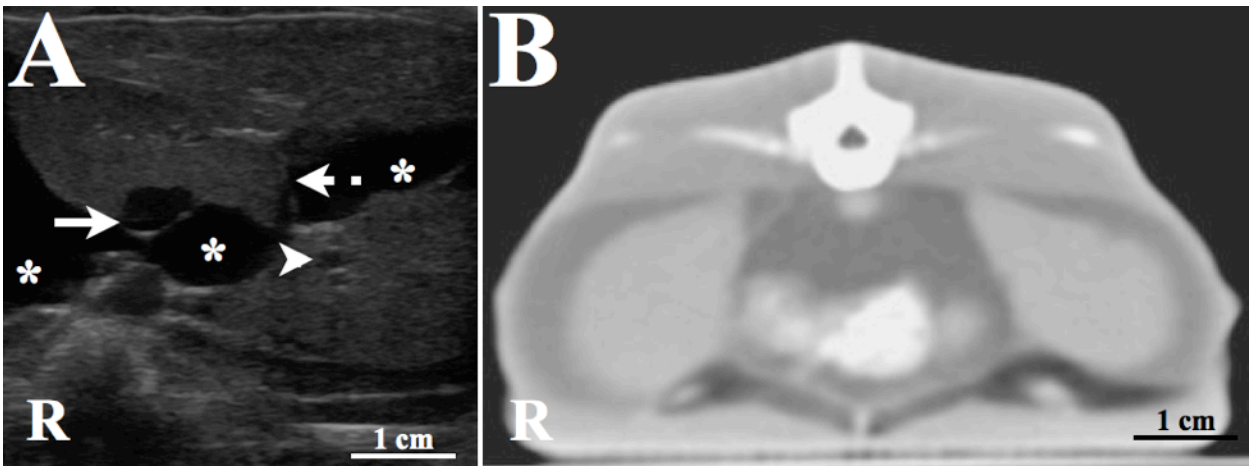

Figure 12. Matched transverse ultrasonographic and contrast-enhanced cross-sectional CT images of the kidneys of a common tegu with bilateral renal pseudocysts. Note the markedly dilated ureter on the right kidney (arrow) in comparison with the normal ureter on the left kidney (arrowhead). Dotted arrow indicates the pseudocysts wall. *

luxations, and bone and joint infections [67]. In the CT technique, tissue density can be assessed directly on the image, using the Hounsfield Unit scale; therefore, CT can therefore be used for monitoring the therapy of metabolic bone disease [8,67].

The bony structures are well evident in CT scans whereas the soft tissues are less defined. It

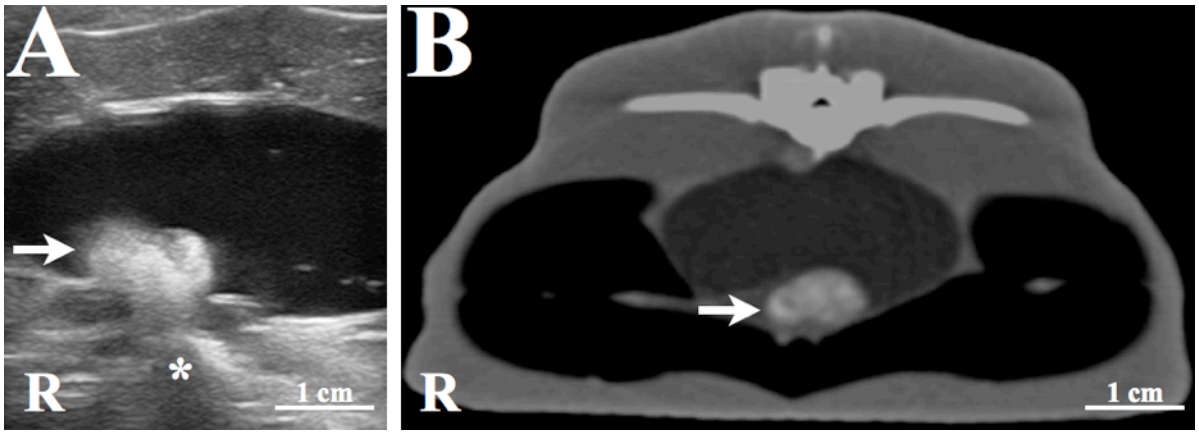

Figure 11. Matched transverse ultrasonographic and contrast-enhanced cross-sectional CT images of a calculus in the cloaca of a common tegu. Note the distal shadowing artefact produced by the calculus in the

is very likely that the intravenous administration of contrast medium (CM) could significantly enhance visualization of the coelomic organs (Fig. 12).

To date, no data have become available regarding the dose, the infusion rate and the normal contrast enhancement after intravenous administration of CM in reptiles. It is the authors' opinion that a thorough standardization of both the contrast-enhanced CT procedures and the features could be highly beneficial in the diagnosis of several diseases of the head and the coelomic cavity.

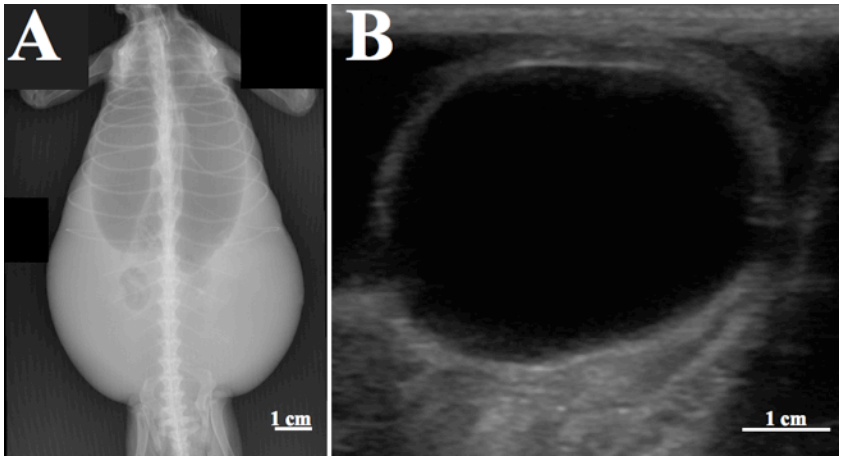

Figure 13. Matched dorso-ventral radiograph and transverse ultrasonographic image of a follicular torsion in a green iguana. Note the coelomic swelling in (A) and the severely enlarged follicle in (B).

The normal CT anatomy of

the lungs is described in some snake species [68]. As previously reported, plain radiographs have a low sensitivity in the detection of pneumonia because the radiographic signs of the disease are evident only at a late stage[28]. Several studies have revealed that CT has a higher sensibility than conventional radiology in the detection and monitoring of bacterial pneumonia in snakes [69-70].

Magnetic Resonance Imaging

The soft tissue high detail feature that is inherent to the MR technique has been demonstrated to be particularly useful in the diagnosis of these problems affecting snakes and lizards [71]: 1) respiratory [72], 2) gastrointestinal [14,73], 3) urinary [73], and 4) neurological[74-75]disorders affecting snakes and lizards. The use of contrast medium (gadolinium; 1 to 2 ml/kg) has been reported some authors[71] to significantly highlight the vasculature in pythons and agamids. Nevertheless, the high cost of equipment, the lengthy duration of the scanning procedure (particularly with low-field MRI) and the lack of detail encountered in small patients are factors that have limited a more frequent use of this technique. Moreover, a complete description of the overall normal anatomic MRI features of snakes and lizards is lacking and only specific segmental tracts are described, such as the brain and the chemosensory systems of the Garter snake (*Tamnophis sirtalis*)[76].

Other Imaging Modalities

Nuclear Medicine (NM) is seldom reported among diagnostic imaging procedures in snakes and lizards. Some authors[8] reports technetium scans to be more sensitive than radiography in the detection of abnormal bone blood flow even if the specificity of the examination appears to be poor. The normal renal uptake of technetium is reported in the green iguana [77] and in the corn snake

(*Pantherophis guttatus*) [78]. Technetium has also been used in an experimental study by Amiel and others (2011) to demonstrate the temperature-dependent blood distribution along the body in snakes. To date, use of nuclear medicine in snakes and lizards, has been discouraged by some authors[79] both because of the poor medical indications emerging from the available studies and due to the implications for radiation regulation and safety.

References

1. Eds Gans, C., Bellairs, A.A., Parsons, T.S., Dawson, W.R., Tinkle, D.W., Kyoko, A., Gans, R., Northcutt, G., Ulinski, P.S., Harvey Pough, F., Billett, F., Maderson, P.F., Huey, R.B., Crews, D., Gaunt, A.S., Adler, K., Liner, E.A. (1970 – 2010) Biology of the Reptilia. Society for the study of Amphibians and Reptiles. Vol. 1-24

2. O'Malley B. Clinical Anatomy and Physiology of Exotic Species: Structure and function of mammals, birds, reptiles and amphibians, 1e. 1st ed. Saunders Ltd.; 2005.

3.Jacobson E ed. Infectious Diseases and Pathology of Reptiles: Color Atlas and Text. 1st ed. CRC Press; 2007.

4. Ed Mader, D.R. (2005a) Reptile Medicine and Surgery. 2nd ed. W.B. Saunders Co. pp1-1242

5. Mitchell M. Diagnosis and management of reptile orthopedic injuries. Veterinary Clinics of NA: Exotic Pet 2002;5:97–114.

6. Zotti A, Selleri P, Carnier P, et al. Relationship between metabolic bone disease and bone mineral density measured by dual-energy X-ray absorptiometry in the green iguana (Iguana iguana). *Vet Radiol Ultrasound* 2004;45:10–16.

7. Mader DR. Metabolic Bone Disease. In: Reptile Medicine and Surgery. Saunders; 2005:841–852.

8. Silverman S. Diagnostic Imaging. In: Reptile Medicine and Surgery. Saunders; 2005:471–489.

9. Klaphake E. A fresh look at metabolic bone diseases in reptiles and amphibians. *Vet Clin North Am Exot Anim Pract* 2010;13:375–392.

10.Snyder PS, Shaw NG, Heard DJ. Two-dimensional echocardiographic anatomy of the snake heart (Python molurus bivittatus). *Vet Radiol Ultrasound* 1999;40:66–72.

11.Schumacher J. Reptile respiratory medicine. Vet Clin of NA: Exotic Pet 2003;6:213–31– viii.

12.Schilliger L, Tessier D, Pouchelon JL. Proposed standardization of the two-dimensional echocardiographic examination in snakes. *J Herp Med Sur* 2006;16.

13.Pees M (2010a) Radiographic investigation. In Diagnostic Imaging of Exotic Pets: Birds, Small Mammals, Reptiles. Eds M.E. Krautwald-Junghanns, M. Pees, S. Reese, T. Tully. Schluetersche Verlagsgesellschaft mbH & Co. pp 310-333

14.Mitchell M, Diaz-Figueroa O. Clinical Reptile Gastroenterology. *Vet Clin North Am Exot Anim Pract* 2005;8:277–2984. Mader DR. Reptile Medicine and Surgery. 2nd ed. Saunders; 2005.

15.Funk RS. Diarrhea. In: Reptile Medicine and Surgery. Saunders; 2005.

16.Canny C. Gross anatomy and imaging of the avian and reptilian urinary system. *Sem Av Exot Pet Med* 1998;7:72–80.

17.Stahl SJ. Veterinary management of snake reproduction. *Vet Clin North Am Exot Anim Pract* 2002;5:615

18.Funk RS. Lizard reproductive medicine and surgery. *Vet Clin North Am Exot Anim Pract* 2002;5:579–613.

19.Gnudi G, Volta A, Di Ianni F, et al. Use Of Ultrasonography And Contrast Radiography For Snake Gender Determination. *Vet Radiol Ultrasound* 2009;50:309–311.

20.Williams J. Orthopedic radiography in exotic animal practice. *Vet Clin North Am Exot Anim Pract* 2002;5:1–22.

21.Preziosi R, Diana A, Florio D, et al. Osteitis deformans (Paget's disease) in a Burmese python (Python molurus bivittatus) – A case report. *Vet J* 2007;174:669–672.

22.Schonbauer M, Loupal G, Schonbauer-Langle A. [Osteoid chondrosarcoma in a desert monitor (Varanus griseus)]. *Berl Munch Tierarztl Wochenschr* 1982;95:193–194

23.Hernandez-Divers SM, Garner MM. Neoplasia of reptiles with an emphasis on lizards. *Vet Clin of NA: Ex Pet* 2003;6:251–273.

24.Cowan ML, Monks DJ, Raidal SR. Osteosarcoma in a woma python (Aspidites ramsayi). *Aus Vet J* 2011;89:520–523.

25.Gal J, Jakab C, Balogh B, et al. First occurrence of periosteal chondroma (juxtacortical chondroma) in Uromastyxmaliensis (Reptilia: Sauria: Agamidae). *Acta Vet Hung* 2007;55:327–331.

26.Fitzgerald KT, Vera R. Spinal Osteopathy. In: Reptile Medicine and Surgery. Saunders; 2005:906–912.

27.Mader DR. Radiographic anatomy. In: Reptile Medicine and Surgery. Saunders; 2005:1097–1102.

28.Murray MJ. Pneumonia and Lower Respiratory Tract Disease. In: Reptile Medicine and Surgery. Saunders; 2005:865–877.

29.Smith D, Dobson H, Spence E. Gastrointestinal studies in the green iguana: technique and reference values. *Vet Radiol Ultrasound* 2001;42:515–520.

30.Klein W. Role of the post-hepatic septum on breathing during locomotion in Tupinambis merianae (Reptilia: Teiidae). *J Exp Biol* 2003;206:2135–2143.

31.Schumacher J, Toal RL. Advanced radiography and ultrasonography in reptiles. *Sem in Av Ex Pet Med* 2001;10:162–168.

32.Pees M, Krautwald-Junghanns ME. Urinary tract. In: Diagnostic Imaging of Exotic Pets: Birds, Small Mammals, Reptiles (Vet S). Schluetersche; 2010.

33.Selleri P, Hernandez-Divers SJ. Renal Diseases of Reptiles. *Vet Clin NA: Ex An Pract* 2006;9:161–174.

34.Hernandez-Divers S, J IC. Renal Diseases in Reptiles: Diagnosis and Clinical Management. In: Reptile Medicine and Surgery. Saunders; 2005:878–892.

35.Pees M. Ultrasonography. In: Diagnostic Imaging of Exotic Pets: Birds, Small Mammals, Reptiles (Vet S). Schluetersche; 2010.

36.Hoffmann I. Eye. In: Diagnostic Imaging of Exotic Pets: Birds, Small Mammals, Reptiles (Vet S). Schluetersche; 2010:354–357.

37.Hollingsworth SR, Holmberg BJ, Strunk A, Oakley AD, Sickafoose LM, Kaas, PH Comparison of ophthalmic

measurements obtained via high frequency ultrasound imaging in four species of snakes. *Am J Vet Res* 2007;68: 1111-1114

38.Barten SL. Cardiomyopathy in a kingsnake (Lampropeltis calligaster rhombomaculata). *Vet Med Small Anim Clin* 1980;75:125–129.

39.Rishniw M,Carmel BP. Atrioventricular valvular insufficiency and congestive heart failure in a carpet python. *Aus Vet J* 1999;77:580-583

40.Schilliger L, Vanderstylen D, Pietrain J, et al. Granulomatous myocarditis and coelomic effusion due to Salmonella enterica arizonae in a Madagascar Dumerili's boa (Acrantophis dumerili, Jan. 1860). *J Vet Cardiol* 2003;5:43–45.

41.Schilliger L, Tréhiou-Sechi E, Petit AMP, et al. Double valvular insufficiency in a Burmese python (Python molurus bivittatus, Linnaeus, 1758) suffering from concomitant bacterial pneumonia. *J Zoo Wildl Med* 2010;41:742–744.

42.Kik MJ, Mitchell A. Reptile cardiology: A review of anatomy and physiology, diagnostic approaches, and clinical disease. *Sem Av Ex Pet Med* 2005;14:52–60.

43.Jensen B, Wang T. Hemodynamic consequences of cardiac malformations in two juvenile ball pythons (Python regius). *J Zoo Wildl Med* 2009;40:752–756.

44.Schroff S, Schmidt V, Kiefer I, et al. Ultrasonographic diagnosis of an endocarditis valvularis in a Burmese python (Python molurus bivittatus) with pneumonia. *J Zoo Wildl Med* 2010;41:721–724.

45.Pizzi R, Pereira YM, Rambaud YF, et al. Secundum atrial septal defect in a Komodo dragon (Varanus komodoensis). *Vet Rec* 2009;164:472–473.

46.Holland MF, Hernandez-Divers S, Frank PM. Ultrasonographic appearance of the coelomic cavity in healthy green iguanas. *J Am Vet Med Ass* 2008;233:590–596.

47.Sainsbury AW, Gili C. Ultrasonographic anatomy and scanning technique of the coelomic organs of the bosc monitor (Varanus exantematicus). *J Zoo Wildl Med* 1991:421–433.

48.Isaza R, Ackerman N, Jacobson ER. Ultrasound imaging of the coelomic structures in the Boa constrictor (Boa constrictor). *Vet Radiol Ultrasound* 1993;34:445–450.

49.Pees M, Kostka V. Liver. In: Diagnostic Imaging of Exotic Pets: Birds, Small Mammals, Reptiles (Vet S). Schluetersche; 2010.

50.Isaza R, Ackerman N, Schumacher J. Ultrasound-Guided Percutaneous Liver Biopsy In Snakes. *Vet Radiol & Ultrasound* 1993;34:452–454.

51.Starck JM. Functional morphology and patterns of blood flow in the heart of Python regius. *J Morphol* 2009;270:673–687.

52.Pees M. Gastrointestinal tract. In: Diagnostic Imaging of Exotic Pets: Birds, Small Mammals, Reptiles (Vet S). Schluetersche; 2010.

53.Fox H. The urogenital System in Reptiles. In Biology of the Reptilia. Vol. 6. Eds C. Gans, T.S. Parsons. Academic

Press. 1977; 1-157.

54.Morris PJ, AC A. Determination of Sex in White-Throated Monitors (Varanus albigularis), Gila Monsters (Heloderma suspectum), and Beaded Lizards (H. horridum). *J Zoo Wildl Med* 1996:371–377.

55.Gilman CA, Wolf BO. Use of portable ultrasonography as a nondestructive method for estimating reproductive effort in lizards. *J Exp Biol* 2007;210:1859–1867.

56.Stahlschmidt Z, Brashears J, Denardo D. The use of ultrasonography to assess reproductive investment and output in pythons. *Biol J of the Linn Soc* 2011;103:772–778.

57.Martínez-Torres M, Guzmán-Rodríguez R, Cárdenas-León M, et al. Follicular Development And Ovulation Determined By Ultrasound Imaging In The Viviparous Lizard Barisia Imbricata (Reptilia: Anguidae). The Southwestern Naturalist 2012;51:401–406.

58.Love NE, Douglass JP, Lewbart G, et al. Radiographic And Ultrasonographic Evaluation Of Egg Retention And Peritonitis In Two Green Iguanas (Iguana Iguana). *Vet Radiol Ultrasound* 1996;37:68–73.

59.Kiefer I, Pees M. Genital Tract. In: Diagnostic Imaging of Exotic Pets: Birds, Small Mammals, Reptiles (Vet S). Schluetersche; 2010.

60.Mehler SJ, Rosenstein DS, Patterson JS. Imaging Diagnosis—Follicular Torsion In A Green Iguana (Iguana Iguana) With Involvment Of The Left Adrenal Gland. *Vet Radiol & Ultrasound* 2002;43:343–345.

61.Stacy BA, Vidal JD, Osofsky A, et al. Ovarian Papillary Cystadenocarcinomas in a Green Iguana (Iguana iguana). *J Comp Pathol*2004;130:223–228.

62.Kiefer I, Pees M. Computed Tomography. In: Diagnostic Imaging of Exotic Pets: Birds, Small Mammals, Reptiles (Vet S). Schluetersche; 2010:358–367.

63.Ritman EL. Micro-Computed Tomography—Current Status And Developments. *Annu Rev Biomed Eng* 2004;6:185–208.

64.Schumacher J, Yelen T. Anesthesia and Analgesia. In: Reptile Medicine and Surgery. Saunders; 2005:442–452.

65.Bertelsen MF. Squamates (Snakes and Lizards). In: Zoo animal and wildlife immobilization and anesthesia. Wiley-Blackwell; 2007:233–244.

66.Rahal SC, Teixeira CR, Vulcano LC, et al. Use of an osteoconductive compound as an aid in the management of a maxillary fracture in a boa constrictor. *Can Vet J* 2011;52:300.

67.Pees M. Skeletal system. In: Diagnostic Imaging of Exotic Pets: Birds, Small Mammals, Reptiles (Vet S). Schluetersche; 2010:378–393.

68.Pees M, Kiefer I, THIELEBEIN J, et al. Computed Tomography Of The Lung Of Healthy Snakes Of The Species Python Regius, Boa Constrictor, Python Reticulatus, Morelia Viridis, Epicrates Cenchria, And Morelia Spilota. *Vet Radiol Ultrasound* 2009;50:487–491.

69.Pees MC, Kiefer I, Ludewig EW, et al. Computed tomography of the lungs of Indian pythons (Python molurus). *Am*

J Vet Res 2007;68:428–434.

70.Pees M, Kiefer I, Oechtering G, et al. Computed tomography for the diagnosis and treatment monitoring of bacterial pneumonia in Indian pythons (Python molurus). *Vet Rec* 2008;163:152–156.

71.Wyneken J. Computed Tomography and Magnetic Resonance Imaging Anatomy of Reptiles. In: Reptile Medicine and Surgery. Saunders; 2005:1088–1096.

72.Pees M, Kiefer I, Ludewig E, et al. Comparative use of modern imaging techniques for the diagnosis of pneumonia in three Indian pythons (Python morulus). TIERAERZTLICHE PRAXIS AUSGABE KLEINTIERE HEIMTIERE 2006;{34}:{275–282}.

73.Ludewig EW, Pees M. Magnetic Resonance Imaging. In: Diagnostic Imaging of Exotic Pets: Birds, Small Mammals, Reptiles (Vet S). Schluetersche; 2010:368–377.

74.Mariani CL. The Neurologic Examination and Neurodiagnostic Techniques for Reptiles. *Vet Clin North Am Exot Anim Pract* 2007;10:855–891.

75.Zimmerman DM, Douglass M, Sutherland-Smith M, et al. Compressive myelopathy of the cervical spine in Komodo dragons (Varanus komodoensis). *J Zoo Wildl Med* 2009;40:207–210.

76. Anderson CL, Kabalka GW, Layne DG, Dyke JP, Burgardt G. Noninvasive high field MRI brain imaging of the garter snake (Tamnhophis sirtalis). *Copeia,* 2000;1:265-269

77.Greer LL, Daniel GB, Shearn-Bochsler VI, et al. Evaluation of the use of technetium Tc 99m diethylenetriamine pentaacetic acid and technetium Tc 99m dimercaptosuccinic acid for scintigraphic imaging of the kidneys in green iguanas (Iguana iguana). *Am J Vet Res* 2005;66:87–92.

78.Sykes JM4, Schumacher J, Avenell J. Preliminary evaluation of 99mTechnetium diethylenetriamine pentaacetic acid, 99mTechnetium dimercaptosuccinic acid, and 99mTechnetium mercaptoacetyltriglycine for renal scintigraphy in corn snakes (Elaphe guttata guttata). *Vet Radiol Ultrasound* 2006;47:222–227.

79.Hernandez-Diver S J, Innis CJ.. Renal Diseases in Reptiles: Diagnosis and Clinical Management. In Reptile Medicine and Surgery. 2nd edn. Ed D.R. Mader. Saunders. 2005;878-892

CHAPTER 2

SCIENTIFIC OUTLINE AND AIMS OF THE THESIS

The aim of this PhD thesis is to describe the normal diagnostic imaging features (Radiology, Ultrasonography and CT) of some snake and lizard species. After an accurate review of literature some research topics were selected in order to fill the existing gaps in the medical and medical imaging veterinary field. The diagnostic imaging modalities used in the experimental studies were selected on the basis of their availability in the general veterinary practices in order to provide useful references for the veterinary clinicians. The experimental studies are presented in two sections;

Diagnostic imaging studies of the head

1. The gross and cross sectional anatomy of the head of some snake and lizards species is described and matched with corresponding radiographic and computed tomographic images. The normal radiographic and computed tomographic technique and features are presented and discussed.

Diagnostic imaging studies of the coelomic cavity

2. The normal gross and cross sectional anatomy of the coelomic cavity of some lizard species is described and matched with corresponding computed tomographic images. The normal computed tomographic technique and features are presented and discussed.

3. The normal gross and cross sectional anatomy of the coelomic cavity of some snake species is described and matched with the normal ultrasonographic features. The normal ultrasonographic technique together with some useful ultrasonographic parameters are presented and discussed.

4. The technique and the normal features of upper gastro-intestinal studies in the ball python are presented and discussed. Normal patterns of contrast medium distribution and normal transit times are reported and discussed.

DIAGNOSTIC IMAGING OF THE HEAD

CHAPTER III

NORMAL RADIOGRAPHY AND COMPUTED TOMOGRAPHY OF THE HEAD OF THE BOA CONSTRICTOR.

This chapter was adapted from: Banzato T, Russo E, Di Toma A, Palmisano G, Zotti A. Evaluation of radiographic, computed tomographic, and cadaveric anatomy of the head of boa constrictors. *American Journal of Veterinary Research* 2011;72:1592-1599.

Abstract

The objective of this study was to evaluate the radiographic, computed tomographic (CT), and cadaveric anatomy of the head of boa constrictors (*Boa constrictor*). 4 *Boa constrictor imperator* cadavers have been used for the anatomical and computed tomographic studies. The cadavers weighed 3.4 to 5.6 kg and had a body length ranging from 189 to 221 cm. Radiographic and CT images were obtained with a high-detail screen-film combination and conventional CT was performed with a slice thickness of 1.5 mm. Radiographic images were obtained in VD, dorsoventral, and left and right LL recumbency; CT images were obtained with animals positioned in ventral recumbency directly laying on a plastic support. At the end of the radiographic and CT imaging session, 2 heads were sectioned following a stratigraphic approach; the other 2, carefully maintained in the same position on the plastic support, were moved into a freezer (–20°C) until completely frozen and then sectioned into 3-mm slices, respecting the imaging protocol. The frozen sections were cleaned and then photographed on each side. Anatomic structures were identified and labeled on gross anatomic images and then on the corresponding CT or radiographic image with the aid of the available literature. Radiographic and CT images provided a high detail for the visualisation of bony structures; soft tissues were not easily identified on radiographic and CT images. Results provide an atlas of stratigraphic and cross-sectional gross and radiographic and CT anatomy of the heads of boa constrictors that might be useful in the interpretation of any imaging modality in this species.

Introduction

In the past 2 decades, reptiles have become increasingly popular as pets and the demand for specialist veterinary services has similarly increased. Boa constrictors (*Boa constrictor*) are one of the most common species among captive snakes.[1] However, the lack of an univocal reference for the normal anatomy and clinical aspects of the so-called nonconventional (ie, exotic) species is a limiting factor for the development of high-level clinical practice.

The gradual increase in use of imaging techniques such as radiography, CT, and magnetic resonance imaging has improved diagnostic abilities in veterinary practice and research. Nevertheless, routine use of such equipment should be accompanied by a thorough knowledge of the normal stratigraphic and cross-sectional anatomy of each imaged species. The role of existing cross-sectional anatomic atlases of dogs,[2–8] cats,[9] rabbits,[10,11] horses,[12] foals,[13] and the heads of some wild species, such as loggerhead sea turtles,[14] bottlenose dolphins,[15] and California sea lions,[16] should be interpreted from this standpoint.

To the best of our knowledge, ophidian anatomic literature is dated and focused almost entirely on single organs or systems.[17–19] Moreover, there are only a few publications regarding imaging in snakes,[20–27] and those report no information on the head region in those species most widespread as pets. Therefore, the purpose of the study reported here was to elucidate the relationship between boa constrictor head anatomy and its radiographic and CT appearance; the intention was to select images to illustrate the main peculiarities of this species with minimal attention to organs or structures for which images have been published elsewhere.

Materials and Methods

Animals

Four *Boa constrictor imperator* cadavers were obtained for this study; 3 were male and 1 was female, and snakes weighed from 3.4 to 5.6 kg and with a body length ranging from 189 to 221 cm.All the animals were referred to the University of Padua Department of Veterinary Clinical Sciences for specialty examination and were euthanized, with their owners' consent, because of advanced clinical conditions. A complete postmortem examination was performed on each snake, which revealed pneumonia in 3 cases and egg retention in 1 case. Gross examination ruled out any lesion in the head of each subject.

Anatomical procedures

To minimize postmortem changes, the heads were dissected immediately after death and radiographic and CT studies were performed on each specimen. Right and left laterolateral and dorsoventral and ventrodorsal x-ray views were obtained by use of conventional x-ray equipment[a] (140 kVp; 600 mA) and a high-detail screen-film combination.[b] The CT images were obtained in transverse and sagittal planes by means of a single-slice third-generation CT scanner[c] by use of the following scanning protocol to ensure optimal image quality: axial acquisition mode, rotation time of 7.6 seconds, voltage of 75 kV, amperage of 80 mA, and slice thickness of 1.5 mm; the images were then displayed in a bone tissue window (window length, 500; window width, 3,000). Some technical tests both using higher kVp and higher mA (with lower rotation time) on the same specimens were performed, however, the images displayed here represent the best-quality result

All specimens were immediately dissected after the imaging procedures. Two heads were dissected following a stratigraphic approach (Figures 1 and 2), whereas the remaining 2 specimens were designated for cross-sectional anatomic studies following the same planes of the CT studies:

transverse (Figures 4–8) and sagittal (Figures 9 and 10). These latter specimens were placed on a plastic support and, immediately upon CT scan completion, moved to a freezer (–20°C), carefully maintained in the same position as in the CT study, for 24 hours. Cross-sectional anatomic dissection was performed strictly following the imaging protocol by means of electric band saw. However, each section was 3 mm thick and therefore included 2 contiguous CT slices. The difference between the CT and anatomic slice thickness was meant to curtail the likelihood of cut errors (which would be greater with a finer slice thickness) and therefore to maintain the best correlation between the cuts and the imaging sections. Slices of each animal were cleaned with water, numbered, and photographed on the cranial and caudal surfaces.Individual anatomic structures were first identified in the anatomically dissected and cross-sectioned heads on the basis of anatomic references and then correlated to the corresponding structures in the radiographs and CT scans. Because of the absence of a single reference for the anatomic nomenclature, individual anatomic structures were named following the only international publications on ophidian anatomy presently available.[28–33] Not all the structures identified in the cadavers were identified on the radiographs and CT scans and vice versa.

Imaging procedures

To overcome the superimposition of structures, radiograph and dissection photographs were matched. Dorsoventral (Figure 1) and right lateral (Figure 2) radiographic images of the head were matched with corresponding images obtained during superficial and deep plane stratigraphic dissection. Lines were superimposed on a photograph of a boa constrictor head to indicate the approximate levels of the sections of the CT studies (Figures 4–10). Matched transverse (Figures 4–8) and sagittal (Figures 9 and 10) sections obtained from the cross-sectional studies were selected.

Results

The limited quality of the CT images was the consequence of an intrinsic lack of resolution in the CT technique applied to small-sized specimens and the inability to reduce the field of view of the device to less than the limit of 16 cm.

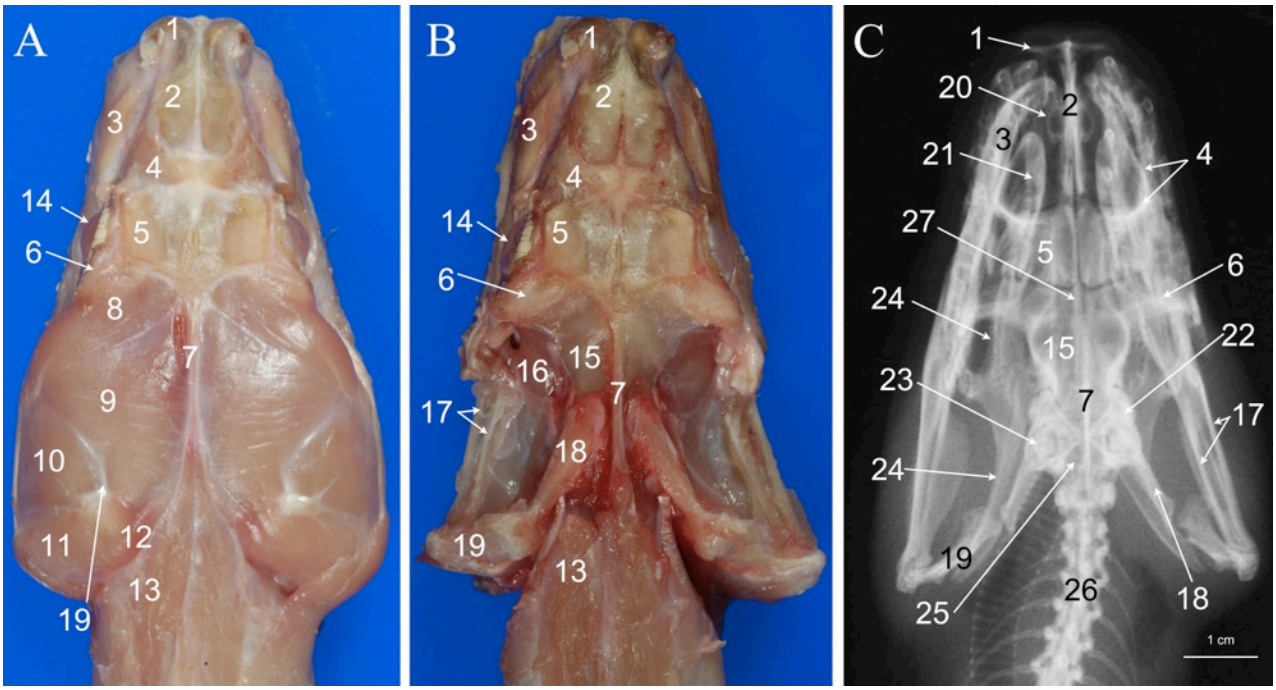

Figure 1—Dorsoventral photographic (superficial [A] and deep plane [B] dissections) and radiographic (C) views of the head of a boa constrictor. A—Only skin was removed. B—Musculus adductor mandibulae externus anterior, musculus adductor mandibulae externus medialis, musculus adductor mandibulae externus posterior, musculus occipito-quadrato-mandibularis, musculus cervico-mandibularis, and musculus adductor mandibularis internus were removed. 1 = Premaxilla. 2 = Nasal bone. 3 = Maxilla. 4 = Prefrontal bone. 5 = Frontal bone. 6 = Postorbital bone. 7 = Parietal crest. 8 = Musculus adductor mandibulae externus anterior. 9 = Musculus adductor mandibulae externus medialis. 10 = Musculus adductor mandibulae externus posterior. 11 = Musculus occipito-quadrato-mandibularis. 12 = Musculus cervico-mandibularis. 13 = Musculus transversospinalis. 14 = Eye. 15 = Parietal bone. 16 = Harderian gland. 17 = Articular and surangular bone. 18 = Supratemporal bone. 19 = Quadrate bone. 20 = Septomaxilla. 21 = Palatine bone. 22 = Otooccipital bone. 23 = Lagena. 24 = Pterygoid bone. 25 = Occipital bone. 26 = Vertebrae.

All the clinically relevant structures of the head were indicated in the cross-sectional and anatomic dissections. A small amount of mucus could be seen in the oral cavity of the cross-sectioned head (Figures 4–8) because the animal was affected by pneumonia.

Bony structures of the head were evident on radiographs and CT scans. The bones composing the lower jaw had less than the minimum resolution level for radiographs and CT scans, so they appeared as a unique bone. Soft tissues were poorly defined on radiographs; only the masticatory

muscles were evident on the dorsoventral and ventrodorsal radiographs as a soft tissue opacity behind and around the supratemporal and quadrate bone. On the CT scans, most of the head soft tissues were not distinctly recognizable.

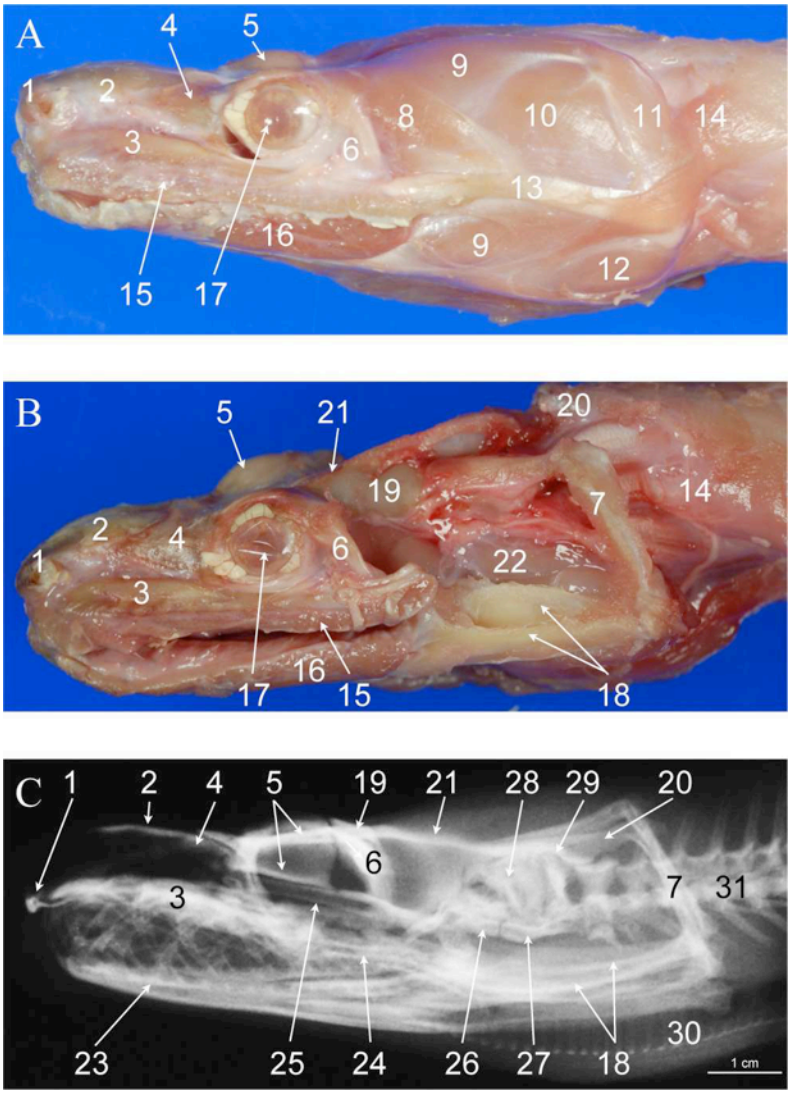

Figure 2—Right lateral photographic (superficial [A] and deep plane [B] dissections) and radiographic (C) views of the head of a boa constrictor. 7 = Quadrate bone. 8 = Musculus adductor mandibulae anterior externus. 9 = Musculus adductor mandibulae medialis externus. 10 = Musculus adductor mandibulae posterior externus. 13 = Maxillo-mandibular ligament. 14 = Musculus cervico-mandibularis. 15 = Supralabial glands. 16 = Infralabial glands. 17 = Eye. 18 = Articular and surangular bone. 19 = Parietal bone. 20 = Supratemporal bone. 21 = Parietal cresta. 22 = Protractor pterygoidei. 23 = Dentary bone. 25 = Parasphenoid rostrum. 26 = Sphenoid bone. 27 = Basioccipital bone. 28 = Otooccipital bone. 29 = Supraoccipital bone. 30 = Trachea. 31 = Vertebrae. *See* Figure 1 for

Discussion

Reptiles, like mammals, have great anatomic variability among species, but unlike mammals, also have extreme individual variability. It is important not to use results of the present study for interpretation of imaging of other snake species unless specific differences among the species under analysis and boa constrictors are well-known.

Snakes are the only vertebrates known to ingest whole prey larger in mass and diameter than themselves. This ability derives from a unique head anatomy not found among other animals.

The snake skull is composed of a snout and a braincase that represent the fixed regions of the skull. To these are loosely attached the palatomaxillary apparatus (divided into maxilla and pterigoideus), which are homologous to the maxilla, and a series of bones (supratemporal, quadrate,

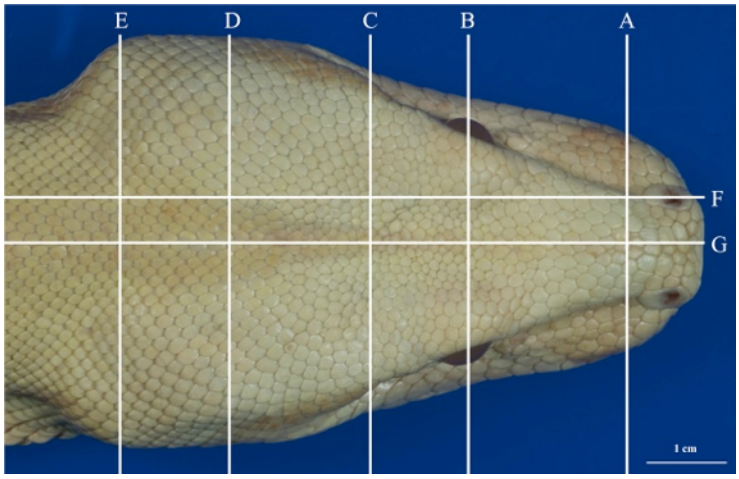

Figure 3—Photograph of the head of a boa constrictor (*Boa constrictor*); lines (A-G) indicate the approximate levels of CT sections.

articular, surangular, dentary, coronoid, and splenial). Together, these bones are homologous to the jaw in mammalians (Figures 1–10). The 2 sides of the lower jaw are divided and independent of each another (Figure 1) and attached by a loose fold of skin and mucosa.

The joints between the supratemporal and quadrate bones and the lower jaw are extremely loose (Figures 1, 2, and 8); this makes positioning of the snake head during imaging studies difficult because it is hard to obtain perfect symmetry between the 2 sides of the head. For this reason, evaluation of symmetry of a radiograph is better performed by positioning the snout and braincase, because of their fixed position.

The bony structures of the skull were evident with CT and radiographic techniques. Nonetheless, some bones were not detectable as single elements when CT was used, because of their limited size (eg, bones of lower jaw), which was smaller than the minimum resolution in conventional CT

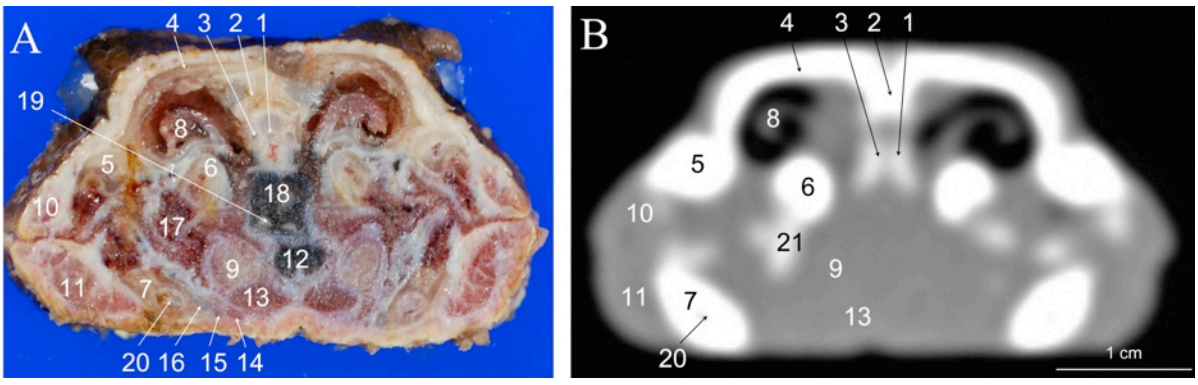

Figure 4—Photograph of an anatomic transverse cross section (A) and CT image (B) at the level of the nasal cavities corresponding to line A in Figure 3. The right side of the head is oriented to the right of the images and the ventral aspect of the head is oriented to the bottom of the images. 1 = Rostrum parasphenoid. 2 = Frontal bone. 3 = Vomer bone. 4 = Prefrontal bone. 5 = Maxilla. 6 = Palatine bone. 7 = Dentary bone 8 = Turbinalia. 9 = Sublingual glands. 10 = Supralabial glands. 11 = Infralabial glands. 12 = Musculus hyoglossus. 13 = Intermandibular muscles. 14 = Musculus constrictor colli. 15 = Sublingual glands. 16 = Meckelian fossa. 17 = Oral cavity. 18 = Trachea. 19 = Cricoid cartilage. 20 = Inferior alveolar canal. 21 = Tooth.

technique. A more accurate evaluation is possible only through high resolution x-ray CT devices such as mini-CT and micro-CT, which are normally used for laboratory animals whose body size is similar to that of the specimens of the present study. However, such technology is not presently

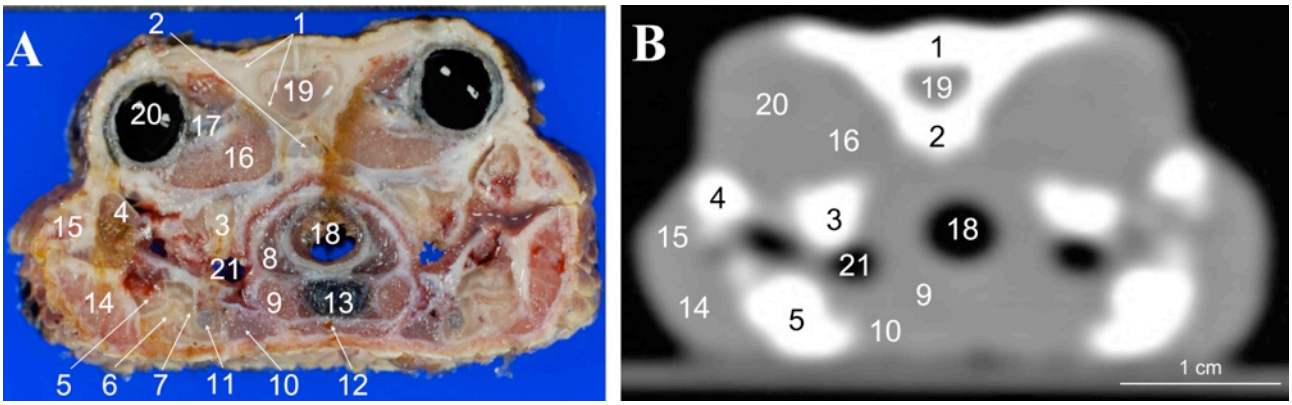

Figure 5— Photograph of an anatomic transverse cross section (A) and CT image (B) at the level of the eyes corresponding to line B in Figure 3. 1 = Frontal bone. 2 = Parasphenoid rostrum. 3 = Palatine bone. 4 = Maxilla. 5 = Dentary bone. 6 = Coronal bone. 7 = Splenial bone. 8 = Musculus dilatator laringis. 9 = Intermandibular muscles. 10 = Musculus neuro-costo-mandibularis (medial fascia). 11 = Meckelian fossa. 12 = Musculus constrictor colli. 13 = Musculus hyoglossus. 14 = Infralabial glands. 15 = Supralabial glands. 16 = Harderian gland. 17 = Optic nerve. 18 = Trachea. 19 = Brain. 20 = Eye. 21 = Oral cavity. *See* Figure 4 for remainder of key.

available in veterinary clinics but only in some specialized research centers.[34]

Snakes have an acrodontal tooth attachment: a dental formation whereby the teeth are consolidated with the summit of the alveolar ridge of the bone without sockets. The teeth are arranged in 1 row on each jaw and 2 rows on each palatomaxillary apparatus. Teeth are periodically replaced throughout a snake's lifetime; dental buds develop on the base and inside the previous tooth while it

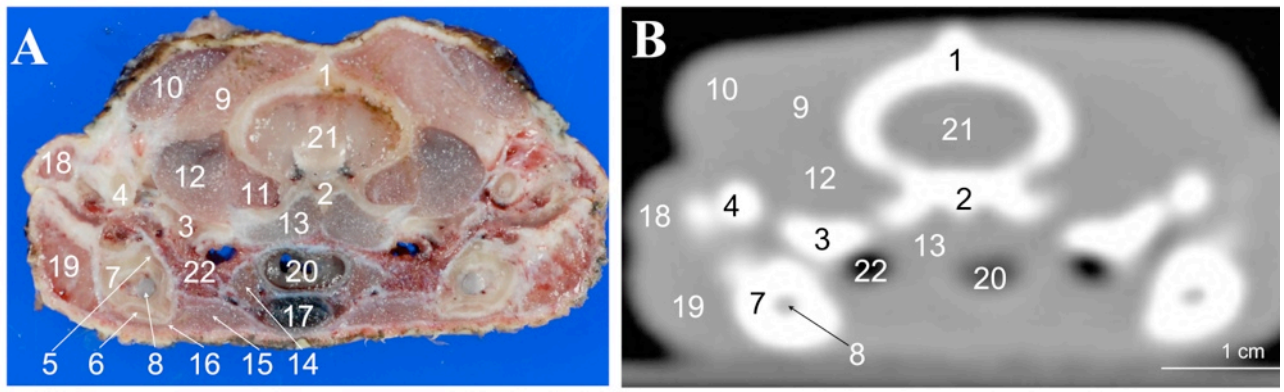

Figure 6— Photograph of an anatomic transverse cross section (A) and CT image (B) at the level of the parietal bone corresponding to line C in Figure 3. 1 = Parietal bone. 2 = Sphenoid bone. 3 = Pterygoid bone. 4 = Ectopterygoid bone. 5 = Coronoid bone. 6 = Splenial bone. 7 = Articular and surangular bones. 8 = Meckelian canal. 9 = Musculus adductor mandibulae externus medialis. 10 = Musculus adductor mandibulae externus anterior. 11 = Musculus adductor mandibulae internus (internal band). 12 = Musculus adductor mandibulae internus (external band). 13 = Musculus protractor pterygoidei. 14 = Intermandibular muscles. 15 = Musculus neuro-costo-mandibularis. 16 = Musculus constrictor colli. 17 = Musculus hyoglossus. 18 = Supralabial glands. 19 = Infralabial glands. 20 = Trachea. 21 = Brain. 22 = Oral cavity. *See* Figure 4 for remainder of key.

is still functional.[30] Tooth and dental cavity anatomy were well visualized on radiographs and CT images (Figures 1, 2, 4–6, and 9).

The musculature of the head is well developed in boa constrictors; the ability of a boa constrictor to catch live prey requires enormous strength in relation to its small head size. The major musculature components are located on the caudolateral side of the head, where the adductor muscles are situated. They are distributed in superficial and deep planes. The musculature of the head was not well visualized on radiographs (Figures 1 and 2) but was evident on CT images (Figures 6–10).

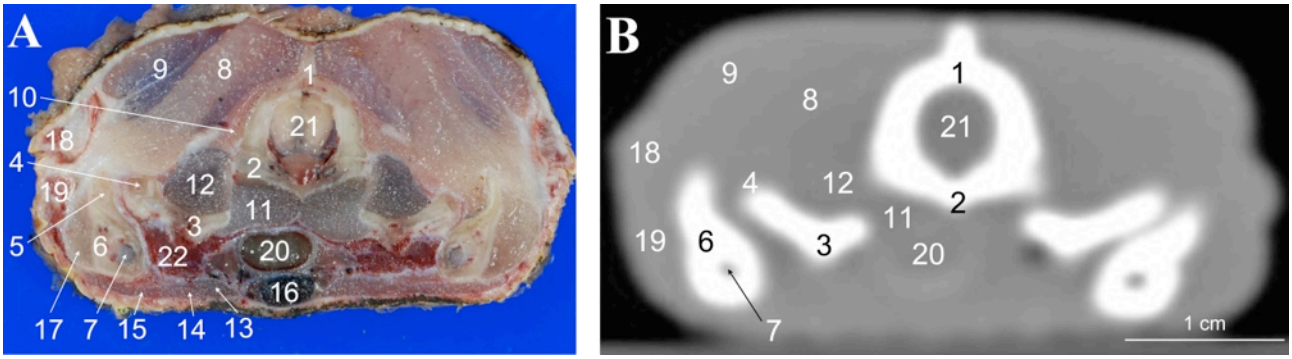

Figure 7— Photograph of an anatomic transverse cross section (A) and CT image (B) at the level of the parietal bone corresponding to line D in Figure 3. 1 = Parietal bone. 2 = Sphenoid bone. 3 = Pterygoid bone. 4 = Ectopterygoid bone. 5 = Coronoid bone. 6 = Articular and surangular bone. 7 = Meckelian canal. 8 = Musculus adductor mandibulae externus medialis. 9 = Musculus adductor mandibulae externus anterior. 10 = Musculus levator mandibulae medialis. 11 = Musculus protractor pterygoid. 12 = Musculus adductor mandibulae internus (internal band). 13 = Intermandibular muscles. 14 = Musculus constrictor colli. 15 = Musculus neuro-costo-mandibolaris. 16 = Musculus hyoioideus. 17 = Musculus adductor mandibulae internus (external band). 18 = Supralabial glands. 19 = Infralabial glands. 20 = Trachea. 21 = Brain. 22 = Oral cavity. *See* Figure 4 for remainder of key.

The snake ear is composed of only inner and middle compounds and completely lacks an external portion. The middle ear is composed of the tympanic cavity (lacking a tympanic membrane), reduced to a narrow fissure, and the ossicular chain (columella and extracolumella [cartilaginous expansion of the distal portion of the columella]), which passes through an air space and inserts medially on the oval window of the cochlea. The inner ear is quite complex; it is composed of the bony and membranous labyrinths. The last part of the cochlear channel is the lagena and is covered by a coat of otoliths (limestone concretions),[35] which were clearly visible on radiographs (Figure 1) and CT images (Figures 9 and 10).

The oral glands in snakes differ greatly depending on the species; boa constrictors have many well-developed oral glands distributed all around the lips (premaxillary, supralabial, and infralabial

glands) and in the oral cavity (sublingual and palatine)[29]; boa constrictors have, like all other boids, no venomous gland. The oral glands were not visualized on radiographs and were difficult to

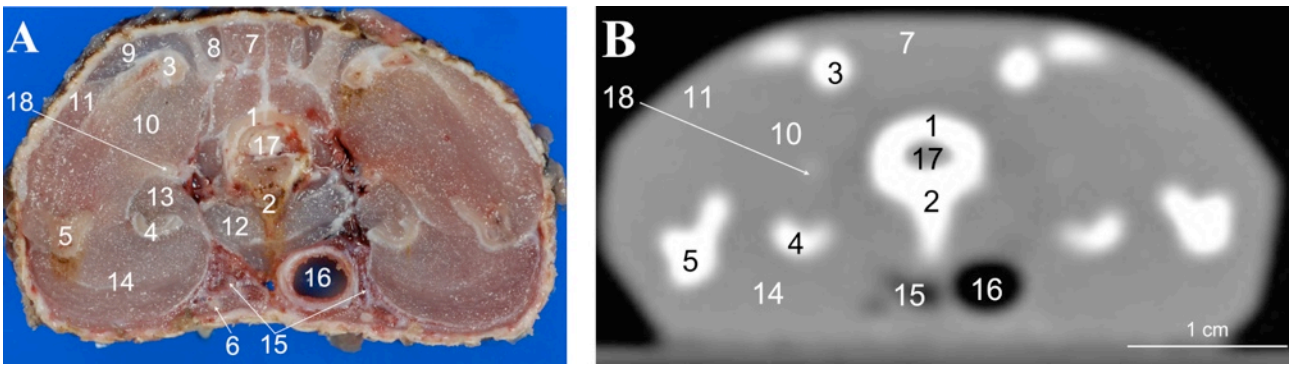

Figure 8— Photograph of an anatomic transverse cross section (A) and CT image (B) at the level of the supratemporal-quadrate joint corresponding to line E in Figure 3. 1 = Occipital bone. 2 = Basioccipital bone. 3 = Supratemporal-quadrate articulation. 4 = Pterygoid bone. 5 = Articular and surangular bones. 6 = Cheratobranchial bone. 7 = Musculus transversospinalis. 8 = Musculus longissimus dorsi. 9 = Musculus cervico-mandibolaris. 10 = Musculus adductor mandibulae externus posterior. 11 = Musculus occipito-quadrato-mandibolaris. 12 = Musculus protractor pterygoid. 13 = Musculus adductor mandibulae internus (internal band). 14 = Musculus adductor mandibulae internus (external band). 15 = Esophagus. 16 = Trachea. 17 = Brain. 18 = Stapes. *See* Figure 4 for remainder of key.

identify in CT images (Figures 1, 2, 4–7, 9, and 10); we hypothesize that use of contrast medium could help in distinguishing oral glands from other structures in living animals.

Snakes possess a well-developed Harderian gland, which is a lachrymal gland extending from the rostral part of the orbit along its medial side and ventral to (and sometimes around) the optic nerve and back into the temporal region.[36] All our specimens had a well-developed Harderian gland surrounding the optic nerve (Figures 1, 5, 6, and 9). The Harderian gland was well visualized on CT scans (Figures 5, 6, and 9); because of the superimposition of other structures, it was not visible in the radiographs (Figure 1).

The small size of the head and presence of a high number of superimposed structures makes correct positioning during imaging studies mandatory. Particular attention must be paid to correctly positioning movable structures, such as jaws.

Radiographs provided a high level of detail regarding the bony structures and could be useful in evaluating pathological changes such as fractures, bone neoplasia, and bone demineralization. Soft tissue definition was poor, and detailed evaluation was difficult.

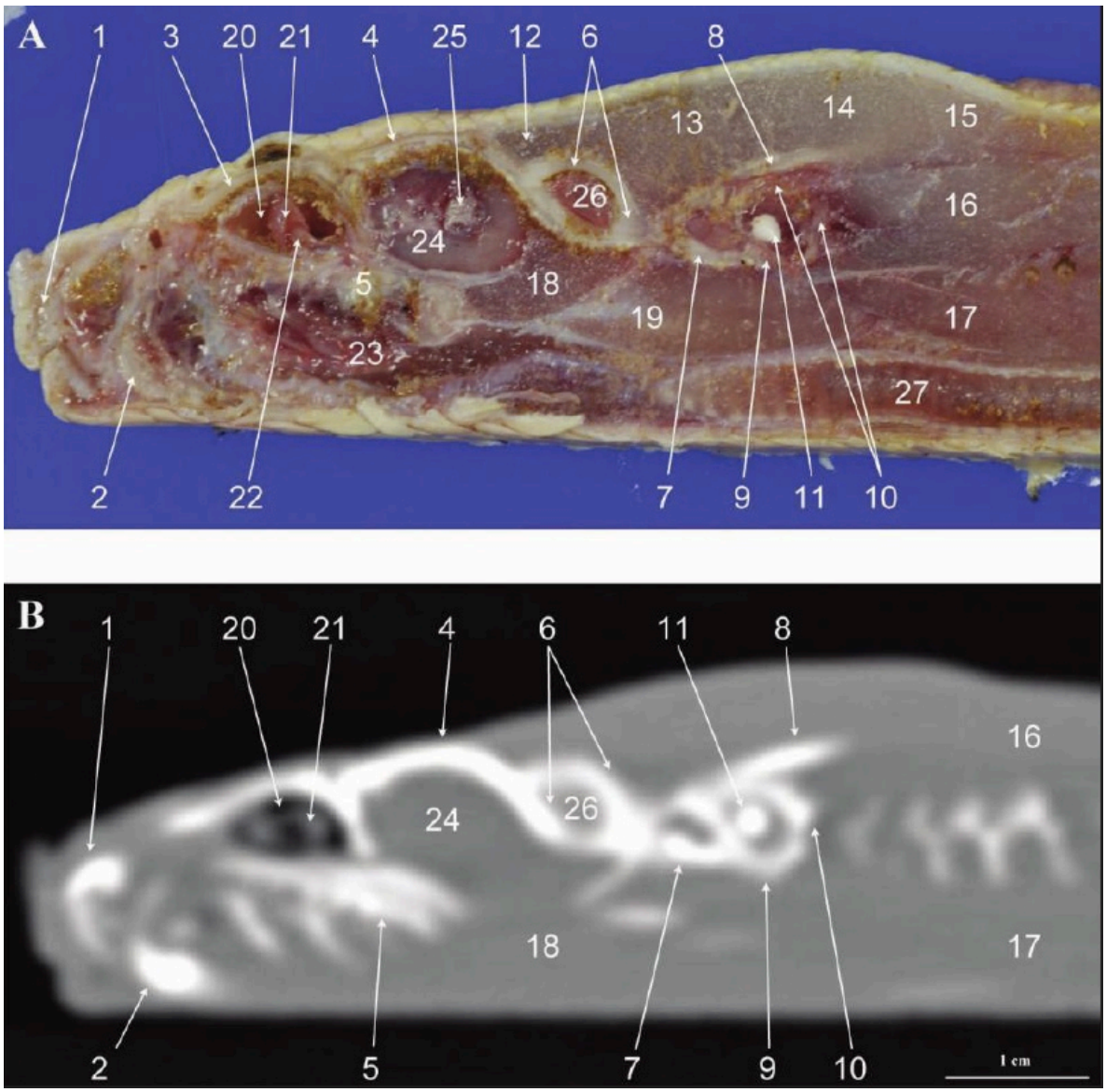

Figure 9—Photograph of an anatomic sagittal cross section (A) and CT image (B) at the level of the internal ear and retro-orbital region corresponding to line F in Figure 3. The sections are displayed with the cranial side to the left and the ventral part to the bottom of the images. 1 = Maxilla. 2 = Dentary bone. 3 = Nasal bone. 4 = Frontal bone. 5 = Palatine bone. 6 = Parietal bone. 7 = Prootic bone. 8 = Supratemporal bone. 9 = Basioccipital bone. 10 = Otoccipital bone. 11 = Lagena. 12 = Musculus adductor mandibulae externus anterior. 13 = Musculus adductor mandibulae externus medialis. 14 = Musculus adductor mandibulae externus posterior. 15 = Musculus cervico mandibularis. 16 = Musculus longissimus dorsi. 17 = Musculus subvertebralis. 18 = Musculus levator pterygoidei. 19 = Musculus protractor pterygoidei. 20 = Nasal cavity. 21 = Chonchae. 22 = Jacobson's organ. 23 = Oral cavity. 24 = Harderian gland. 25 = Optic nerve. 26 = Brain. 27

Most of the main boa constrictor head structures were well visualized on CT scans. Nevertheless, as in mammal CT studies, soft tissues with similar structure and density, such as glands and muscles, are difficult to distinguish, particularly in cadavers, where the lack of vascularization reduces contrast. We believe that in live animals, injection of contrast medium could provide better differentiation. Moreover, multislice helical scanners (enabling reduction of slice thickness to

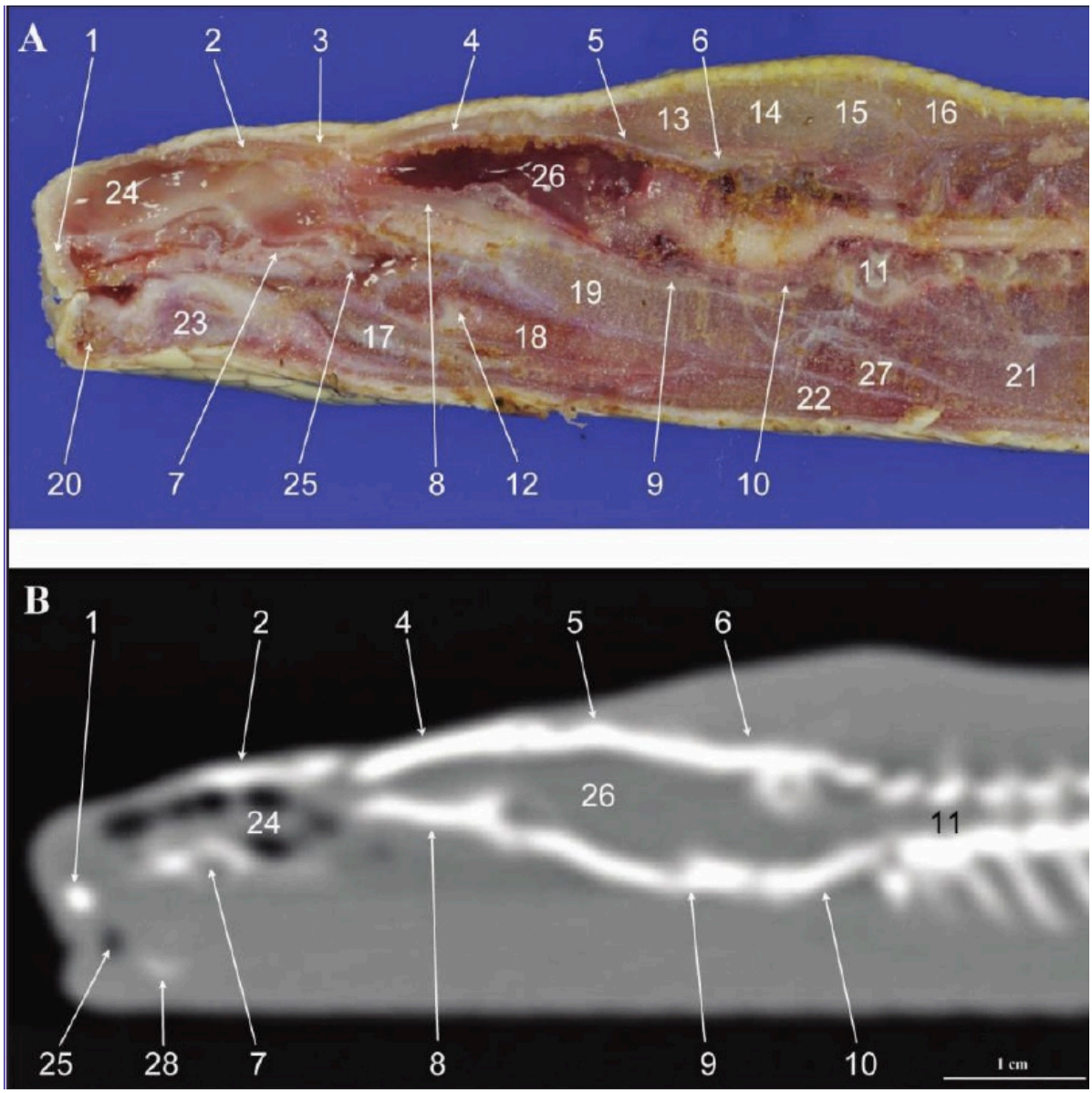

Figure 10—Photograph of an anatomic sagittal cross section (A) and CT image (B) in midsagittal plane corresponding to line G in Figure 3. 1 = Premaxilla. 2 = Nasal bone. 3 = Prefrontal bone. 4 = Frontal bone. 5 = Parietal bone. 6 = Supraoccipital bone. 7 = Palatine bone. 8 = Parasphenoid rostrum. 9 = Sphenoidal bone. 10 = Basioccipital bone. 11 = Vertebrae. 12 = Arytenoid cartilages. 13 = Musculus adductor mandibulae externus anterior. 14 = Musculus adductor mandibulae externus medialis. 15 = Musculus adductor mandibulae externus posterior. 16 = Musculus cervico mandibularis. 17 = Musculus hyoglossus. 18 = Laringeal muscles. 19 = Musculus protractor pterygoidei. 20 = Infralabial glands. 21 = Musculus subvertebralis. 22 = Musculus constrictor colli. 23 = Sublingual glands. 24 = Nasal cavities. 25 = Oral cavity. 26 = Brain. 27 = Esophagus. 28

submillimetric values) with dynamic field of view could provide higher-quality images and a better resolution of bone and soft tissues.

References

1. Lindemann L, Harding J. University of Michigan Museum of Zoology. Animal Diversity Web. *Boa constrictor*: boa constrictor. Available at: animaldiversity.ummz.umich.edu/site/accounts/information/Boa_constrictor.html. Accessed Jul 6, 2010.

2. Zook BC, Hitzelberg RA, Bradley EW. Cross-sectional anatomy of the Beagle thorax. *Vet Radiol Ultrasound* 1989;30:277–281.

3. Feeney DA, Fletcher TA, Hardy RM. Atlas of correlative imaging anatomy of the normal dog. Ultrasound and computed tomography. Philadelphia: WB Saunders Co, 1991;1–382.

4. George TF II, Smallwood JE. Anatomic atlas for computed tomography in the mesaticephalic dog: head and neck. *Vet Radiol Ultrasound* 1992;33:217–240.

5. Smallwood JE, George TF II. Anatomic atlas for computed tomography in the mesaticephalic dog: caudal abdomen and pelvis. *Vet Radiol Ultrasound* 1992;33:143–167.

6. Smallwood JE, George TF II. Anatomic atlas for computed tomography in the mesaticephalic dog: thorax and cranial abdomen. *Vet Radiol Ultrasound* 1993;34:65–84.

7. De Rycke LM, Gielen IM, can Meervenne SA, et al. Computed tomography and cross-sectional anatomy of the normal canine brain. *Am J Vet Res* 2005;66:1743–1756.

8. De Rycke LM, Saunders JH, Gielen IM, et al. Magnetic resonance imaging, computed tomography and cross-sectional anatomy of the normal canine nasal cavities and paranasal sinuses in the mesaticephalic dog. *Am J Vet Res* 2003;64:1093–1098.

9. Samii FV, Biller SD, Koblik DP. Normal cross section anatomy of the feline thorax and abdomen: comparison of computed tomography and cadaver anatomy. *Vet Radiol Ultrasound* 1998;39:504–511.

10. Van Caelenberg A, De Rycke LM, Hermans K, et al. Computed tomography and cross-sectional anatomy of the head in healthy rabbits. *Am J Vet Res* 2010;71:293–303.

11. Zotti A, Banzato T, Cozzi B. Cross-sectional anatomy of the rabbit neck and trunk: Comparison of computed tomography and cadaver anatomy. *Res Vet Sci* 2009;87:171–176.

12. Morrow LK, Park RD, Spurgeon LT, et al. Computed tomographic imaging of the equine head. *Vet Radiol Ultrasound* 2000;41:491–497.

13. Smallwood JE, Wood BC, Taylor WE, et al. Anatomic reference for computed tomography of the head of the foal. *Vet Radiol Ultrasound* 2002;43:99–117.

14. Arencibia A, Rivero MA, De Miguel I, et al. Computed tomographic anatomy of the head of the loggerhead sea turtle (*Caretta caretta*). *Res Vet Sci* 2006;81:165–169.

15. Liste F, Palacio J, Ribes V, et al. Anatomic and computed tomographic atlas of the newborn bottlenose dolphin (*Tursiops truncatus*). *Vet Radiol Ultrasound* 2006;47:453–460.

16. Dennison ES, Schwarz T. Computed tomographic imaging of the normal immature California sea lion head (*Zalophus californianus*). *Vet Radiol Ultrasound* 2008;49:557–563.

17. Eds Gans, C., Bellairs, A.A., Parsons, T.S., Dawson, W.R., Tinkle, D.W., Kyoko, A., Gans, R., Northcutt, G., Ulinski, P.S., Harvey Pough, F., Billett, F., Maderson, P.F., Huey, R.B., Crews, D., Gaunt, A.S., Adler, K., Liner, E.A. (1970 – 2010) Biology of the Reptilia. Society for the study of Amphibians and Reptiles. Vol. 1-24

18. O'Malley B. *Clinical anatomy and physiology of exotic species: structure and function of mammals, birds, reptiles and amphibians*. Philadelphia: Saunders Ltd, 2005;77–88.

19. Mader DR. *Reptile medicine and surgery*. 2nd ed. Philadelphia: WB Saunders Co, 2006.

20. Snyder PS, Shaw NG, Heard DJ. Two-dimensional echocardiographic anatomy of the snake heart (*Python molurus bivittatus*). *Vet Radiol Ultrasound* 1999;40:66–72.

21. Schumacher J, Toal RL. Advanced radiography and ultrasonography in reptiles. *Semin Avian Exot Pet Med* 2001;10:162–168.

22. Maisano JA, Rieppel O. The skull of the Round Island boa, *Casarea dussumieri schlegel*, based on high-resolution x-ray computed tomography. *J Morphol* 2007;268:371–384.

23. Pees M, Kiefer I, Ludewig EW, et al. Computed tomography of the lungs of Indian pythons (*Python molurus*). *Am J Vet Res* 2007;68:428–434.

24. Pees M, Kiefer I, Oechtering G, et al. Computed tomography for the diagnosis and treatment monitoring of bacterial pneumonia in Indian pythons (*Python molurus*). *Vet Rec* 2008;163:152–156.

25. Pees MC, Kiefer I, Thielebein J, et al. Computed tomography of the lung of healthy snakes of the species *Python regius*, *Boa constrictor*, *Python reticulatus*, *Morelia viridis*, *Epicrates cenchria* and *Morelia spilota*. *Vet Radiol Ultrasound* 2009;50:487–491.

26. Pees M, Bochmann M, Krautwald-Junghanns ME, et al. Vergleichende röntgenologishe Darstellung des Respirationstraktes von Schlangen mittels konventioneller hochausflösender Film-Folien-Kombination und einem digitalen Detektorsystem. *Berl Munch Tierarztl Wochenschr* 2010;123:177–185.

27. Rieppel O, Kley NJ, Maisano JA. Morphology of the skull of the white-nosed blindsnake, *Liotyphlops albirostris* (Scolecophidia: Anomalepididae). *J Morphol* 2009;270:536–557.

28. Edgeworth FH. *The cranial muscles of vertebrates*. Cambridge: Cambridge University Press, 1935;405–430.

29. Taub AM. Ophidian cephalic glands. *J Morphol* 1966;118:529–542.

30. Grassè P. Traité de zoologie. Vol 14. 2nd ed. Paris: Masson et Cie, 1970;360–375.

31. Kochva E. Oral glands of the reptilia. In: Gans C, Kyoko A, eds. *Biology of the reptilia*. Vol 8. London: Academic Press, 1970;43–100.

32. Van Wallach S. The pulmonary system: The lungs of snakes. In: Gans C, Gaunt AS, eds. *Biology of the reptilia*. Vol 19. Ithaca, NY: Society for the Study of Amphibians and Reptiles, 1998;117–126.

33. Cundall D, Irish F. The snake skull. In: Gans C, Gaunt AS, Adler K, eds. *Biology of the reptilia*. Vol 20. Ithaca, NY: Society for the Study of Amphibians and Reptiles, 2008;444–460.

34. Bartling HS, Stiller W, Semmler W, et al. Small animal computed tomography imaging. *Curr Med Imaging Rev* 2007;3:45–59.

35. Murray MJ. Aural abscesses. In: Mader DR, ed. *Reptile medicine and surgery*. 2nd ed. Philadelphia: WB Saunders Co, 2006;742–743.

36. Underwood G. The eye. In: Gans C, Thomas S, eds. *Biology of the reptilia*. Vol 2. London: Academic Press, 1970;48–70.

CHAPTER IV

NORMAL RADIOGRAPHY AND COMPUTED TOMOGRAPHY OF THE HEAD OF LIZARDS

*This chapter was adapted from:*Banzato T, Selleri P, Veladiano IA, Martin A, Zanetti E, Zotti A. Comparative evaluation of the cadaveric, radiographic and computed tomographic anatomy of the heads of green iguana (Iguana iguana), common tegu (Tupinambis merianae) and bearded dragon (Pogona vitticeps). *BMC Veterinary Research* 2012, 8.

Abstract

Radiology and computed tomography are the most commonly available diagnostic tools for the diagnosis of pathologies affecting the head and skull in veterinary practice. Nevertheless, accurate interpretation of radiographic and CT studies requires a thorough knowledge of the gross and the cross-sectional anatomy. Despite the increasing success of reptiles as pets, only a few reports over their normal imaging features are currently available. The aim of this study is to describe the normal cadaveric, radiographic and computed tomographic features of the heads of the green iguana, tegu and bearded dragon. 6 adult green iguanas, 4 tegus, 3 bearded dragons, and, the adult cadavers of : 4 green iguana, 4 tegu, 4 bearded dragon were included in the study. 2 cadavers were dissected following a stratigraphic approach and 2 cadavers were cross-sectioned for each species. These latter specimens were stored in a freezer (-20°C) until completely frozen. Transversal sections at 5 mm intervals were obtained by means of an electric band-saw. Each section was cleaned and photographed on both sides. Radiographs of the head of each subject were obtained. Pre- and post-contrast computed tomographic studies of the head were performed on all the live animals. CT images were displayed in both bone and soft tissue windows. Individual anatomic structures were first recognised and labelled on the anatomic images and then matched on radiographs and CT images. Radiographic and CT images of the skull provided good detail of the bony structures in all species. In CT contrast medium injection enabled good detail of the soft tissues to be obtained in the iguana whereas only the eye was clearly distinguishable from the remaining soft tissues in both the tegu and the bearded dragon. The results provide an atlas of the normal anatomical and in vivo radiographic and computed tomographic features of the heads of lizards, and this may be useful in interpreting any imaging modality involving these species.

Introduction

Nowadays, reptiles are treated at veterinary practices in a context where both reptile and amphibian medical expertise is constantly improving as more advanced knowledge of these species is scientifically validated[1]. Owners now expect and demand more targeted and expert diagnostic testing for their animals, on the basis of these advances[1]. Reptile medicine has in fact stirred a certain interest in recent years, which is illustrated by the numerous publications validating diagnostic, surgical and anesthesiological techniques in reptile patients[2-14].

Radiographic evaluation of the skull and vertebral column is the most economic and readily available imaging modality for the exotic animal clinician[1]. Furthermore, routine access to CT is becoming increasingly common and many specialty practices have a CT scanner on site[1]. Nevertheless, accurate interpretation of radiographic and CT studies requires a thorough knowledge of the gross and the cross-sectional anatomy[15-16].

To the best of our knowledge, no comprehensive description of the radiographic and computed tomographic features of lizard heads is currently available. Therefore, the aim of this study is to describe and compare the normal radiographic and CT features of the head of some of the most popular pet lizards. Green iguanas and bearded dragons are common reptile pets[17-18]; tegus have recently become popular among collectors and breeders, although no official data exist on this topic.

This study has resulted in a series of tables matching the normal anatomic, radiographic and computed tomographic features of these species.

To thxe best of authors' knowledge, to the date a univocal anatomical reference for the species taken in account in this work is not available; nevertheless, the anatomy of closely related species has been thoroughly described. Several references describing the anatomy of the head of lizards are actually available[19-28].

Materials and Methods

Animals

Three species belonging to three different families of lizards were the object of this study: the green iguana (*Iguana iguana*, infraorder *Iguania*, family *Iguanidae*), the common tegu (*Tupinambis merianae*, infraorder *Scincomopha*, family *Teiidae*) and the bearded dragon (*Pogona vitticeps*, infraorder *Iguania*, family *Agamidae*).

The heads from adult cadavers of 4 green iguanas (3 females and 1 male, mean length 85.1 ±18.1 cm, mean weight 2824±856 g), 4 tegus (2 females and 2 males, mean length 42.5 ± 15.1 cm, mean weight 1587 ± 785 g) and 4 bearded dragons (1 female and 3 males, mean length 18.1±7.1 cm, mean weight 385±49 g) were dissected for this study. The animals were referred to the Radiology Unit of the Department of Animal Medicine, Production and Health at the University of Padua (Italy) for specialty examination and were euthanized because of advanced clinical conditions. A complete post-mortem gross examination was performed on each lizard and revealed pneumonia in 4 cases (2 iguanas and 2 bearded dragons), egg retention in 3 cases (1 iguana and 2 tegus), diffuse abscesses in 2 cases (1 tegu and 1 iguana); no lesions were evident in 3 cases (1 tegu, 2 bearded dragons).

Additionally, 13 live adult animals – 6 iguanas (4 males and 2 females, mean length 90.8±20.1 cm, mean weight 3298±922 g), 4 tegus (1 male and 3 females, mean length 55.2±22.1 cm, mean weight 2156 ± 655 g) and 3 bearded dragons (3 females, mean length 22.1 ± 5.4 cm, mean weight 455±75 g) – referred to the above facilities for specialty examination were included in the study. The pathologies affecting the animals did not involve the head in any of the cases and no pathological findings were evident at clinical examination of the head. For this reason, the imaging procedures were extended to the head of the animal upon prior consent from the owner [a].

Imaging procedures

Complete radiographic studies of the head, including LL (left lateral), right lateral, VD (ventrodorsal) and dorsoventral projections, were performed on all specimens and live animals. Radiographs were obtained by means of a computed radiography device (Kodak Point of Care CR-360 System- Carestream Health, Inc – Rochester, USA). All radiographs were displayed with a bone-edge slight enhancement filter.

CT examination was performed on all the live subjects. These animals were sedated with sevofluorane (Sevofluorane 100%, Baxter Spa, Rome, Italy) administered through a face mask. All CT studies were performed with the animals lying on ventral recumbency with the head towards the gantry. Pre- and post- contrast CT images were obtained in transverse planes by means of a third-generation CT scanner (Tomoscan® LX, Philips Medical Systems, Amsterdam, Holland). The CT parameters were: axial acquisition mode, rotation time of 2.9 seconds, voltage of 120 kV, amperage of 125 mA, and slice thickness of 1.5 mm. Contrast medium (Optiray® 300mg/ml, Covidien Spa, Italy) was injected directly into the caudal vein at the dose of 2.2 ml/kg bw. The images were then displayed in a bone tissue window (window length: 500; window width: 2,000) and a soft tissue window (window length: 40; window width: 400). Only post-contrast images have been reported.

Anatomical dissections

Stratigraphic gross anatomical dissection of the cadaver heads was performed in 2 green iguanas, 2 tegus and 2 bearded dragons. The dissections were performed within 24 hours of death in each patient to minimise post-mortem changes. Two green iguana, 2 Tegu, and 2 bearded dragon cadaver heads were designated for cross-sectional studies. These latter specimens were placed on a plastic

support, in ventral recumbency with the legs adherent to the body, immediately after death; soon after they were stored into a freezer (-20°C) and kept there until completely frozen. Cross-sectional anatomic dissection was performed by means of an electric band-saw. Contiguous 5 mm sagittal slices were obtained starting at the snout and reaching the cranial portion of the lungs. The slices were cleaned with water, numbered and photographed on the cranial and caudal surfaces.

The individual anatomic structures were first identified in the anatomically dissected and cross-sectioned heads, on the basis of anatomic references, and then matched with the corresponding structures in the radiographs and CT scans.

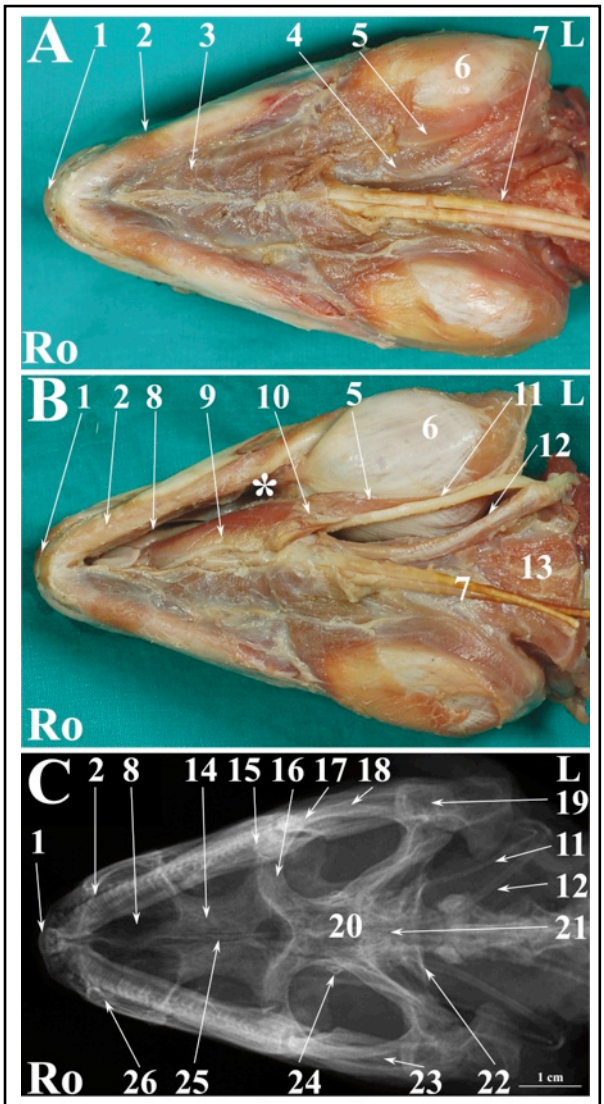

Figure 1. Normal radiographic anatomy of the head of the green iguana in VD projection. A. Ventral view in a superficial plane of stratigraphic dissection (only skin was removed) of the head of an iguana. B. Ventral view of stratigraphic dissection after removal of Musculus constrictor colli and Musculus intermandibularis (lower part of the image) and a deeper plane of dissection (upper part of the image) of the head of an iguana (deeper plane of dissection is labelled with * on the image). C. VD radiographic projection of the head of an iguana. Ro is rostral, L is left.1. Premaxillary bone; 2. Dentary bone; 3. Musculus intermandibularis; 4. Musculus geniohyoideus; 5. Musculus hyoglossus; 6. Musculus pterygoideus typicus; 7. Ceratobranchial 1 process of the hyobranchial skeleton; 8. Vomer bone; 9. Musculus genioglossus; 10. Tendinous band; 11. Ceratohyal process of the hyobranchial skeleton; 12. Ceratobranchial 2 process of the hyobranchial skeleton; 13. Musculus omohyoideus; 14. Palatine bone; 15. Ectopterygoid bone; 16. Pterygoid bone; 17. Jugal bone; 18. Postorbital bone; 19. Articular bone + quadrate bone; 20. Parietal bone; 21. Basioccipital bone; 22. Paraoccipital process of otooccipital bone; 23. Adductor fossa; 24. Epipterygoid bone; 25; Interpterygoid vacuiti; 26. Maxillary bone.

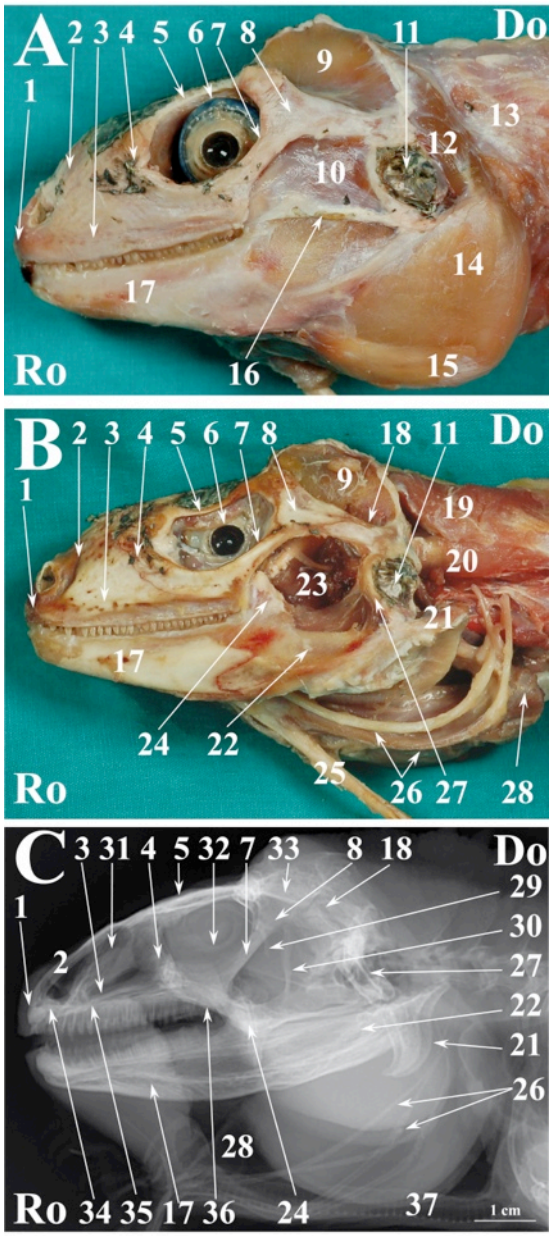

Figure 2. Normal radiographic anatomy of the head of the green iguana in LL projection. A. LL photographic image in a superficial plane of the stratigraphic dissection of the head of an iguana (only skin was removed). B. LL photographic image in a deep plane of the stratigraphic dissection of the head of an iguana. C. LL radiographic projection of the head of an iguana. Ro is rostral, Do is dorsal. 1. Premaxillary bone; 2. Nasal bone; 3. Maxillary bone; 4. Prefrontal bone; 5.Frontal bone; 6. Eye; 7. Jugal bone; 8. Postorbital bone; 9. Musculus adductor mandibulae externus medialis; 10. Musculus adductor mandibulae externus superficialis; 11. Ear; 12. Musculus depressor mandibulae; 13. Musculus episternocleidomastois; 14. Musculus pterygoideus typicus; 15. Musculus intermandibularis posterior; 16. Quadrato-maxillary ligament; 17. Dentary bone; 18. Squamosal bone 19. Musculus trapezius + Musculus clavicle dorsalis; 20. Musculus episternocleidomastoid; 21. Articular bone; 22. Angular bone + Surangular bone; 23. Adductor chamber; 24; Coronoid bone; 25. Ceratobranchial process of hyobranchial skeleton; 26. Hyobranchial skeleton; 27. Quadrate bone; 28. Oesophagus; 29. Pila metoptica; 30. Epipterygoid bone; 31. Nasal glands; 32. Scleral ossicles; 33. Parietal bone; 34. Vomer bone; 35; Palatine bone; 36; Pterygoid bone; 37. Trachea.

Results

Most of the clinically relevant structures of the head were recognised both in cross-sectional and anatomic dissections (Figures 1-9).

Figures 1, 4 and 7 show matched images of the ventral view of the stratigraphically dissected heads and VD radiographic projections of the corresponding species. Figures 2, 5 and 8 show matched images of the LL views of the stratigraphically dissected heads and LL radiographic projections of the corresponding species. Right lateral and dorsoventral radiographic projections were not shown because the radiographic images were identical to the LL and VD projections, respectively.

Figures 1A, 4A and 7A show ventral views of the superficial plane of the stratigraphic dissection (only skin was removed). Figures 1B, 4B and 7B show ventral views of the stratigraphically dissected heads: 1) after removal of musculus constrictor colli and musculus intermandibularis, and, 2) at a deeper dissection plane (the deeper dissection plane is marked on the figure). Two dissection planes – superficial, where only skin was removed (Figures 2A, 5A, 8A), and deep (Figures 2B, 5B, 8B) – are shown in LL views of the stratigraphically dissected heads.

The bony structures were clearly defined on the

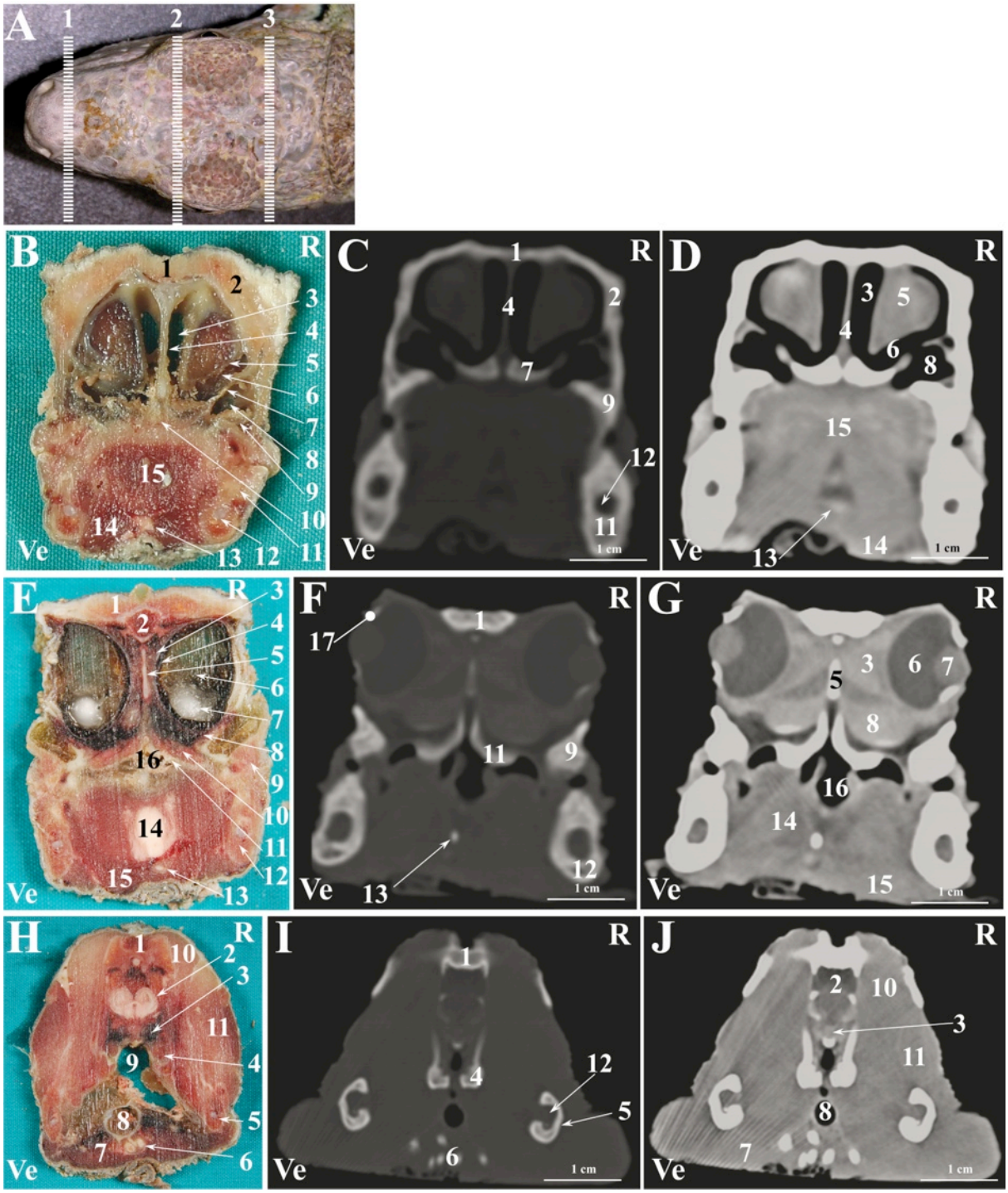

Figure 3. **Normal computed tomographic anatomy of the head of the green iguana.** A. Photograph of the head of an iguana; lines (1-3) indicate the approximate levels of matched cross-sections and CT images. B-J: Matched images of cross-sectional gross anatomy (B-E-H), CT image displayed in bone window (WW: +2000; WL: +500) (C-F-I) and CT image displayed in soft tissue window (WW: +400; WL: +40)(D-G-L) corresponding to: line 1 (B-C-D), line 2 (E-F-G) and line 3 (H-I-J) as depicted in Figure 3A. R is right and Ve is ventral. **B-C-D:** 1. Nasal bone; 2. Prefrontal bone; 3. Stammteil; 4. Nasal septum; 5. Nasal glands; 6. Subconcal recess; 7.Vomer bone; 8. Choanal tube; 9. Maxillary bone; 10. Cavum oris; 11. Dentary bone; 12. Meckelian fossa; 13. Entoglossal process of the basihyal bone; 14. Musculus geniohyoideus + Musculus hyoglossus + Musculus intermandibularis; 15. Tongue. **E-F-G:** 1. Frontal bone; 2. Brain; 3. Harderian glands; 4. Choroid plexus; 5. Interorbital septum; 6. Vitreous humor; 7. Lens; 8. Sinus orbitalis; 9. Maxillary bone; 10. Palatine glands; 11. Palatine bone; 12. Dentary bone; 13: Entoglossal process of the basihyal bone; 14. Tongue; 15. Musculus geniohyoideus + Musculus hyoglossus + Musculus intermandibularis; 16. Cavum oris; 17. Scleral ossicles. **H-I-J:** 1. Parietal bone**;** 2. Brain; 3. Vena cerebralis media; 4. Sphenoid bone; 5. Angular bone + Surangular bone; 6. Hyobranchial skeleton; 7. Musculus intermandibularis+ Musculus genioyhoideus + Musculus hyoglossus + Musculus pterygoideus + Musculus omohyoideus + Musculus stermohyoideus + Musculus ceratohyoideus; 8. Trachea; 9. Oesophagus; 10. Musculus adductor mandibulae externus medialis; 11. Musculus adductor mandibulae externus superficialis; 12. Adductor fossa.

radiographs of all species (Figures 1C, 2C, 4C, 5C, 7C, 8C). Some soft tissues, such as the

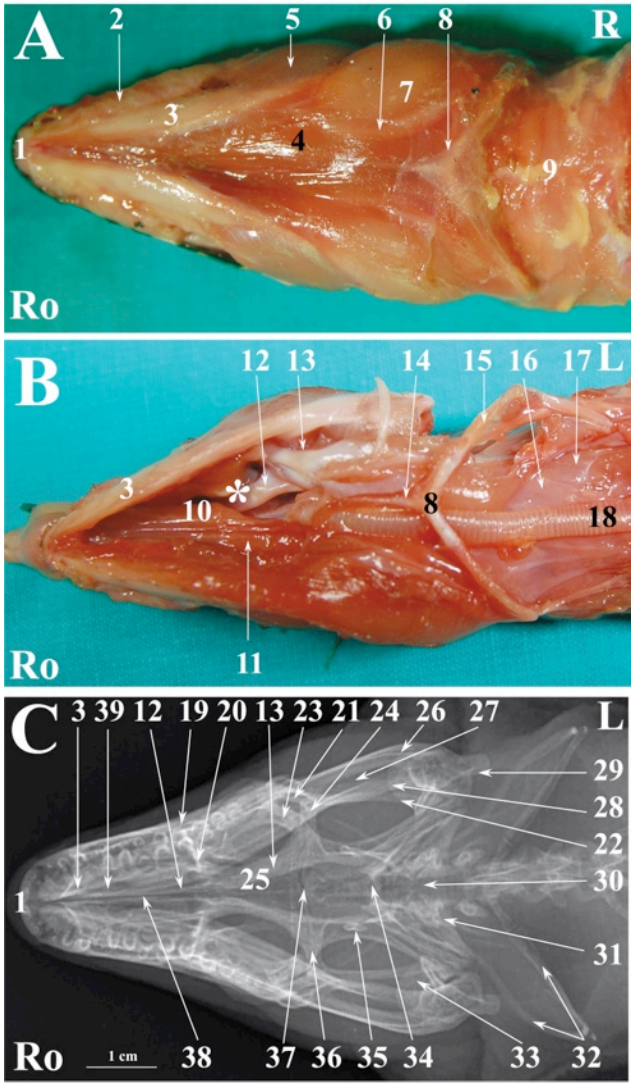

Figure 4. Normal radiographic anatomy of the head of the common tegu in VD projection. A. Ventral view in a superficial plane of stratigraphic dissection (only skin was removed) of the head of a tegu. B. Ventral view of stratigraphic dissection after removal of Musculus constritor colli and Musculus intermandibularis (lower part of the image) and a deeper plane of dissection (upper part of the image) of the head of a tegu (deeper plane of dissection is labelled with * on the image). C. VD radiographic projection of the head of a tegu. Ro is rostral, L is left.1. Premaxillary bone; 2. Infralabial glands; 3. Dentary bone; 4. Musculus intermandibularis; 5. Musculus adductor mandibulae externus superficialis; 6. Musculus hyoglossus; 7. Musculus pterygoideus; 8. Basihyal bone; 9. Musculus constrictor colli; 10. Tongue ; 11. Oesophagus; 12. Palatine bone; 13. Pterygoid bone; 14. Entoglossal process of hyobranchial skeleton; 15. Ceratobranchial process of hyobranchial skeleton; 16. Musculus omohyoideus; 17. Musculus sternohyoideus; 18. Trachea; 19. Maxillary bone; 20. Prefrontal bone; 21. Jugal bone; 22. Squamosal bone; 23. Ectopterygoid bone; 24. Postorbital bone; 25. Frontal bone; 26. Surangular bone; 27. Adductor fossa; 28. Angular bone; 29. Articular bone; 30. Basioccipital + Sopraoccipital bones; 31. Paraoccipital process of otooccipital bone; 32. Hyobranchial skeleton; 33. Quadrate bone; 34. Parietal bone; 35. Epipterygoid bone; 36. Postfrontal bone; 37. Parieto-frontal suture; 38. Interpterygoid vacuity; 39 Vomer bone.

oesophagus, the trachea and the masticatory muscles, could be also identified.

A selection of matched cross-sections and CT images are shown in Figures 3, 6 and 9. In Figures 3A, 6A and 9A, the lines superimposed on the photographs indicate the approximate level of the matched images displayed in the corresponding figures. The level of the cross-sections displayed in the images is similar for all the species considered in order to emphasise the comparative imaging features. A small amount of fluid was noticed in the oesophagus of the cross-sectioned iguanas (Figure 3H).

Discussion

The skull of lizards belonging to the infraorder *Iguania* is roughly triangular in dorsal view, with a short pre-orbital region. It retains all the characteristics of the ancestral lizard skull with no secondary closure of the skull openings[15].

The main difference between

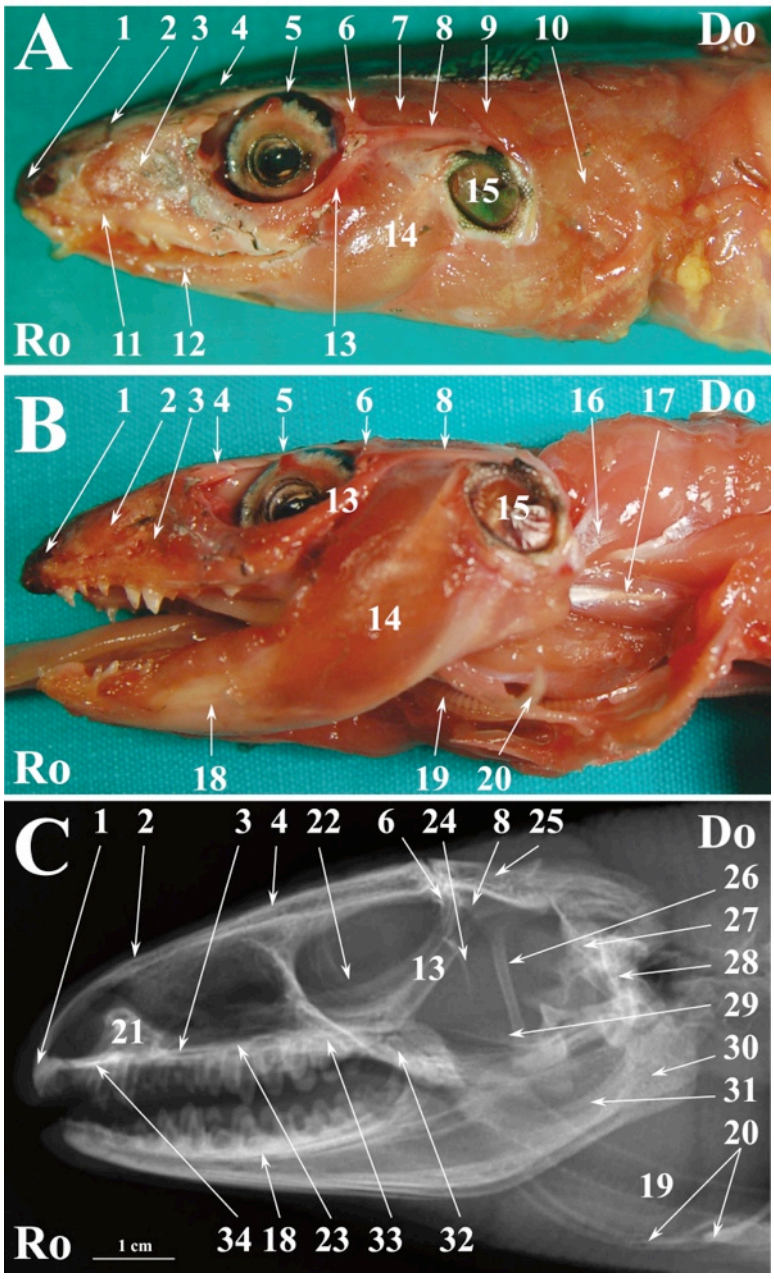

Figure 5. **Normal radiographic anatomy of the head of the common tegu in LL projection.** A. LL photographic image in a superficial plane of the stratigraphic dissection of the head of a tegu (only skin was removed). B. LL photographic image in a deep plane of the stratigraphic dissection of the head of a tegu C. LL radiographic projection of the head of a tegu. Ro is rostral, Do is dorsal. 1. Premaxillary bone; 2. Nasal bone; 3. Maxillary bone; 4. Frontal bone; 5. Eye; 6. Postorbital bone; 7. Musculus adductor mandibulae externus medialis; 8. Squamosal bone; 9. Musculus depressor mandibulae; 10. Musculus constrictor colli; 11. Supralabial glands; 12. Infralabial glands; 13. Jugal bone; 14. Musculus adductor mandibulae externus superficialis; 15. Ear; 16. Musculus obliquus capitis magnus; 17. Musculus spinalis; 18. Dentary bone; 19. Trachea; 20. Hyobranchial skeleton; 21. Septomaxilla; 22. Scleral ossicles; 23. Palatine bone; 24. Pila metoptica; 25. Parietal bone; 26. Epipterygoid bone; 27. Occipital bone; 28. Quadrate bone; 29. Rostrum parasphenoid; 30. Articular bone; 31. Angular + Surangular bone; 32. Pterygoid bone; 33. Coronoid bone; 34. Vomer bone.

Iguanidae and *Agamidae* is in the nature of tooth implantation – acrodontal rather than pleurodontal – although most agamids have at least some pleurodont teeth in the front lower jaw[15].

Standard positioning is a prerequisite for good film quality[29]. As in snakes, the junctions between the bones composing the lower jaw are relatively loose[13]. Therefore, radiographic positioning quality should be evaluated, in our opinion, primarily through the symmetry and superimposing of the bilateral structures of the snout and neurocranium both in lateral and sagittal projections.

All the radiographs and CT images shown in the figures were obtained from live animals. It is the authors' opinion that, although a direct comparison between anatomical and diagnostic images was not possible, a significant correlation in the matched images was achieved.

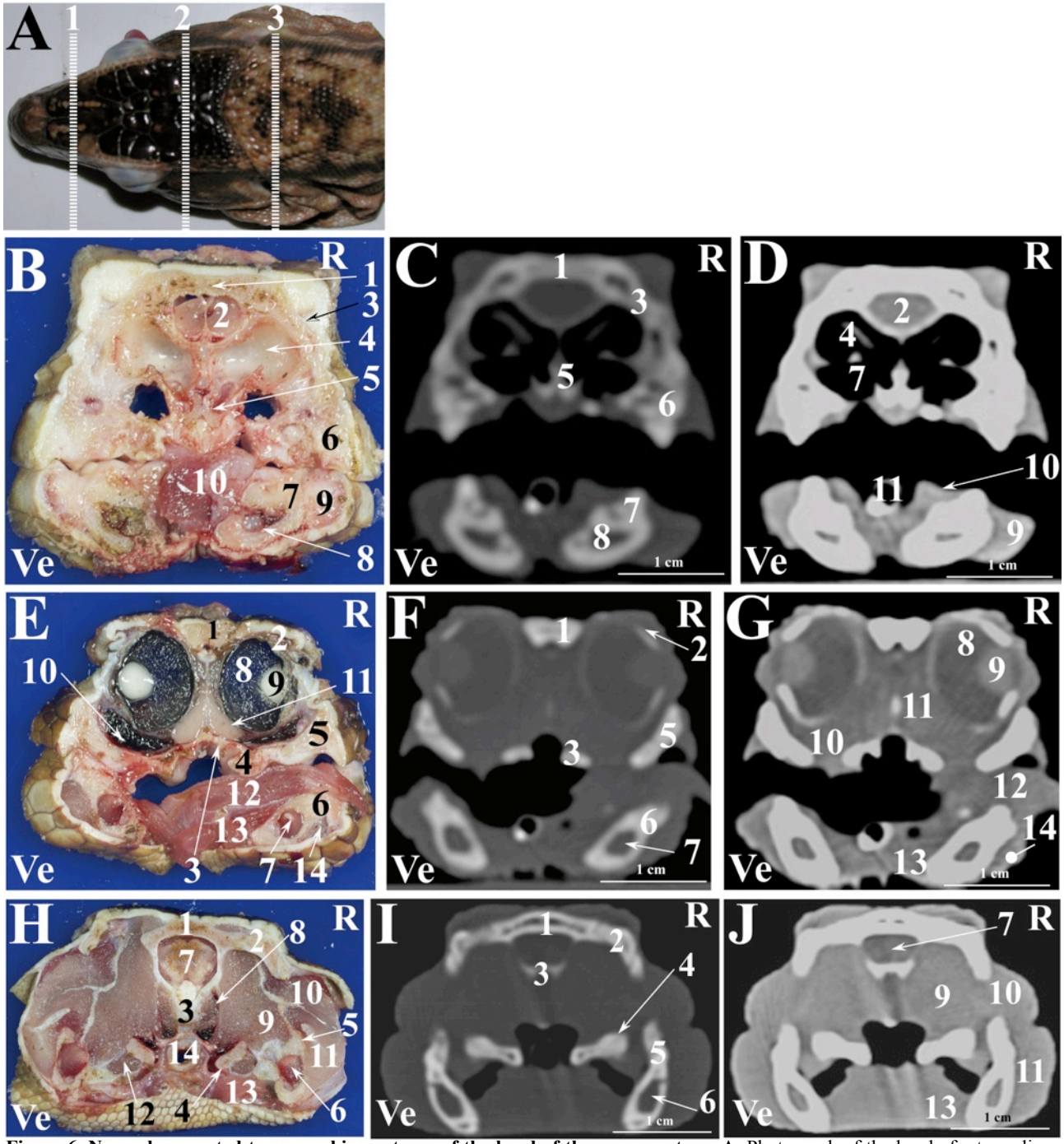

Figure 6. **Normal computed tomographic anatomy of the head of the common tegu.** A. Photograph of the head of a tegu; lines (1-3) indicate the approximate levels of matched cross-sections and CT images. B-J: Matched images of cross-sectional gross anatomy (B-E-H), CT image displayed in bone window (WW: +2000; WL: +500)(C-F-I) and CT image displayed in soft tissue window (WW: +400; WL: +40) (D-G-J) corresponding to: line 1 (B-C-D), line 2 (E-F-G) and line 3 (H-I-J) as depicted in Figure 6A. R is right and Ve is ventral. **B-C-D:** 1. Nasal bone; 2. Nasal glands 3. Prefrontal bone; 4. Nasal conchae; 5. Septomaxilla; 6. Maxillary bone; 7. Dentary bone; 8. Meckelian canal 9. Infralabial glands; 10. Tongue; 11. Trachea. **E-F-G:** 1. Frontal bone; 2. Scleral ossicles; 3. Palatine bone; 4. Palatine gland; 5. Maxillary bone; 6. Dentary bone; 7. Meckelian canal; 8. Eye; 9. Lens; 10. Sinus orbitalis; 11. Harderian gland; 12. Tongue; 13. Musculus intermandibularis + Musculus geniohyoideus + Musculus genioglossus + Musculus hyoglossus; 14. Infralabial glands**. H-I-J**: 1. Parietal bone; 2. Squamosal bone; 3. Sphenoid bone; 4. Pterygoid bone; 5. Angular bone + Surangular bone; 6. Adductor fossa; 7. Brain; 8. Musculus longus colli; 9. Musculus adductor mandibulae externus profundus; 10. Musculus abductor mandibularis externus medialis; 11. Musculus intermandibularis posterior; 12. Musculus pterygoideus typicus + Musculus pterygoideus atypicus; 13. Musculus intermandibularis + Musculus geniohyoideus + Musculus pterygoideus typicus + Musculus hyoglossus; 14. Trachea.

Moreover, the use of contrast medium enabled good visualisation of the soft tissues and overcame the lack of soft tissue detail encountered in other similar works performed only on cadavers[8].

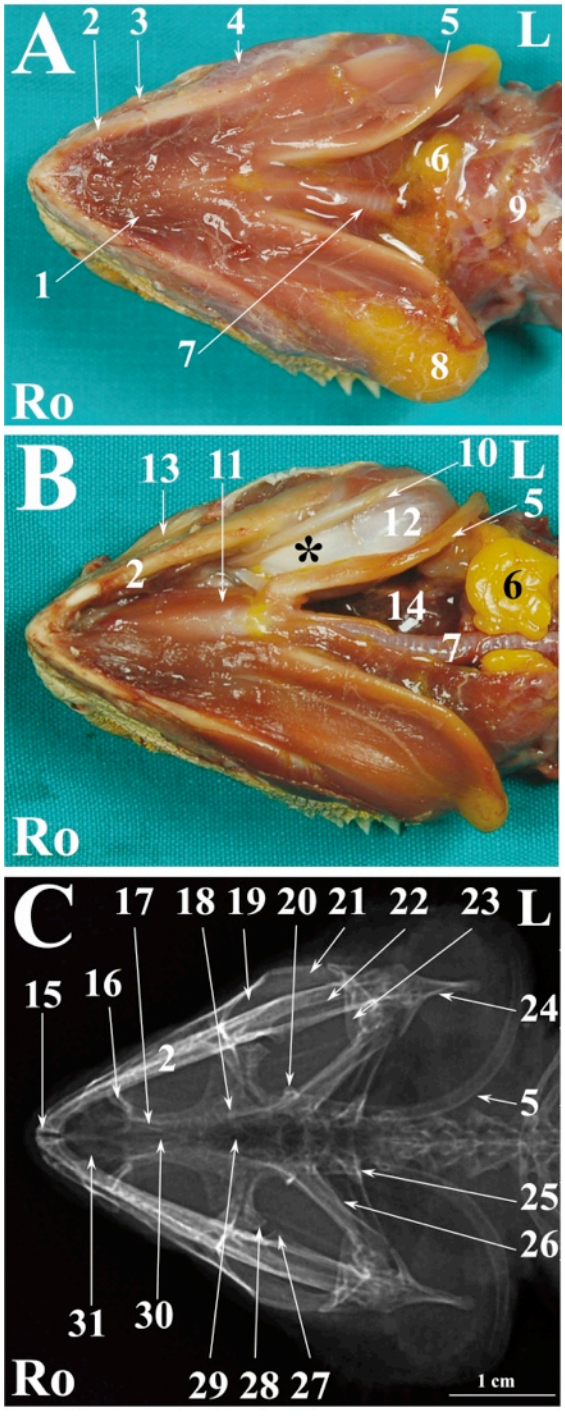

Figure 7. Normal radiographic anatomy of the head of the bearded dragon in VD projection. A. Ventral view in a superficial plane of stratigraphic dissection (only skin was removed) of the head of a bearded dragon. B. Ventral view of stratigraphic dissection after removal of Musculus constrictor colli and Musculus intermandibularis (lower part of the image) and a deeper plane of dissection (upper part of the image) of the head of a bearded dragon (deeper plane of dissection is labelled with * on the image). C. VD radiographic projection of the head of a bearded dragon. Ro is rostral, L is left.1. Musculus intermandibularis; 2. Dentary bone; 3. Supralabial gland; 4. Musculus adductor mandibulae externus supeficialis; 5. Ceratobranchial 1 process of hyobranchial skeleton; 6. Fat body; 7. Trachea; 8. Fat body; 9. Musculus constrictor colli; 10. Ceratohyal 2 process of hyobranchial skeleton; 11. Basihyal bone; 12. Musculus pterygoideus typicus; 13. Maxillary bone; 14. Oesophagus; 15. Premaxillary bone; 16. Prefrontal bone; 17. Palatine bone; 18. Frontal bone; 19. Jugal bone; 20. Epipterygoid bone; 21; Squamosal bone; 22. Angular bone + Surangular bone; 23. Quadrate bone; 24. Articular bone; 25. Paraoccipital process of otooccipital bone; 26. Pterygoid bone; 27. Coronoid bone; 28. Ectopterygoid bone; 30. Interpterygoid vacuiti; 31. Vomer bone.

The CT images of the iguana (Figure 3) provided good detail when displayed both in bone and soft tissue windows. The CT images of the tegu (Figure 6) displayed in a bone window provided good detail of the bony structures whereas in the images displayed in a soft tissue window only the eyes were clearly distinguishable from the remaining soft tissues. The CT images of the bearded dragon (Figure 9) were of a relatively lower quality in both the bone and soft tissue windows. This lack of detail is due to the small size of this species and to the impossibility to reduce the field of view of our CT scanner to less than 16 cm. Despite this lack of detail, most of the bony structures were identified in CT images displayed in the bone window. In the CT images displayed in the soft tissue window, only the eyes and the Harderian glands were distinguishable from the other soft tissues of the head.

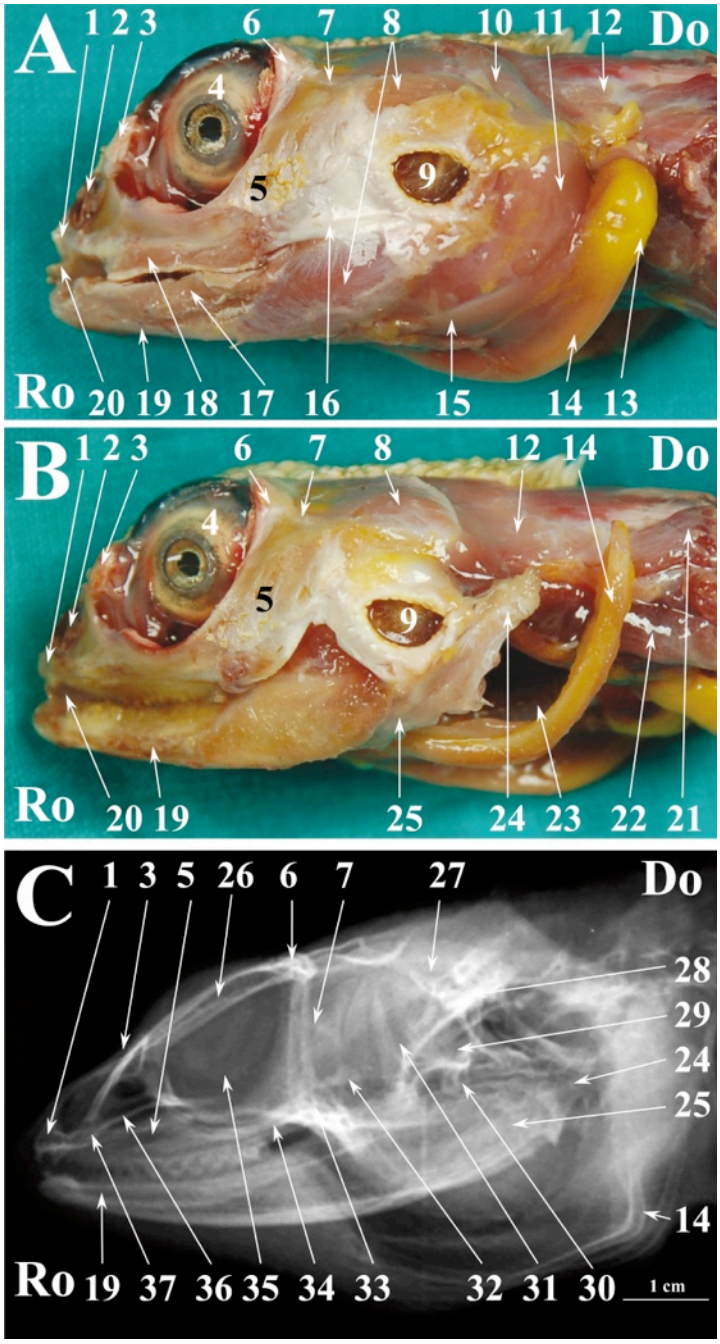

Figure 8. Normal radiographic anatomy of the head of the bearded dragon in LL projection. A. LL photographic image in a superficial plane of the stratigraphic dissection of the head of a bearded dragon (only skin was removed). B. LL photographic image in a deep plane of the stratigraphic dissection of the head of a bearded dragon. C. LL radiographic projection of the head of a bearded dragon. Ro is rostral, Do is dorsal. 1. Premaxillary bone; 2. Nostril; 3. Prefrontal bone; 4. Eye; 5. Maxillary bone; 6. Postorbital bone; 7. Jugal bone; 8. Musculus adductor mandibulae externus superficialis; 9. Ear; 10. Musculus adductor mandibulae externus medialis; 11. Musculus pterygoideus typicus; 12. Musculus depressor mandibulae; 13. Fat body; 14. Ceratobranchial process of hyobranchial skeleton; 15. Musculus sphincter colli; 16. Quadrato maxillary ligament; 17. Infralabial glands; 18. Supralabial gland; 19. Dentary bone; 20. Tongue; 21. Musculus trapezius + Musculus clavicle dorsalis; 22. Musculus episternocleidomastoid; 23. Trachea; 24. Articular bone; 25. Angular bone + Surangular bone; 26. Frontal bone; 27. Parietal bone; 28. Squamosal bone; 29. Paraoccipital process of otooccipital bone; 30. Quadrate bone; 31. Epipterygoid bone; 32. Coronoid bone; 33. Ectopterygoid bone; 34. Pterygoid bone; 35. Scleral ossicles; 36. Palatine bone; 37. Vomer bone.

The nasal cavity of all three species was clearly visible both in VD (Figures 1C, 4C, 7C) and LL (Figures 2C, 5C, 8C) radiographs. The septomaxilla and the nasal glands were very prominent in the LL radiographic projection of the iguana (Figure 2C), giving the nasal cavities an overall higher radiopacity than in the tegu (Figure 5C) and the bearded dragon (Figure 8C). The nasal cavity of the iguana appeared almost entirely occupied by the nasal glands both in cross-sections and CT scans (Figures 6B,C,D). The nasal glands in the bearded dragon (Figures 9B,C,D) were similar in appearance but less prominent in the nasal cavity. The nasal glands in the tegu were more medially located and less evident both in cross-sections and in CT images (Figures 6B,C,D).

The scleral ossicles were clearly visible both in the iguana (Figure

2C) and the tegu (Figure 5C) in LL radiographic projections, whereas they appeared less evident in the LL radiographic projection involving the bearded dragon (Figure 8C). Furthermore, the scleral ossicles were evident in CT images of all the examined species (Figures 3F,G, 6F,G, 9F,G) but were hardly visible in anatomic cross-sections (Figures 3E, 6E, 9E).

The bones composing the lower jaw were not individually evident either in LL or VD radiographic projections in any of the examined species because the sutures between the bones of the lower jaw are smaller than the minimum radiologic resolution.

The oesophagus was well defined in LL radiographs of all the examined species (Figures 2C, 5C, 8C). It appeared as a U-shaped radiolucency bordering the caudal aspect of the lower jaw in the iguana (Figure 2C) and bearded dragon (Figure 8C) whereas it appeared straighter in the tegu (Figure 5C). Furthermore, the dorsal portion of the oesophagus is partially superimposed on the highly developed masticatory muscles in the iguana and bearded dragon (Figures 2A and 8A, respectively) and is grossly much larger, as can be seen in the radiographs.

The trachea was clearly identified in the LL radiographic projection partially superimposed on the ventral aspect of the oesophagus in the iguana (Figure 2C) and tegu (Figure 5C), while it was difficult to identify in the bearded dragon (Figure 8C). In the iguana (Figure 2C) the trachea showed a peculiar outline turning two ninety-degree angles at the inlet of the coelomic cavity. All the animals were deeply sedated during the imaging procedures; the authors are unable to determine whether this latter feature is due to muscular relaxation induced by anaesthesia or is normal even in unsedated iguanas.

The eyes were very evident in all the species examined, both in cross-sections and CT images displayed in a soft tissue window (Figures 3E,G, 6E,G, 9E,G). The lens and the vitreous were clearly delineated both in cross-sections and CT images in the iguana (Figures 3E,G) and tegu (Figures 6E,G). The lens and the vitreous were not individually identified either in cross-sections or CT images in the bearded dragon (Figures 9E,G). In the iguana the Harderian glands were hardly

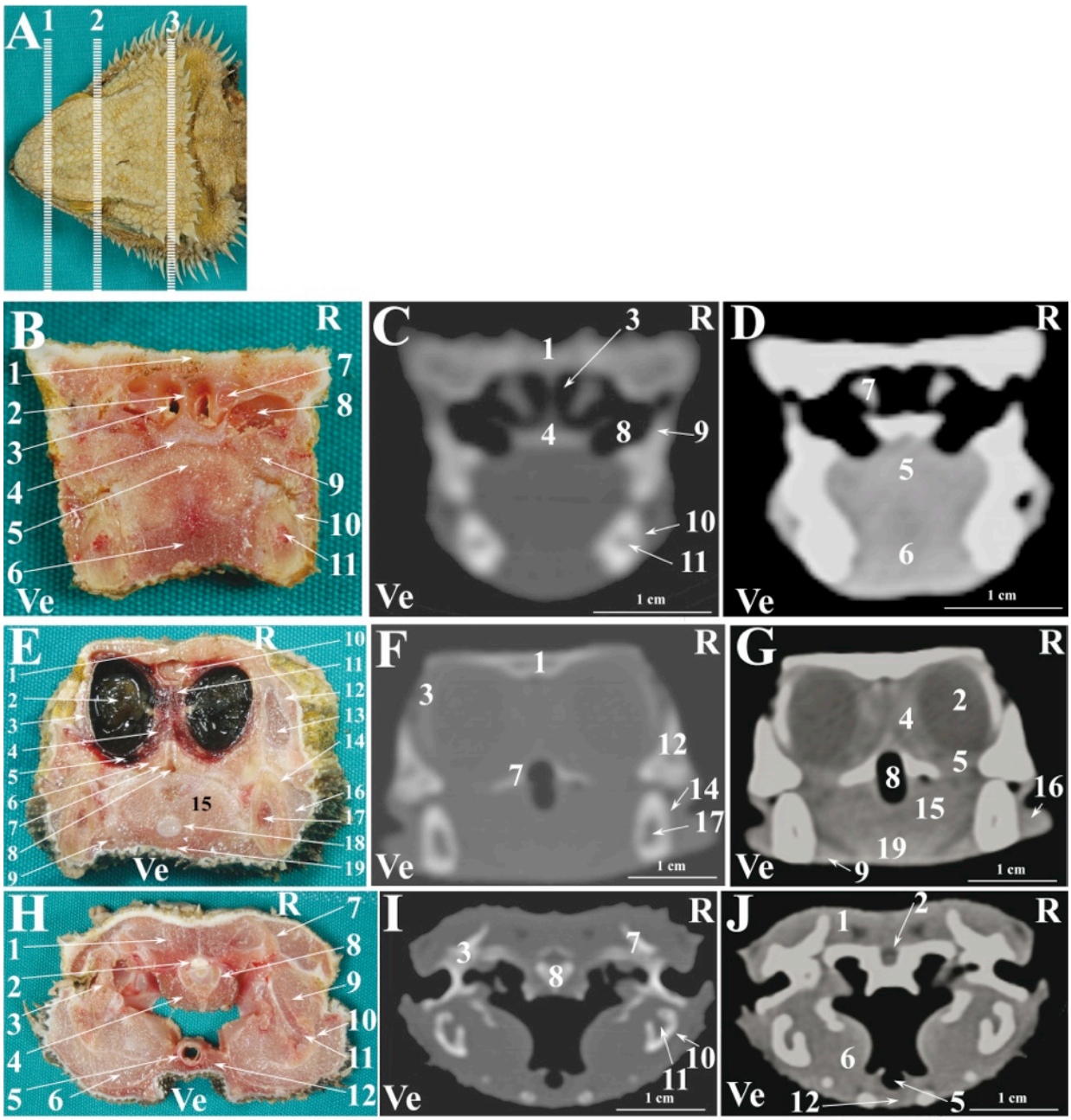

Figure 9. Normal computed tomographic anatomy of the head of the bearded dragon. A. Photograph of the head of a bearded dragon; lines (1-3) indicate the approximate levels of matched cross-sections and CT images. B-J: Matched images of cross-sectional gross anatomy (B-E-H), CT image displayed in bone window (WW: +2000; WL: +500)(C-F-I) and CT image displayed in soft tissue window (WW: +400; WL: +40) (D-G-J) corresponding to: line 1 (B-C-D), line 2 (E-F-G) and line 3 (H-I-J) as depicted in Figure 9A. R is right and Ve is ventral. **B-C-D:** 1. Nasal bone; 2. Nasal septum; 3. Choanae; 4. Vomer bone; 5. Tongue; 6. Musculus intermandibularis + Musculus geniohyoideus + Musculus genioglossus; 7. Nasal glands; 8. Choanal tube; 9. Maxillary bone; 10. Dentary bone; 11. Meckelian canal. **E-F-G:** 1. Frontal bone; 2. Eye; 3. Scleral ossicles; 4. Harderian gland; 5. Sinus orbitalis; 6. Palatine gland; 7. Pterygoid bone; 8. Cavum oris; 9. Sublingual gland; 10. Brain; 11. Choroid plexus; 12; Postorbital bone + Jugal bone; 13. Musculus adductor mandibulae externus superficialis; 14. Dentary bone; 15. Tongue; 16. Infralabial glands; 17. Meckelian canal; 18. Entoglossal process of the hyobranchial skeleton; 19. Musculus intermandibularis + Musculus geniohyoideus + Musculus hyoglossus + Musculus pterygoideus typicus. **H-I-J:** 1. Musculus adductor mandibulae externus medialis; 2. Brain; 3. Quadrate bone; 4. Musculus longus colli; 5. Trachea; 6. Musculus pterygoideus typicus; 7. Postparietal process of otooccipital bone; 8. Orbitosphenoid bone; 9. Musculus adductor mandibularis externus superficialis; 10. Angular bone + Surangular bone; 11. Adductor fossa; 12. Musculus intermandibularis + Musculus geniohyoideus + Musculus ceratohyoideus + Musculus hyoglossus.

visible in cross-sections (Figure 3E) while they were very prominent and clearly distinguishable from the underlying *sinus orbitalis* in CT images (Figure 3G). A radiodense line was noticed on the ventral aspect of the *sinus orbitalis* in post-contrast CT images of the iguana displayed in a soft

tissue window (Figure 3G). In the tegu the Harderian glands were clearly evident in cross-sections (Figure 6H) but were difficult to identify in the CT images (Figure 6L). In the bearded dragon the Harderian glands could be identified both in cross-sections (Figure 9E) and CT images (Figure 9G) but were less evident than in the iguana.

Different pathologies can affect the head of lizards; abscesses, metabolic bone diseases, fractures, osteomyelitis, and neoplasia [30-34]. Many causes can be found for abscesses in the head of reptiles; bites from preys, traumas, infections with pyogenic organism, foreign bodies. Immunocompromised animals, as most captive kept reptiles are, seem to be more prone to develop abscess[31]. Since the key to successful treatment of the reptilian abscess is complete removal of the abscess cavity and surrounding fibrous capsule[31], for a good pre-surgical evaluation both radiographic and CT studies could be helpful to determine the extension and the number of involved structures. Moreover, abscesses may not be apparent externally; in these cases, in order to archive a correct diagnose, CT studies may be mandatory.

Metabolic bone diseases may result from different underlying pathologies[32]. Different techniques have been proposed to diagnose and to evaluate the efficiency of treatment of metabolic bone diseases[2,3,14]. Dual energy x-ray absorptiometry is actually considered the technique of choice to evaluate bone mineral density[35]. Nevertheless, it is authors' opinion that, the high correlation obtained between the mean grey values measured on computed radiology and the bone mineral density measured by dual energy x-ray absorptiometry[36] suggest computed radiology as a valid alternative to other more expensive (CT) or less available techniques (dual energy x-ray absorptiometry) both in the diagnosis and in the evaluation of the efficiency of treatment of metabolic bone diseases in lizards.

Fractures are not uncommon in reptiles and can be both of traumatic or pathological (mostly from metabolic bone diseases) origin[34]. Skull fractures may be difficult to assess on plain radiographs due to both the relatively small size of the individual bone composing the skull and the high number

of superimpositions typical of this technique. Therefor, it is authors' opinion that, CT may be useful to correctly assess skull fractures in lizards and more in general in reptiles.

The mandibula and the maxilla are most common sites of osteomyelitis in the head[30]. Changes in the bony structure include osteolysis and less frequently new bone formation[30]. Plain radiographs may be sufficient for the detection of this pathology[30]; nevertheless, in our opinion, CT scans may provide additional informations about the extension of the infectious process and may aid planning a correct therapy.

Neoplasia is believed to be a common disease in reptiles[33]. Since lizard patients often require sedation for diagnostic imaging procedures[30], it is author's opinion that, CT may be the imaging technique of choice if neoplasia of the head is suspected. The mayor advantages of CT are: the possibility to visualize entirely the extension of the neoplastic process and the possibility to perform CT guided biopsies[37]. It is authors' opinion that, in lizards, the advantages of CT guided biopsies may be limited by the relatively small size of the head of most lizards and it may be difficult to perform the biopsy without damaging adjacent structures. Expensive stereotactic CT biopsy devices may be necessary to safely perform this procedure.

The skull of reptiles develops from a post-hatching cranium, the chondrocranium, to its definitive form in adults, the osteocranium[15]. Often the bones composing the chondrocranium have not reached full adult form[15]. All the tables presented in this work refer to adult animals and care should be taken when using these tables to interpret radiographs or CT studies of immature animals.

References

1. Knipe FM: Principles of Neurological Imaging of Exotic Animal Species. *Vet Clin North Am Exot Anim Pract* 2007; 10:893–907.
2. Pees M: Reptiles. In *Diagnostic Imaging of Exotic Pets.* Edited by Krautwald-Junghanns ME, Pees M, Reese S, Tully T. Hannover, Germany: Schlütersche Verlagsgesellschaft mbH & Co; 2011: 310-459.
3. Mader DR: *Reptile Medicine and Surgery.* 2nd edition. Philadelphia, USA: W.B. Saunders Co; 2006.
4. McFadden MS, Bennet RA, Kinsel MJ, Mitchell MA: Evaluation of the histologic reactions to commonly used suture materials in the skin and musculature of ball pythons (*Python regius*). *Am J Vet Res* 2011; 72:1397-1406.
5. Alworth LC, Hernandez SM, Divers SJ: Laboratory Reptile Surgery. Principles and Techniques. *J Am Assoc Lab Anim Sci* 2011;50:11–26.
6. Stahl SJ, Hernandez-Divers SJ, Cooper TL, Blas-Machado U: Evaluation of transcutaneous pulmonoscopy for examination and biopsy of the lungs of ball pythons and determination of preferred biopsy specimen handling and fixation procedures. *J Am Vet Med Assoc* 2008; 233:440-445.
7. Mc Fadden MS, Bennet RA, Reavill DR, Raegetly GR, Clark-Price SC: Clinical and histologic effects of intracardiac administration of propofol for induction of anesthesia in ball pythons (*Python regius*). *Am J Vet Res* 2011;239:803-807.
8. Olesen MG, Bertelsen MF, Perry SF, Wang T: Effects of preoperative administration of butorphanol or meloxicam on physiologic responses to surgery in ball pythons. *Am J Vet Res* 2008;233:1883-1888.
9. Holland MF, Hernandez-Divers S, Frank PM: Ultrasonographic appearance of the coelomic cavity in healthy green iguanas. *J Am Vet Med Assoc* 2008; 233:590-596.
10. Hollingsworth SR, Holmberg BJ, Strunk A. Comparison of ophthalmic measurements obtained via high-frequency ultrasound imaging in four species of snakes. *Am J Vet Res* 2007; 68:1111-1114.
11. Pees M, Kiefer I, Oechtering G, Krautwald-Junghanns ME: Computed tomography for the diagnosis and treatment monitoring of bacterial pneumonia in Indian pythons (*Python molurus*). *Vet Rec* 2008;163:152-156.
12. Pees MC, Kiefer I, Thielebein J, Oechtering G, Krautwald-Junghanns ME: Computed Tomography of the lung of healthy snakes of the species *Python regius, Boa constrictor, Python reticulatus, Morelia viridis, Epicrates cenchria* and *Morelia spilota*. *Vet Radiol Ultrasound* 2009;50:487–491.
13. Banzato T, Russo E, Di Toma A, Palmisano G, Zotti A: Anatomic imaging of the *Boa constrictor* head: a comparison between Radiography, Computed Tomography and Cadaver Anatomy. *Am J Vet Res* 2011;72:1592-1599.
14. Zotti A, Selleri P, Carnier P, Morgante M, Bernardini D: Relationship between metabolic bone disease and bone

mineral density measured by dual-energy X-ray absorptiometry in the green iguana *(Iguana iguana)*. *Vet Radiol Ultrasound* 2004; 45:10-16.

15. George TF II, Smallwood JE: Anatomic atlas for computed tomography in the mesaticephalic dog: head and neck. *Vet Radiol Ultrasound* 1992;33:217–240.
16. Zotti A, Banzato T, Cozzi B: Cross-sectional anatomy of the rabbit neck and trunk: Comparison of computed tomography and cadaver anatomy. *Res Vet Sci* 2009;87:171–176.
17. Gingel F: Animal Diversity Web.
18. [http://animaldiversity.ummz.umich.edu/site/accounts/information/Iguana_iguana.html]
19. Periat J: Animal Diversity Web. [http://animaldiversity.ummz.umich.edu/site/accounts/information/Pogona_vitticeps.html]
20. Evans SE: The Skull of Lizards and Tuatara. In *Biology of the Reptilia*. Volume 20. Edited by Gans C, Gaunt A. Ithaca, New York: Society for the study of Amphibians and Reptiles; 2008:1-275.
21. Edgeworth FH: The Cranial Muscles of Vertebrates. Cambridge: Cambridge University Press; 1935.
22. Kochva E: Oral Glands of the Reptilia. In *Biology of the Reptilia*. Volume 8. Edited by Gans C, Kyoko A. London and New York: Academic Press, 1970;43-100
23. Underwood G: The Eye. In *Biology of the Reptilia*. Volume 2. Edited by Gans C, Thomas S. London and New York: Academic Press; 1970:48-70.
23. Parsons S: The Nose and Jacobson's organ. In *Biology of the Reptilia*. Volume 2. Edited by
24. Gans C, Parsons TS. New York: Academic Press; 1970: 99-19.
25. Edmund AG: Dentition. In *Biology of the Reptilia*. Volume 1. Edited by Gans C, Bellairs A, Parson TS. New York: Academic Press; 1969:117-200.
26. Haas G: Muscles of the jaws and associated structures in the Rhynchocephalia and Squamata. In *Biology of the Reptilia.* Volume 4. Edited by Gans C, Parsons TS. New York and London: Academic Press; 1973: 285-490
27. Oelrich TM. 1956. The anatomy of the head of Ctenosaura pectinata (Iguanidae).
28. *Misc Publ Mus Zool Univ Mich* 94: 1-122.
29. Digital Morphology: A National Science Foundation Digital Library at the University of Texas at Austin
30. [http://www.digimorph.org/listbygroup.phtml?grp=lizard&sort=SpeciesName].
31. Jones MEH, Curtis N, O'Higgins P, Fagan, M, Evans SE. The Head and Neck Muscles Associated with Feeding in *Sphenodon* (Reptilia: Lepidosauria: Rhynchocephalia). *Palaeontologia Electronica* 2009;12:1-56.
29. Kealy JK, McAllister H, Graham JP. The Radiograph. In *Diagnostic radiology and Ultrasonography of the Dog and*
30. *Cat.* 5th edition. Edited by Kealy JK, McAllister H. Philadelphia, USA: Elseviers Saunders; 2005:1-22.
30. Silverman S: Diagnostic imaging. In *Reptile Medicine and Surgery.* 2nd edition. Edited by Mader DR.

Philadelphia,

31. USA: W.B. Saunders Co; 2006: 471-489.
31. Mader DR: Abscess. In *Reptile Medicine and Surgery.* 2nd edition. Edited by Mader DR. Philadelphia, USA: W.B.
32. Saunders Co; 2006: 715-719.
32. Mader DR: Metabolic Bone Diseases. In *Reptile Medicine and Surgery.* 2nd edition. Edited by Mader DR.
33. Philadelphia, USA: W.B. Saunders Co; 2006: 841-851.
33. Hernadez-Divers SM, Garner MM. Neoplasia of reptiles with an emphasis on lizards. *Vet Clin Exot An* 2003;6:
34. 251-273.
34. Mader DR, Bennet RA, Funk RS, Fitzgerald KT, Vera R, Hernandez-Divers SJ: Surgery. In *Reptile Medicine and*
35. *Surgery.* 2nd edition. Edited by Mader DR. Philadelphia, USA: W.B. Saunders Co; 2006: 581-629.
36. Liewiecky EM, Watts NB, McClung MR, Petak SM, Bachrach LK, Shepherd JA, Downs RW Jr. Official positions of the international society for clinical densitometry. *J Clin Endocrinol Metab* 2004, 89:3651–3655.
37. Vaccaro C, Busetto R, Bernardini D, Anselmi C, Zotti A. Accuracy and precision of computer-assisted analysis of bone density via conventional and digital radiography in relation to dual-energy x-ray absorptiometry. *Am J Vet Res* 2012;73:381-384.
38. Schwarz T, Puchalsky S: Inteventional CT. In *Veterinary Computed Tomography.* Edited by Saunders J,Stark T. Ames: John Wiley & Sons; 2011: 81-87.

DIAGNOSTIC IMAGING OF THE COELOMIC CAVITY

CHAPTER V

NORMAL COMPUTED TOMOGRAPHY OF THE COELOMIC CAVITY OF LIZARDS

This chapter was adapted from: Banzato T, Selleri P, Veladiano IA, Zotti A. Comparative evaluation of the cadaveric and computed tomographic features of the coelomic cavity in the green iguana (*Iguana iguana*), black and white tegu (*Tupinambis merianae*) and bearded dragon (*Pogona vitticeps*). *Anatomia Histologia Embryologia. Corrected proofs, in press* (doi: 10.1111/ahe.12037).

Abstract

Contrast enhanced computed tomographic studies of the coelomic cavity in 4 green iguanas, 4 black and white tegu and 4 bearded dragons were performed using a conventional CT scanner. Anatomical reference cross-sections were obtained from 4 green iguana, 4 black and white tegu and 6 bearded dragon cadavers; the specimens were stored in a – 20° C freezer for 24 hours then sliced at 5-mm intervals. The frozen sections were cleaned with water and photographed on both sides. The individual anatomical structures were identified by means of the available literature; these were labelled first on the anatomical images and then matched on the corresponding computed tomography images. The results provide an atlas of the normal cross-sectional and computed tomographic anatomy of the coelomic cavity in the green iguana, the black and white tegu and the bearded dragon, which is useful in the interpretation of any imaging modality.

Introduction

In the last decade numerous studies describing the normal features of the most commonly used diagnostic imaging techniques in different reptile species have enabled improvement of the diagnostic imaging standards in reptile medicine [1-8]. Some general information regarding the computed tomography technique and the features of the coelomic cavity in lizards is currently available [9-10]. However, to our knowledge, neither comprehensive descriptions nor a direct comparison with cross-sectional anatomy has yet been published.

Although no official data are reported, the large number of dedicated websites, exhibitions and professional and amateur breeders active in the market illustrates that keeping lizards as pets has become increasingly widespread. Moreover, lizards are almost always present in zoos and are often part of private animal collections [11].

Three species of lizards were object of this work: the green iguana (*Iguana iguana* - Linnaeus 1758), the black and white tegu (*Tupinambis merianae* – Duméril & Bibron 1839) and the bearded dragon (*Pogona vitticeps* – Ahl 1926), belonging to the Iguanidae, Teiidae and Agamidae families, respectively.

The anatomy of the coelomic cavity of lizards has already been described in literature[12-22]. However, as far as the authors are aware, a thorough description of the anatomy of the coelomic cavity in the species considered in this work is still not available. Moreover, to the authors' knowledge, no description of the cross-sectional anatomy of the coelomic organs of lizards is currently available.

The aim of this study is to relate the normal cross-sectional anatomy of the green iguana, the black and white tegu and the bearded dragon to the normal CT features of live animals.

Materials and Methods

Animals

4 green iguana (1 male and 3 females, mean length 76.4± 22.2 cm, mean weight 1852±855 g), 4 black and white tegus (2 males, 2 females, mean length 42.3± 19.1 cm, mean weight 953±455 g) and 6 bearded dragon (4 males, 2 females, mean length 22.5± 12.1 cm, mean weight 366±185 g) cadavers were obtained for this study. All animals were privately owned and were presented to the Department of Animal Medicine, Production and Health, Clinical Section, Radiology Unit at the University of Padua (Italy) or to the Clinic for Exotic Animals (Rome, Italy) for specialty examination and were euthanized due to advanced clinical conditions.

Additionally, 4 green iguanas (3 males and 1 female, mean length 96.2± 33.4 cm, mean weight 3085±1053 g), 4 black and white tegus (3 males and 1 female, mean length 66.3± 24.1 cm, mean weight 2024±403 g) and 4 bearded dragons (1 male and 3 females, mean length 26.2± 5.4 cm, mean weight 422±55g) referred to the above mentioned facilities were included in the imaging study. The animals included in the CT studies were all affected by pathologies involving the head, neck, limbs or tail region. The whole body CT studies were all performed upon owner consent; both dissection of the cadavers and the CT scans were performed within the period May-September.

CT studies

CT studies were performed by means of an axial, single slice, 3rd generation CT scanner (Tomoscan® LX, Philips Medical Systems, Amsterdam, Netherlands). Animals were sedated with sevofluorane (Sevofluorane 100%, Baxter Spa, Rome, Italy) administered through a nasal mask. The more aggressive animals were injected with a single bolus of propofol (Propofol 20 mg/ml, Fresenius Kabi Srl, Italy) directly into the caudal vein, at the dose of 3-5 mg/kg. Contrast medium (Optiray® 300mg/ml, Covidien Spa, Italy) was injected directly into the caudal vein, at the dose of

2.2 ml/kg. In order to reduce the procedure duration only post-contrast CT images were obtained. CT scans were performed in all considered species in a cranio-caudal (CC) direction with the animals positioned in ventral recumbency. Furthermore, to overcome the lack of detail deriving both from the small size of the specimens and the inability of our CT scanner to reduce the field of view below the limit of 16 cm, 2 bearded dragons were scanned in a latero-medial (LM) direction. CT images were acquired using a soft tissue algorithm. The following CT parameters have been used in all specimens: axial acquisition mode, rotation time 2,9 s, voltage of 120 kV, amperage of 125 Ma, field of view 16 cm; matrix 512x512 pixels. Slice thickness was adjusted according to the subject undergoing scanning, in order to maximise imaging quality. A slice thickness of 5 mm was used both in green iguanas and black and white tegu; in bearded dragons the slice thickness was set to 1.5 mm for the LM scans and to 3 mm for the CC scans. CT images were displayed in a soft tissue window (Window width: +400; Window level: +40) and in a lung window (Window width: +1500; Window level: -600).

Anatomical dissections

Prior to the beginning of both the cross-sectional and the CT procedures, 2 cadavers for each considered species were dissected to compensate for the lack of unambiguous anatomy references regarding the study species. Moreover, as a consequence of the absence of official nomenclature describing the various gastro-intestinal tract loops, individual loops were identified in the three species and named by adapting the nomenclature proposed by Smith et al. (2001) for the green iguana.

Two green iguana (2 females), 2 black and white tegu (1 male and 1 female) and 4 bearded dragon (3 males and 1 female) cadavers were designated for cross-sectional anatomical studies. The animals were placed on a plastic support immediately following death and stored in a freezer (-20° C) for 24 hours. Five-mm cross-sectional slices were obtained from the coelomic cavity of 2

cadavers of each species by means of an electric band-saw in order to match the CT imaging protocol. Additionally, 2 bearded dragon cadavers were sectioned along the longitudinal plane using the same slice thickness. Thereafter the slices were cleaned with cold water, numbered and photographed on both sides.

Individual anatomical structures were first identified and labelled on the cross-sections, on the basis of the available literature and the dissection results, and then matched to the corresponding structures on the CT scans.

Results

The results of the present study are depicted in Figures 1-12. The comparison between available literature and dissections enabled identification of most of the clinically relevant structures. The main differences noticed among the considered species regarded the gross anatomy of the gastro-intestinal tract. Schematic drawings of the gastro-intestinal tract in the common tegu and the bearded dragon are provided in Figure 1. Each intestinal loop was separately named, adapting the nomenclature proposed by Smith et al. (2001).

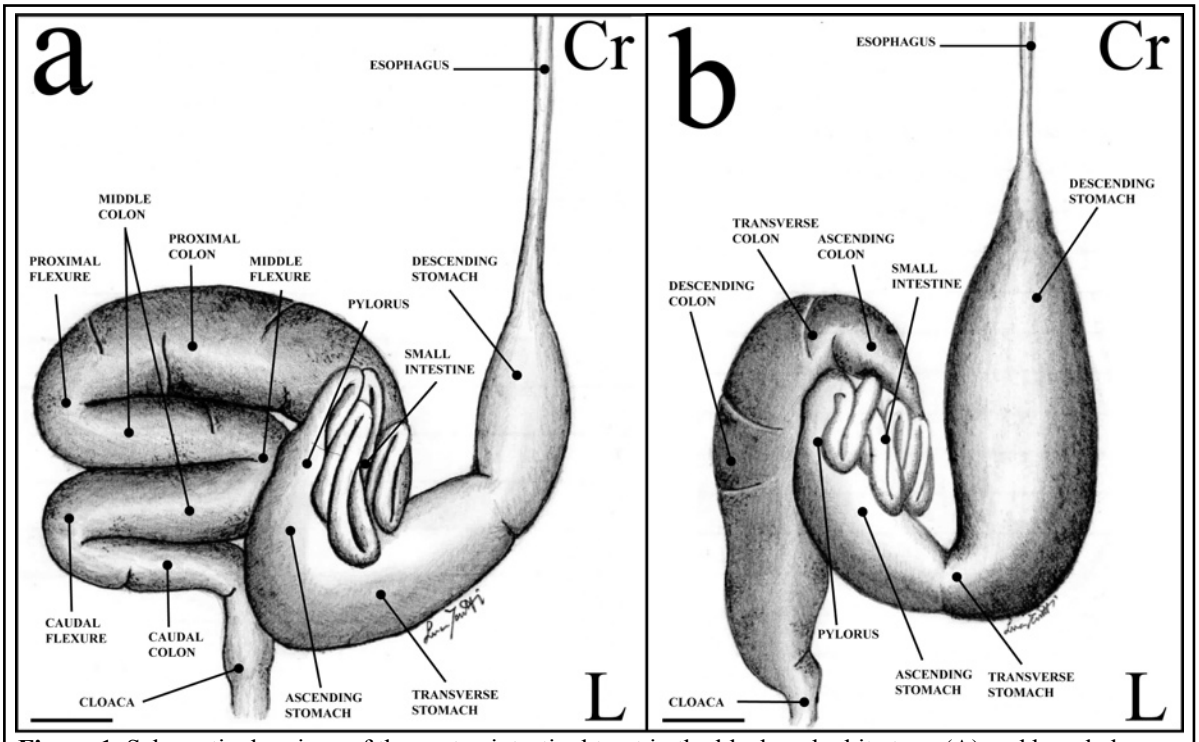

Figure 1. Schematic drawings of the gastro-intestinal tract in the black and white tegu (A) and bearded dragon (B). Ventral view. Cr is cranial; L is left.

The approximate level of the reported matching cross-sections and CT images is displayed in Figure 2. A selection of matched cross-sections and CT images is shown in Figures 3-12. The levels in the matched cross-sections and CT images displayed in Figures 3-12 are similar for all the considered species, in order to emphasise the comparative aspect of this work. A marked distension of the oesophagus, partially displacing the surrounding structures, was noticed in the cross-sections of the green iguana and black and white tegu (Figures 3-6). The use of contrast medium enabled a

good visualisation of the vascular structures for all considered species (Figures 3-12). A selection of matched longitudinal sections and longitudinal CT scans if the bearded dragon is shown in Figure 12.

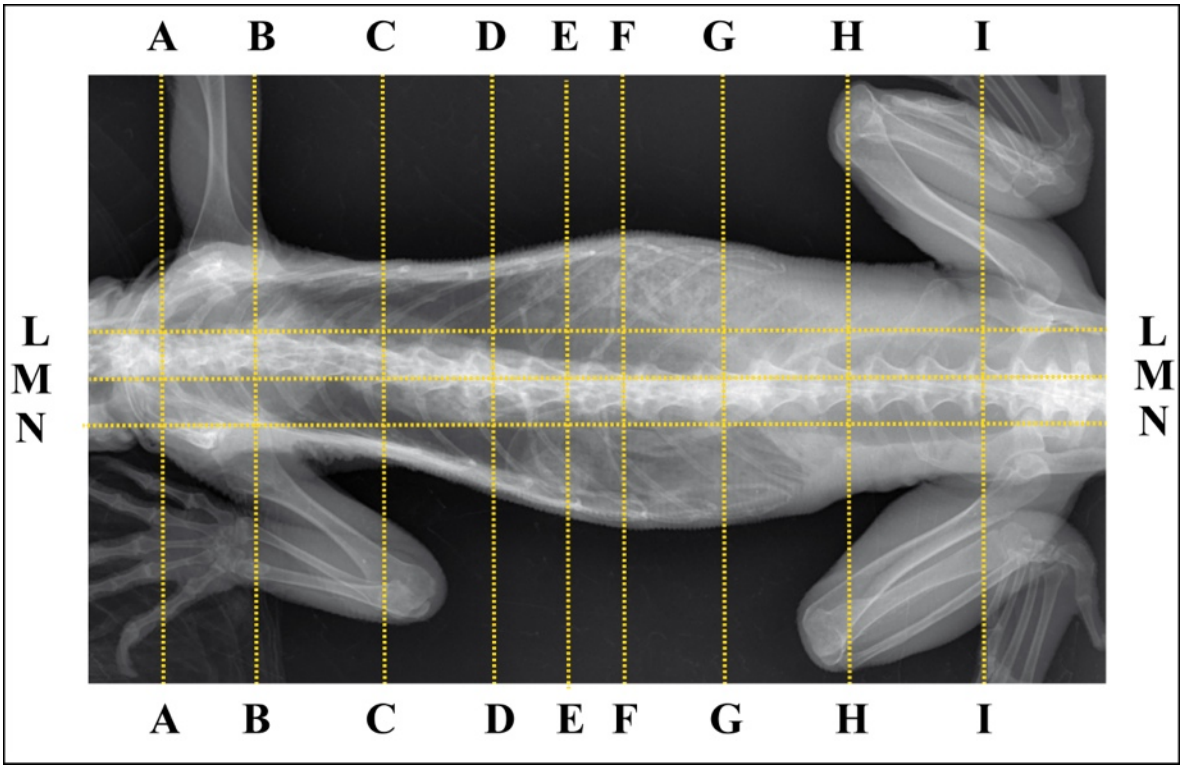

Figure 2. Radiographic dorso-ventral projection of a green iguana; lines A-N indicate the approximate level of the matched cross-sections and the CT images displayed in figures 3-12.

Discussion

The coelomic cavity of the black and white tegu is almost completely divided by what is known as the "post-hepatic septum" into a cranial cavity, containing the lungs and the liver, and a caudal

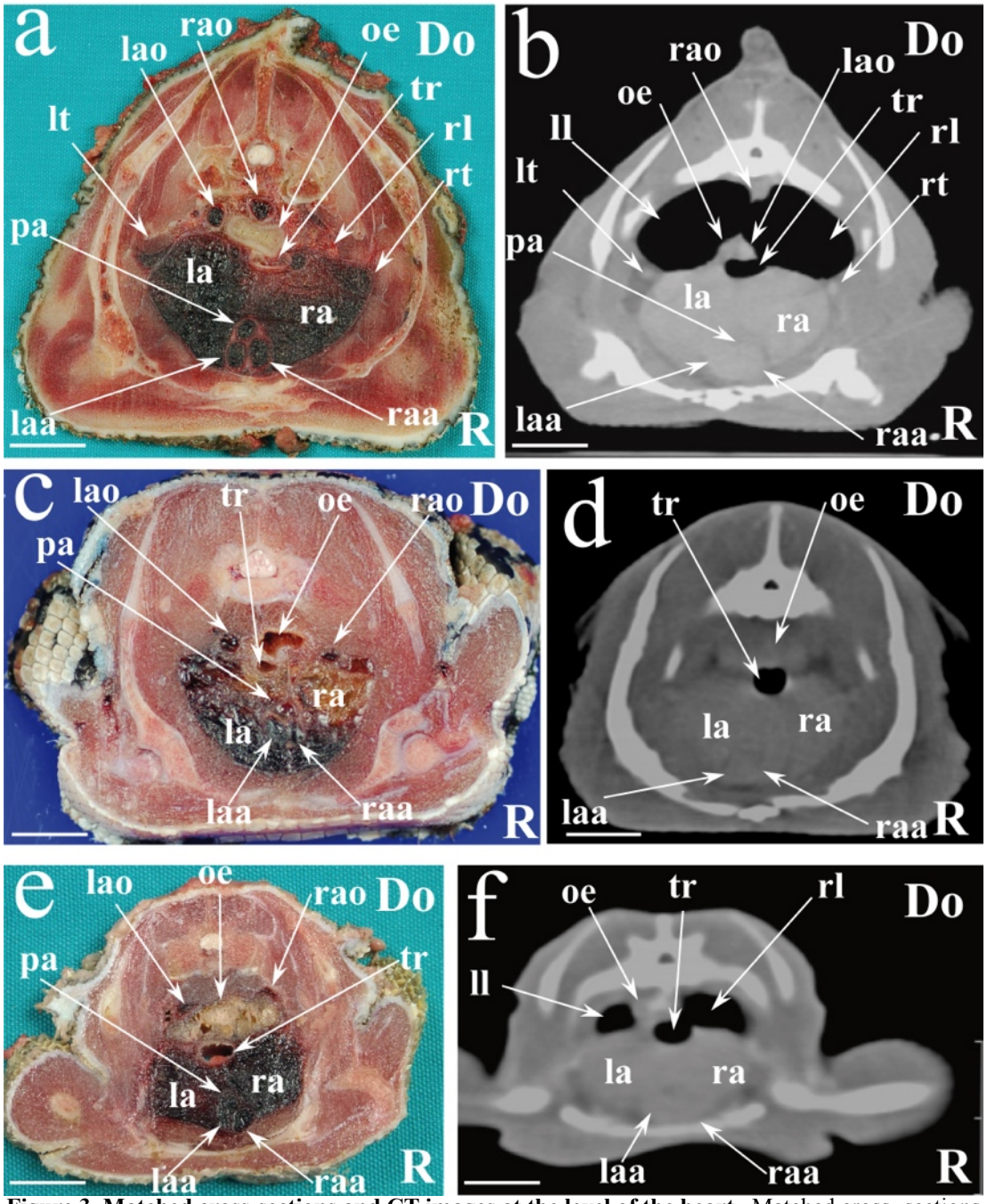

Figure 3. Matched cross-sections and CT images at the level of the heart. Matched cross- sections and CT images displayed in a soft tissue window in a green iguana (A-B), black and white tegu (C-D) and bearded dragon (E-F) at the level of the heart, corresponding to line A in Figure 2. Do is dorsal, R is right. Bar =1 cm. la, left atrium; laa, left aortic arch; lao, left aorta; ll, left lung; lt, left thyroid gland; oe, oesophagus; pa, pulmonary artery; ra, right atrium; raa, right aortic arch; rao, right aorta; rl, right lung; rt, right thyroid gland; tr, trachea.

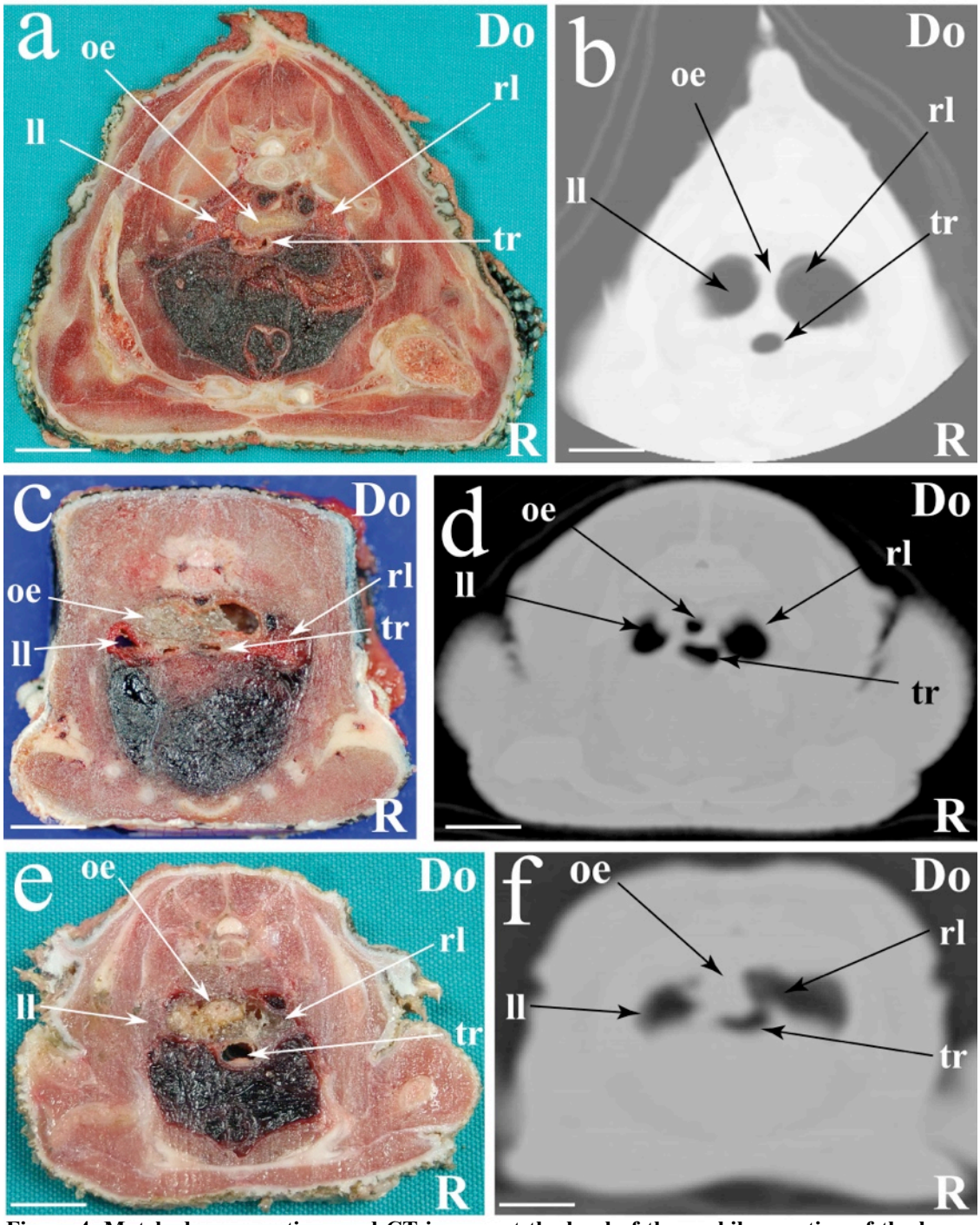

Figure 4. Matched cross-sections and CT images at the level of the prehilar portion of the lungs. Matched cross-sections and CT images, displayed in a lung window, in a green iguana (A-B), black and white tegu (C-D) and bearded dragon (E-F) at the level of the pre-hilar portion of the lungs, corresponding to line B in Figure 2. Do is dorsal, R is right. Bar =1 cm. ll left lung; oe, oesophagus; rl, right lung; tr, trachea.

cavity containing the remaining viscera. The coelomic cavity in the green iguana and bearded dragon presents an undivided pleuro-peritoneal cavity[23-24]. To the best of the authors' knowledge, no reports have become available to date regarding diseases involving the post-hepatic septum. Nevertheless, surgical removal of the post-hepatic septum for experimental purposes led to a displacement of the organs into the coelomic cavity [23]. Although the post-hepatic septum was not

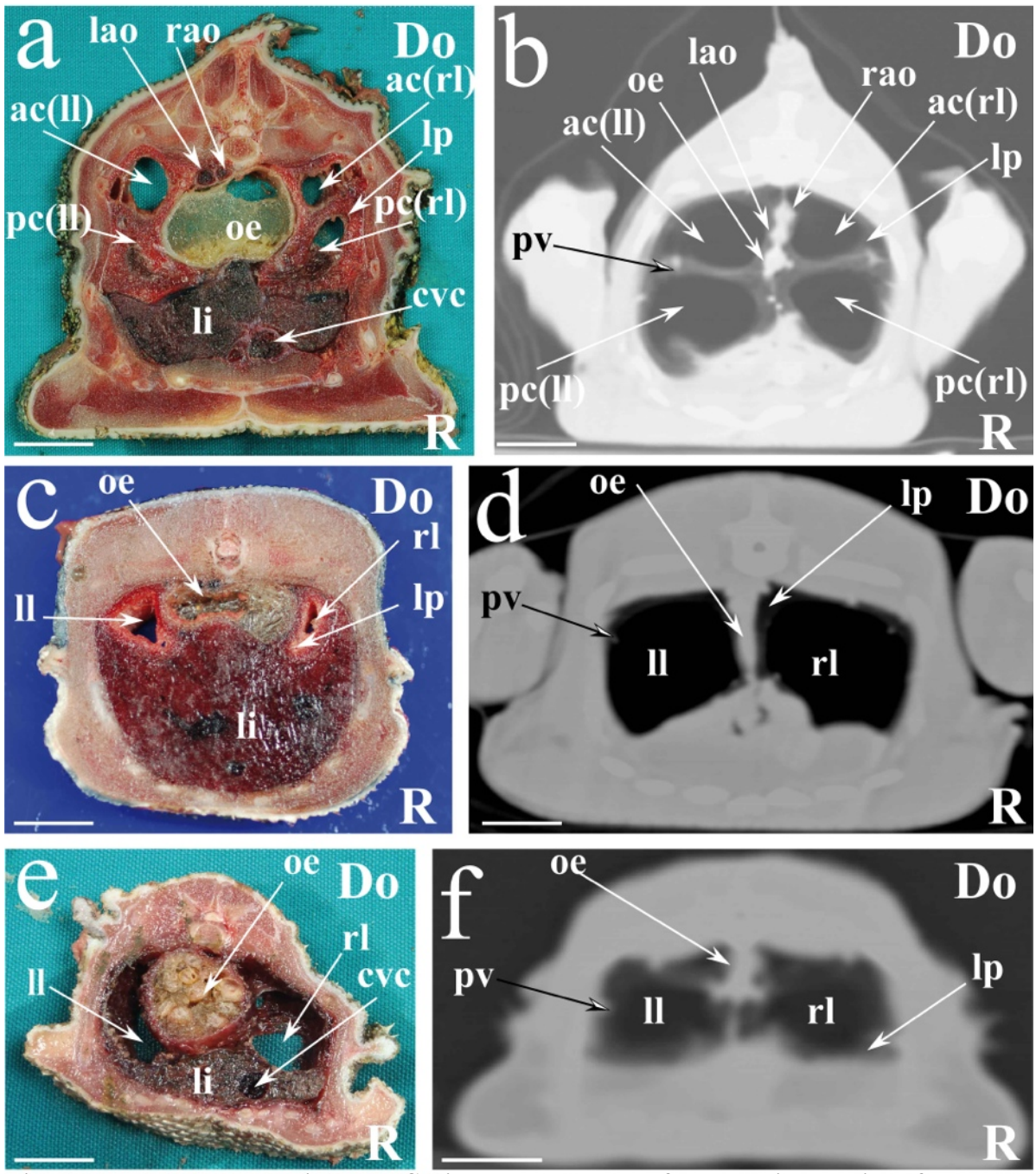

Figure 5. Matched cross-sections and CT images at the level of the posthilar portion of the lungs. Matched cross-sections and CT images displayed in a lung window in a green iguana (A-B), black and white tegu (C-D) and bearded dragon (E-F) at the level of the post-hilar portion of the lungs corresponding to line C in Figure 2. Do is dorsal, R is right. Bar =1 cm. ac(ll), anterior chamber of the left lung; ac(rl), anterior chamber of the right lung; cvc, caudal vena cava; lao, left aorta; li, liver; ll, left lung; lp, lung parenchyma; oe, oesophagus; pc(ll) posterior chamber of the left lung; pc(rl), posterior chamber of the right lung; pv, pulmonary vessels; rao, right aorta; rl, right lung.

identified in the CT scans, the clinician should be aware of this particular structure when evaluating topographic anatomy of organs within the coelomic cavity.

It is the authors' opinion that the dose and the contrast medium administration method were adequate for evaluation of most of the vascular structures. No short-term adverse reactions to the

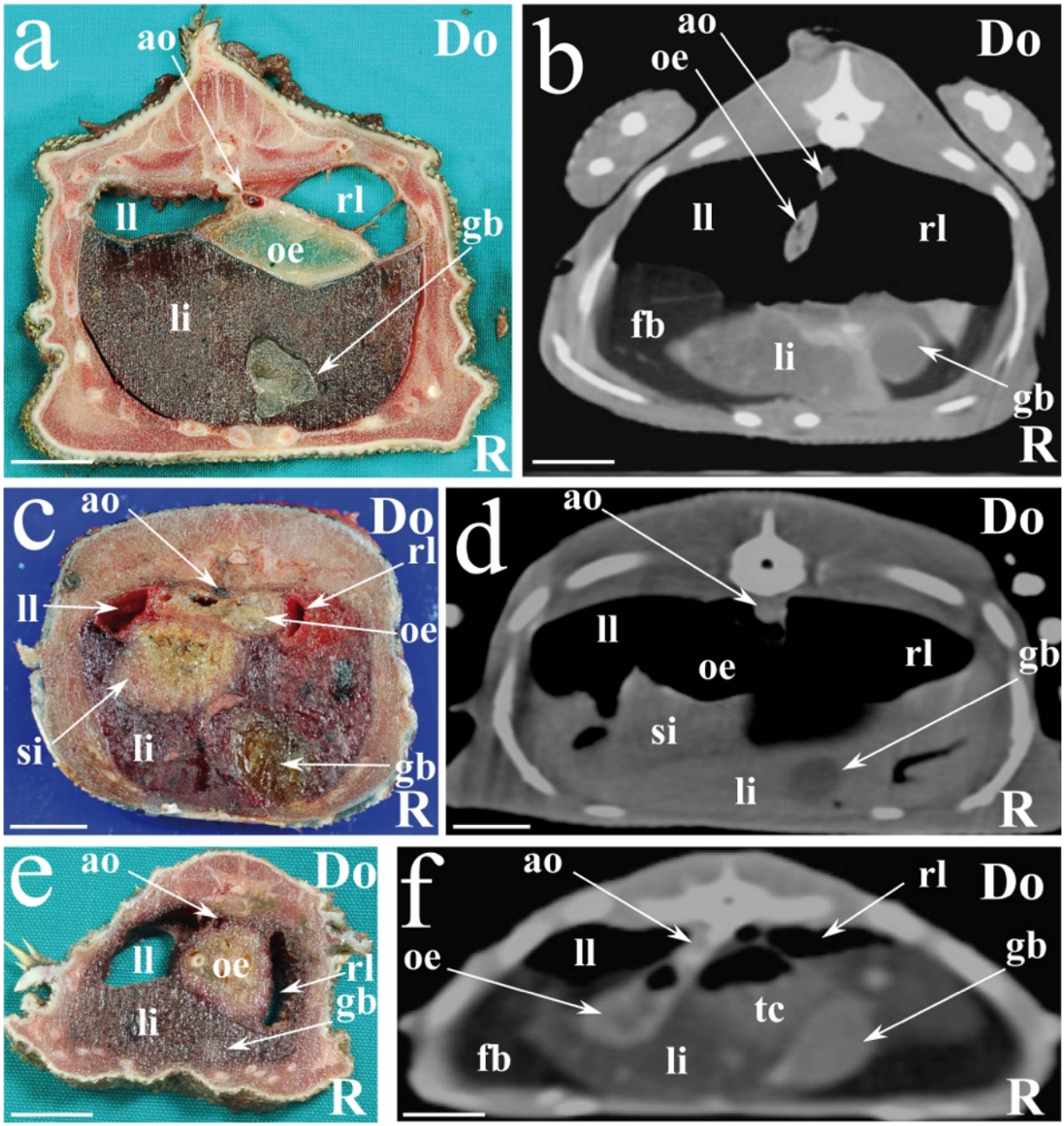

Figure 6. Matched cross-sections and CT images at the level of the liver and gallbladder. Matched cross-sections and CT images displayed in a soft tissue window in a green iguana (A-B), black and white tegu (C-D) and bearded dragon (E-F) at the level of the liver and the gallbladder, corresponding to line D in Figure 2. Do is dorsal, R is right. Bar =1 cm. ao; aorta; fb, fat bodies; gb, gallbladder; li, liver; ll, left lung; oe, oesophagus; rl, right lung; si, small intestine; tc, transverse colon.

contrast medium were evident. The heart was identified in all the considered species immediately caudal to the coelomic cavity inlet (Figure 3). The two atria and the two aortic arches were easily identified, whereas partial volume artefact prevented clear visualisation of the pulmonary artery emerging from the heart (Figure 3 B-D-F). The two aortae were individually identified in the green iguana (Figure 3 B) whereas partial volume artefact between the two aortae and the esophagus was noticed in the black and white tegu and the bearded dragon (Figure 3 D-F).

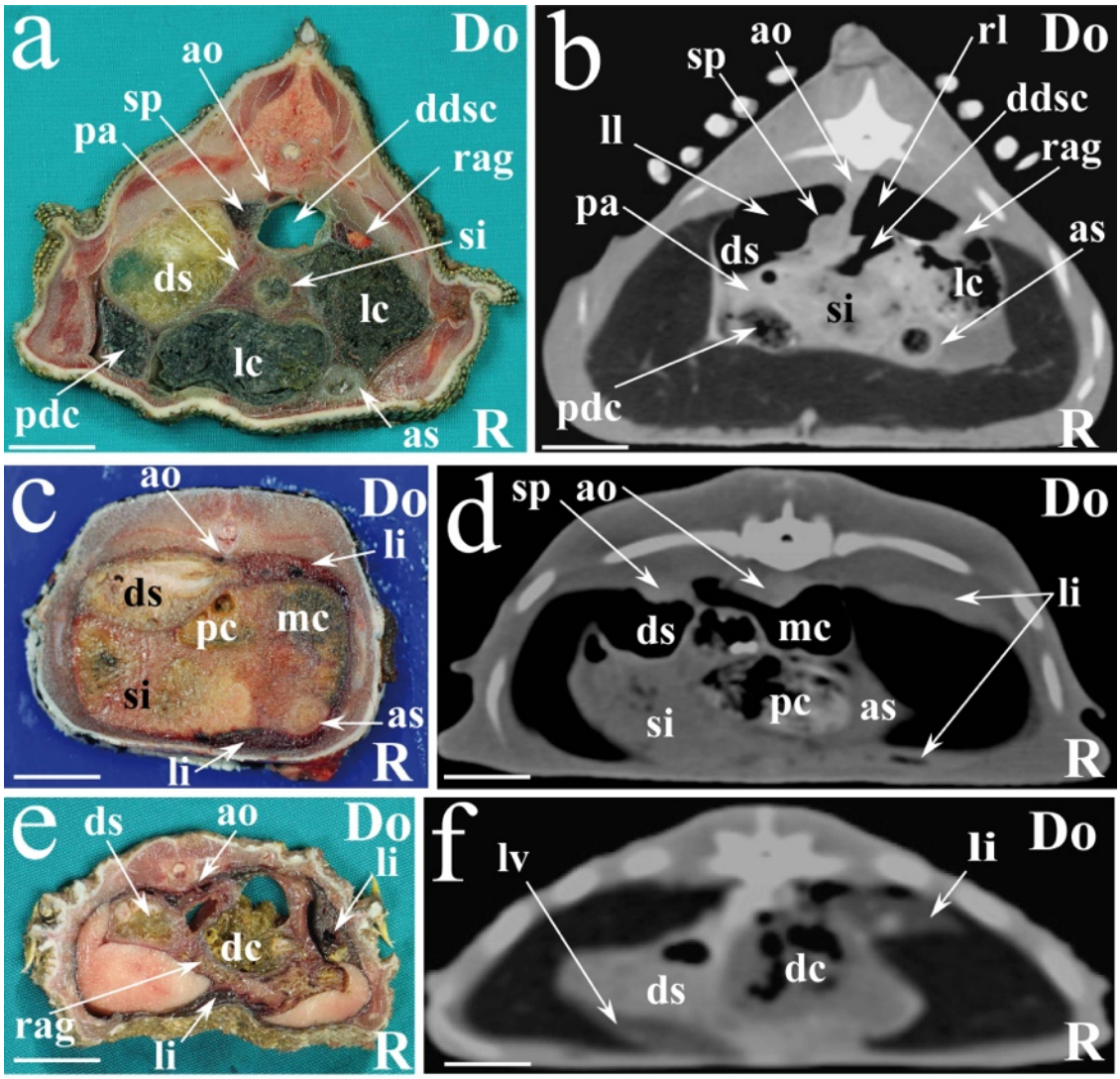

Figure 7. Matched cross-sections and CT images at the level of the spleen. Matched cross- sections and CT images displayed in a soft tissue window in a green iguana (A-B), black and white tegu (C-D) and bearded dragon (E-F) at the level of the spleen, corresponding to line E in Figure 2. Do is dorsal, R is right. Bar =1 cm. ao, aorta; as, ascending stomach; dc, descending colon; ddsc, distal descending small colon; ds, descending stomach; lc, large colon; li, liver; ll, left lung; mc, middle colon; pa, pancreas; pc, proximal colon; pdc, proximal descending colon; rag, right adrenal gland; rl, right lung; si, small intestine; sp, spleen.

The lung parenchyma in the pre-hilar portion of the lungs appeared, in all the considered species, as a thin, faintly outlined, structure surrounding an air-filled cavity (Figure 4 B-D-F). In the post-hilar portion of the lungs the parenchyma was barely visible in the black and white tegu (Figure 5D) and in the bearded dragon (Figure 5F), whereas large transverse septa were evident in the green iguana (Figure 5B). CT has already been proven to represent the gold standard in the diagnosis of pulmonary disease in snakes [25]; it is the authors' opinion that CT might improve the diagnostic accuracy regarding pulmonary diseases even in lizards.

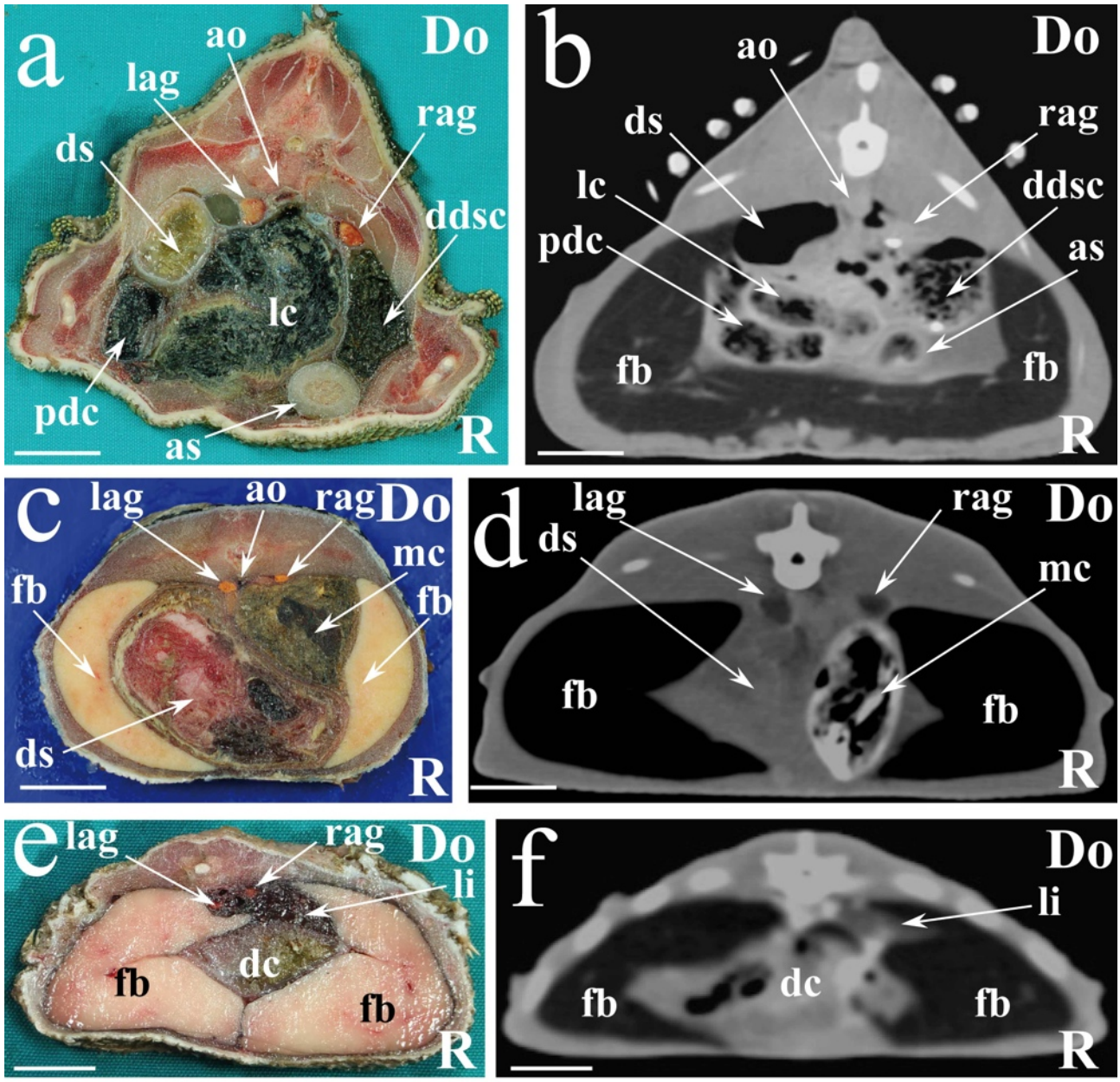

Figure 8. Matched cross-sections and CT images at the level of the adrenal glands. Matched cross-sections and CT images displayed in a soft tissue window in a green iguana (A-B), black and white tegu (C-D) and bearded dragon (E-F) at the level of the adrenal glands, corresponding to line F in Figure 2. Do is dorsal, R is right. Bar =1 cm. ao, aorta; as, ascending stomach; dc, descending colon; ddsc, distal descending small colon; ds; descending stomach; fb, fat bodies; lag, left adrenal gland; lc, large colon; li, liver; mc, middle colon; pdc, proximal descending colon; rag, right adrenal gland.

The liver was clearly distinguishable from the surrounding fat bodies and showed a compact appearance in all the species considered (Figure 6 B-D-F). Some contrast-enhanced parenchymatous vessels were evident in the green iguana (Figure 6 B) as well as in the bearded dragon (Figure 6F). In both the black and white tegu (Figure 7 C-D) and the bearded dragon (Figure 7 E-F, 8 E-F, 9 E-F), a liver lobe extending caudally in a dorso-lateral position was evident on the right side of the coelomic cavity. The gallbladder wall was detected in the green iguana (Figure 6B)

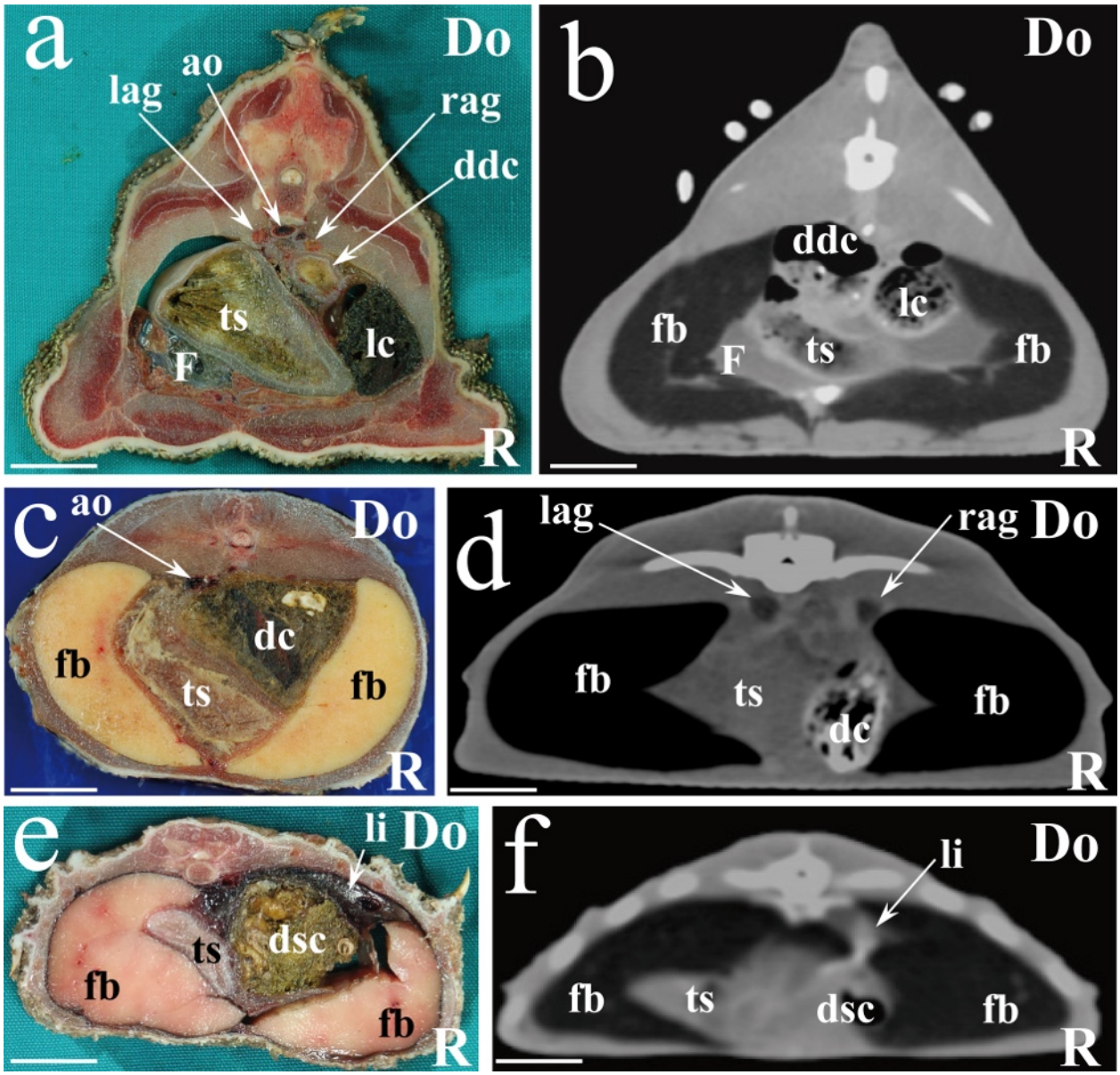

Figure 9. Matched cross-sections and CT images at the level of the transverse portion of the stomach. Matched cross-sections and CT images displayed in a soft tissue window of a green iguana (A-B), black and white tegu (C-D) and bearded dragon (E-F) at the level of the transverse portion of the stomach, corresponding to line G in Figure 2. Do is dorsal, R is right. Bar =1 cm. F = Free fluid. ao, aorta; dc, distal colon; ddc, distal descending colon; dsc, descending colon; fb, fat bodies; lag, left adrenal gland; lc, large colon; li, liver; rag, right adrenal gland; ts, transverse stomach.

and the bearded dragon (Figure 6F) whereas no wall resulted in the black and white tegu (Figure 6D).

The stomach had a similar C-shaped appearance both in the green iguana (Figures 7A-B, 8A-B, 9 A-B) and the black and white tegu (Figures 1A, 7B-C, 8B-C, 9B-C). The descending stomach was located in a dorso-lateral position to the left of the midline; the transverse stomach was located caudally and crossed the midline at the level of the caudal pole of the adrenal glands (Figure 9 A-B-C-D). The ascending stomach was located in a ventral position to the right of the midline, with the

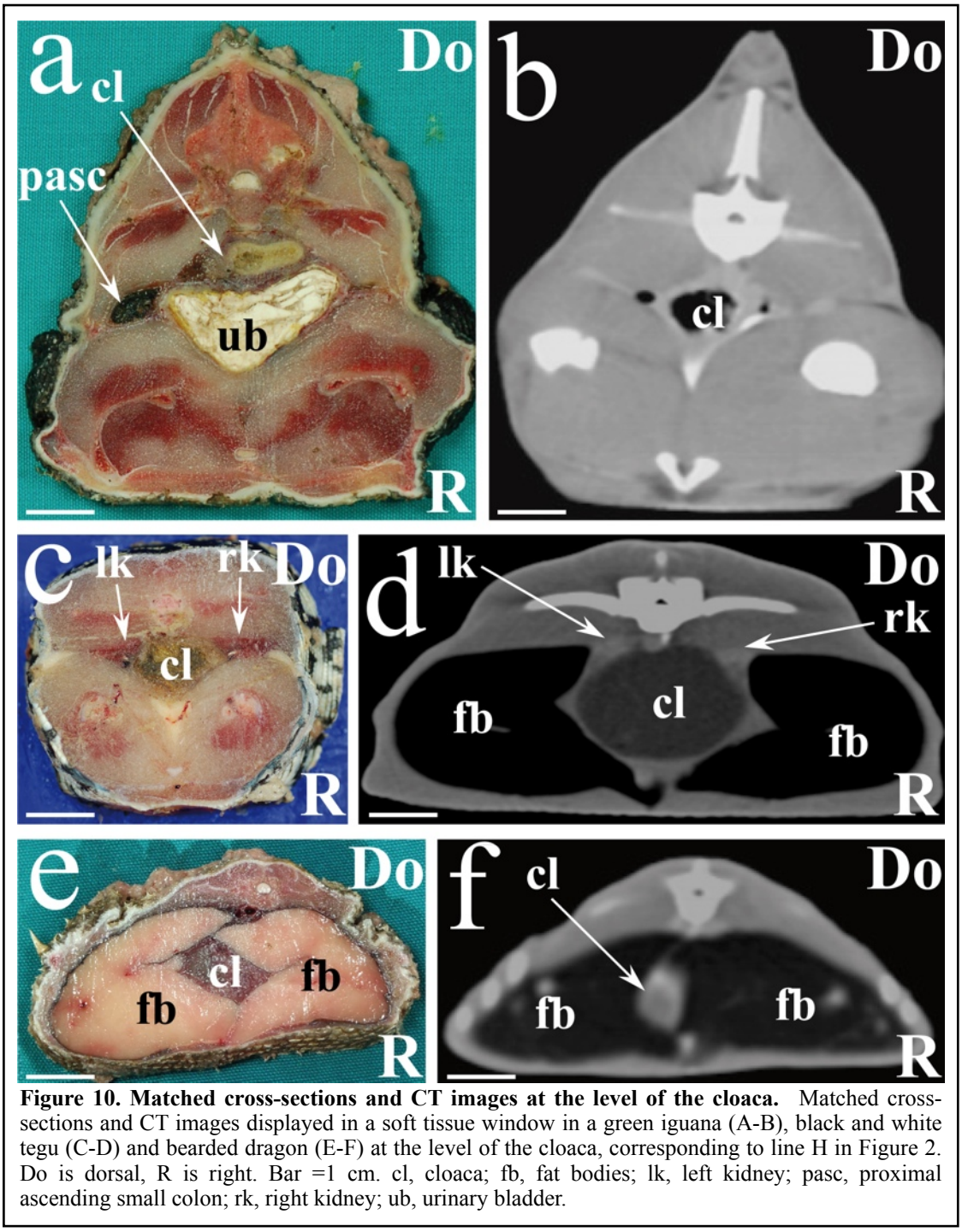

Figure 10. Matched cross-sections and CT images at the level of the cloaca. Matched cross-sections and CT images displayed in a soft tissue window in a green iguana (A-B), black and white tegu (C-D) and bearded dragon (E-F) at the level of the cloaca, corresponding to line H in Figure 2. Do is dorsal, R is right. Bar =1 cm. cl, cloaca; fb, fat bodies; lk, left kidney; pasc, proximal ascending small colon; rk, right kidney; ub, urinary bladder.

pylorus immediately caudal to the liver (Figures 1A, 7A-B-C-D, 8A-B). In the bearded dragon the stomach was J-shaped and entirely occupied the left side of the coelomic cavity; the ascending portion of the stomach was short and the pylorus was located more caudally than in the green iguana and black and white tegu (Figures 1B, 7E-F). In all the considered species, the small intestine was positioned almost completely and immediately caudal to the liver (Figure 7). Only in the green iguana were individual small intestinal loops evident (Figure 7B). The large intestine was

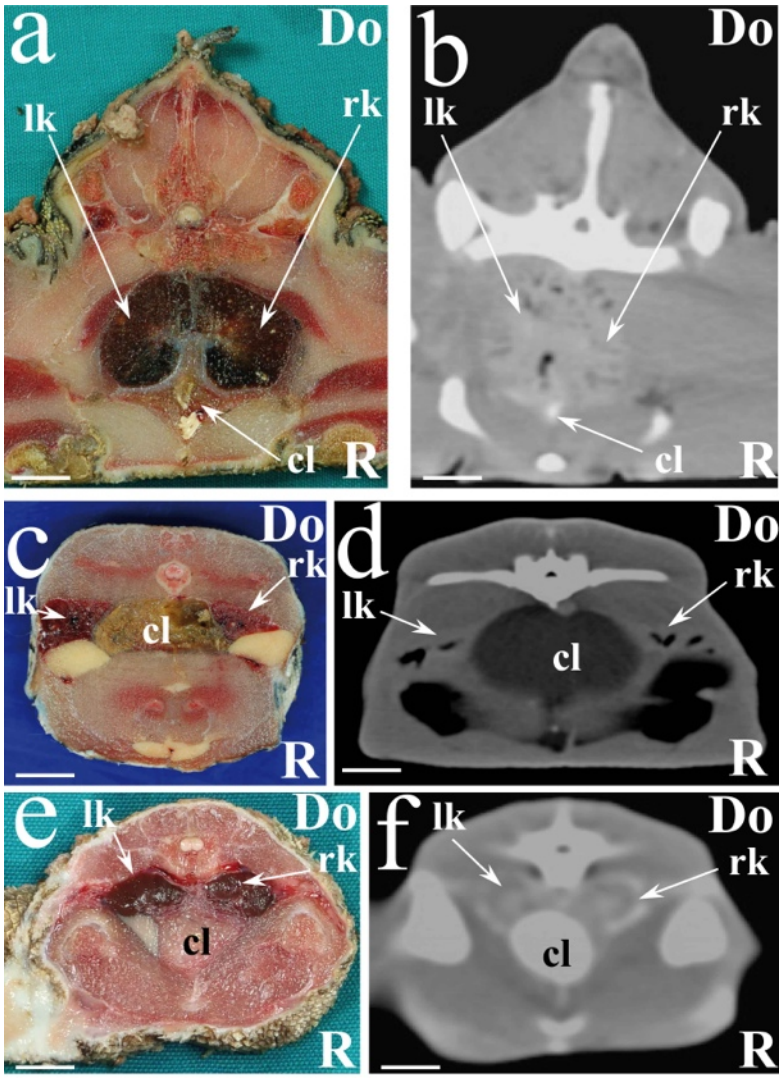

Figure 11. Matched cross-sections and CT images at the level of the kidneys. Matched cross- sections and CT images displayed in a soft tissue window in a green iguana (A-B), black and white tegu (C-D) and bearded dragon (E-F) at the level of the kidneys, corresponding to line G in Figure 2. Do is dorsal, R is right. Bar =1 cm. cl, cloaca; lk, left kidney; rk, right kidney.

particularly obvious in all the CT-scanned tegus (Figures 7D, 8D, 9D) due to its hyperattenuating content.

The spleen was identified in the green iguana (Figure 7B) and the black and white tegu (Figure 7D) as a small, rounded, soft tissue density, partially silhouetting with the descending stomach. The pancreas was identified only in the green iguana as a soft tissue density interposed between the small intestinal loops (Figure 7A-B).

The urinary bladder was detected ventral to the cloaca (Figure 10A) in the cross-sectioned iguanas, whereas no urinary bladder could be observed in the CT-scanned subjects (Figure 10B). In all the CT-scanned black and white tegus (Figure 10D) the cloaca was markedly distended with a fluid content. A clear opacification of the urine was noticed only in the bearded dragon (Figure 11F).

In the green iguana (Figure 11 A-B) and bearded dragon (Figure 11 E-F) the kidneys were completely embedded within the pelvic girdle whereas in the black and white tegu the kidneys extended a few centimetres into the coelomic cavity (Figures 10C-D, 11C-D). The renal parenchyma showed an inhomogeneous appearance in the green iguana (Figure 11B) and common

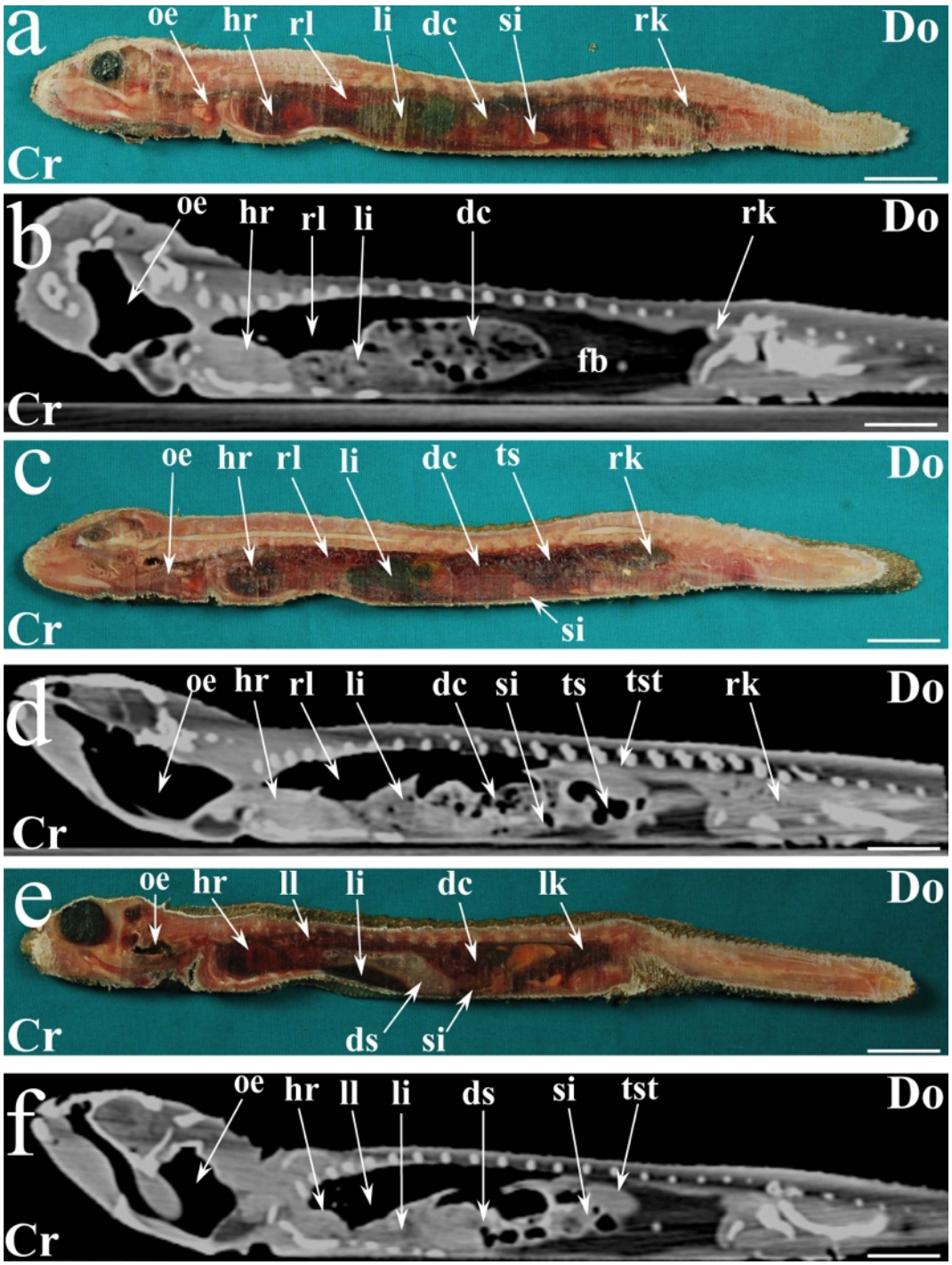

Figure 12. Longitudinal cross-sections and CT images of the bearded dragon. Matched longitudinal cross-sections and longitudinal CT images displayed in a soft tissue window for a bearded dragon, corresponding to lines L (A-B), M (C-D), N (E-F) in Figure 2. Cr is cranial, Do is dorsal. Bar = 1 cm. dc, descending colon; ds, descending stomach; fb, fat bodies; hr, heart; li, liver; lk, left kidney; ll, left lung; oe, oesophagus; rk, right kidney; rl, right lung; si, small intestine; ts, transverse stomach; tst, testicle.

black and white tegu (Figure 11D) whereas it appeared quite homogeneous in the bearded dragon (Figure 11F). A clear opacification of the kidneys was evident only in the bearded dragon (Figure 11F). Reproductive organs were identified only in the CT scans of 2 male bearded dragons (Figure 12D-F). All the CT scans and the dissections were performed during the period May-September;

such a period coincides with the sexual resting season for this species of lizard. It is the authors' opinion that the small physiological size of the gonads during this period might have prevented their visualization both in the dissections and in the CT scans.

In the matched LM cross-sections and CT images of the bearded dragon, which are displayed in Figure 12, most of the clinically relevant structures have been identified. Some authors[10] suggest, in the event of using old CT scanners, that smaller specimens be scanned in a LM direction in order to overcome the inability of those CT scanners to reproduce isotropic voxels. Results of the present study suggest that patient positioning should be determined only on the basis of a clinician's preferences and that both CC and LM positions provide quality images for diagnostic imaging.

References

1.

1. Zotti A, Selleri P, Carnier P, Morgante M, Bernardini D. Relationship between metabolic bone disease and bone mineral density measured by dual-energy X-ray absorptiometry in the green iguana (Iguana iguana). *Vet Radiol Ultrasound* 2004;45:10–16.
2. Arencibia A, Rivero MA,De Miguel I, Contreras S, A. Cabrero A, Oros J.. Computed tomographic anatomy of the head of the loggerhead sea turtle (*Caretta caretta*). *Res Vet Sci* 2006;81:165–169.
3. Valente AL, Cuenca R, Zamora M, Parga ML, Lavin S,Alegre F,Marco I. Computed tomography of the vertebral column and coelomic structures in the normal loggerhead sea turtle (Caretta caretta). *Vet J* 2007;174:362-370.
4. Holland MF, Hernandez-Divers S, Frank PM. Ultrasonographic appearance of the coelomic cavity in healthy green iguanas. *J Am Vet Med Assoc* 2008; 233:590–596.
5. Banzato T, Russo E, Di Toma A, Palmisano G, Zotti A. Anatomic imaging of the *Boa constrictor* head: a comparison between radiography, computed tomography and cadaver anatomy. *Am J Vet Res* 2011;72:1592–1599.
6. Banzato T, Russo E, Finotti L, Zotti A. Development of a technique for contrast radiographic examination of the gastrointestinal tract in ball pythons (*Python regius*). *Am J Vet Res* 2012; 73: 996-1001.
7. Banzato T, Russo E, Finotti L, Milan MC, Gianesella M, Zotti A. Ultrasonographic anatomy of the coelomic organs of boid snakes (*Boa constrictor imperator*, *Python regius*, *Python molurus molurus*, and *Python curtus*). *Am J Vet Res* 2012;73:634-645.
8. Banzato T, Selleri P, Veladiano IA, Martin A, Zanetti E, Zotti A. Comparative evaluation of the cadaveric, radiographic and computed tomographic anatomy of the heads of green iguana (*Iguana iguana*), common tegu (*Tupinambis merianae*) and bearded dragon (*Pogona vitticeps*). *BMC Vet Res* 2012;**8**:53 doi: 10.1186/1746-6148-8-53.
9. Silverman S. Diagnostic imaging. In: Reptile Medicine and Surgery. (Mader, D.R., ed.), 2nd edition. Philadelphia: W.B. Saunders Co, 2006:471–489.
10. Kiefer I, Pees M. Computed tomography. In: Diagnostic Imaging of Exotic Pets (Krautwald-Junghanns, M.E., M. Pees, S. Reese, and T. Tully, eds.). Hannover: Schlütersche Verlagsgesellschaft mbH & Co, 2011: 358.
11. Uetz P: The Reptile database**.** [www.reptile-database.org]. Accessed 15 June 2012.
12. Gardner Lynn W. The Thyroid. In: Gans C, and Parsons TS, eds. *Biology of the Reptilia*, Vol. 3. London and New York: Academic Press, 1970:201-234.
13. Miller RM, Lagios MD. The Pancreas. In: Gans C, Parsons TS, eds. *Biology of the Reptilia*, Vol. 3. London and New York: Academic Press 1970: 319-324.

14. Ottaviani G, Tazzi A.. The Lymphatic System. In: Gans, C., and T.S. Parsons, eds. Biology of the Reptilia, Vol. 6. London and New York: Academic Press 1977;315-322.
15. Parsons TS, Cameron JE. Internal Relief of the Digestive Tract. In: Gans C, Parsons TS, eds. *Biology of the Reptilia*. Vol. 6. London and New York: Academic Press, 1977:192-212.
16. Fox H. The Urinogenital System of Reptiles. In: Gans C, Parson TS, eds. *Biology of the Reptilia*. Vol. 6. London and New York : Academic Press 1977:24-109.
17. Farrel PA, Gamperl KA, Francis T.. Comparative aspects of heart morphology. In: Gans C, Gaunt AS, eds. *Biology of the Reptilia*. Vol. 14. Ithaca, New York: Contributions to Herpetology SSAR, 1998:375-419.
18. Tanaka Y. Structure of the Reptilian Spleen. In: Gans C, Gaunt AS, eds. *Biology of the Reptilia*. Vol. 19. Ithaca, New York: Society for the Study of Amphibians and Reptiles 1998:533-580.
19. Smith D, Dobson H, Spence E. Gastrointestinal studies in the green iguana: technique and reference values. *Vet Radiol Ultrasound* 2001;42:515-520.
20. Soriano JC. Saurios. In: Orti RM, Garcia PM, Soriano JC, eds. Atlas de anatomia de animales exoticos. (), Barcelona: Masson SA 2004:125-129.
21. O' Malley B (ed.),. Clinical Anatomy and Physiology of Exotic Species: Structure and function of mammals, birds, reptiles and amphibians. Philadelphia: Saunders Ltd 2005:1-269.
22. Perry SF. Lungs: Comparative anatomy, functional morphology, and evolution. In: Gans C, Gaunt AS, eds. *Biology of the Reptilia*. Vol.19. Ithaca, New York: Society for the Study of Amphibians and Reptiles, 1998:1-97.
23. Klein W, Abe AS, Andrade DV, Perry SF. Structure of the Posthepatic Septum and Its Influence on Visceral Topology in the Tegu Lizard, *Tupinambis merianae* (Teiidae: Reptilia). *J Morphol* 2003;258:151–157.
24. Klein W, Andrade DV, Abe AS, Perry SF. Role of the post-hepatic septum on breathing during locomotion in *Tupinambis merianae* (Reptilia: Teiidae). *J Exp Biol* 2003;206:2135-2143.
25. Pees MC, Kiefer I, Ludewig EW, Schumacher JP, Krautwald-Junghanns ME, Oechtering GU. Computed tomography of the lungs of Indian pythons (Python molurus). *J Am Vet Med Assoc* 2007;64:428-434.

CHAPTER VI

ULTRASONOGRAPHIC ANATOMY OF THE COELOMIC ORGANS OF BOID SNAKES

This chapter was adapted from: Banzato T, Russo E, Milan MC, Gianesella M, Finotti L, Zotti A. Ultrasonographic anatomy of the coelomic organs of the boid snakes (Boa constrictor, Python regius, Python molurus, Python curtus). *2012. American Journal of Veterinary Research 73, 634-345.*

Abstract

16 Ball pythons (*Python regius*; 7 males, 8 females, and 1 immature), 10 Indian rock pythons (*Python molurus molurus*; 5 males, 4 females, and 1 immature), 12 *Python curtus* (5 males and 7 females), and 8 boa constrictors (*Boa constrictor imperator*; 4 males and 4 females) where object of this study. All snakes underwent complete ultrasonographic evaluation of the coelomic cavity; chemical restraint was not necessary. A dorsolateral approach to probe placement was chosen to increase image quality and to avoid injury to the snakes and operators. Qualitative and quantitative observations were recorded. The liver, stomach, gallbladder, pancreas, small and large intestine, kidneys, cloaca, and scent glands were identified in all snakes. The hemipenes were identified in 10 of the 20 (50%) male snakes. The spleen was identified in 5 of the 46 (11%) snakes, and ureters were identified in 6 (13%). In 3 sexually immature snakes, the gonads were not visible. One (2%) snake was gravid, and 7 (15%) had small amounts of free fluid in the coelomic cavity. Statistical analysis revealed a significant positive correlation between several measurements (diameter and thickness of scent glands, gastric and pyloric walls, and colonic wall) and body length (snout to vent) and body weight.

Introduction

Ultrasonography is already considered a valuable tool in the clinical evaluation of reptiles: the ultrasonographic appearance of the coelomic organs in green iguanas (*Iguana iguana*),[2] loggerhead sea turtles (*Caretta caretta*),[3] Bosc monitors (*Varanus exantematicus*),[4] and boa constrictors (*Boa constrictor*)[5] has been reported. The purpose of the study reported here was to characterize the ultrasonographic appearance of the coelomic organs of Ball pythons (*Python regius*), Indian rock pythons (*Python molurus molurus*), *Python curtus*, and boa constrictors (*Boa constrictor imperator*), with particular emphasis on comparative aspects. In a previous ultrasonographic study,[5] a ventral approach to probe placement was used on anesthetized snakes. We also sought to determine whether a dorsolateral approach to ultrasonography could be used in conscious snakes, which could potentially provide a faster yet reliable, clinical useful ultrasonographic technique.

Materials and Methods

Animals

The study involved 2 parts. For the first part (anatomic evaluation), cadavers were used of 3 boa constrictors (1 male and 2 females), 10 *P curtus* (3 males and 7 females), 4 Indian rock pythons (3 males and 1 female) and 6 Ball pythons (3 males and 3 females). These 23 snakes had died from various causes and their bodies had been stored at –20°C for a mean of 1 month. For the second part (ultrasonographic evaluation), 46 privately owned boid snakes were used (16 Ball pythons [7 males, 8 females, and 1 immature], 12 *P curtus* [5 males and 7 females], 10 Indian rock pythons [5 males, 4 females, and 1 immature], and 8 boa constrictors [4 males and 4 females]). Twenty of the live snakes (10 Ball pythons, 4 *P curtus*, 3 Indian rock pythons, and 3 boa constrictors) were evaluated between July and September 2010 and 26 (6 Ball pythons, 8 *P curtus*, 7 Indian rock pythons, and 5 boa constrictors) were evaluated in October and November of the same year. All snakes were considered healthy on the basis of their medical history and physical examination findings. Last meal and reproductive status were recorded for each snake. This study was performed with approval of the Padua University Ethical Committee.

Anatomic evaluation

Snake cadavers were dissected prior to ultrasonographic evaluation of live snakes to overcome the lack of unambiguous anatomic references for the species in this study. All necropsy findings were carefully documented, and all coelomic organs (including major blood vessels) were identified and named in accordance with the most recent information on snake anatomy.[6–18] Photographs were obtained as part of this documentation.

Imaging procedures

Ultrasonographic examination of the coelomic cavity was performed on each snake by use of the same dorsolateral approach to probe placement. Each scan was performed with snakes positioned in ventral recumbency. Constant environmental temperature, set at 27°C, was maintained by means of a heater. Chemical restraint was not necessary; for the more aggressive subject, the head was kept inside a cotton sack to avoid injury to the snake or operator. For each evaluation, ultrasonographic coupling gel was applied to the dorsolateral surfaces of the body and the tail. Images were obtained with a 6- to 10-MHz linear array transducer connected to a commercial sonographic scanner (Logiq P5, GE Healthcare, Milano, Italy); a standoff pad was not used. The transducer frequency was adjusted throughout each examination to obtain the best imaging quality. In small subjects (Ball pythons) the frequency was set at 10 MHz, whereas in large subjects (Indian rock pythons, boa constrictors, and *P curtus*), the frequency was set from 6 to 8 MHz. Each examination was completed within 15 to 30 minutes. All coelomic organs were evaluated in both longitudinal and transverse scan planes. Findings are reported in the order of appearance during ultrasonography, starting at the tail.

Statistical analysis

Measurement values are reported as mean ± SD. The distribution of data regarding the anatomic structure measurements was tested for normality by means of graphic methods (histograms and Q-Q plots) and the Shapiro-Wilk test. When data were normally distributed, correlations between body weight or body length and thickness of the scent glands, colonic wall, gastric wall, and pyloric wall were evaluated by performing linear regression and calculating Pearson correlation coefficients (r). When data were not normally distributed, Spearman correlation coefficients (ρ) were calculated for non normally distributed values. All analyses were performed with commercially available

software(GraphPad Prism, version 4.00 for Windows, GraphPad Software Inc, San Diego, Calif.). Values of $P < 0.05$ were considered significant.

Results

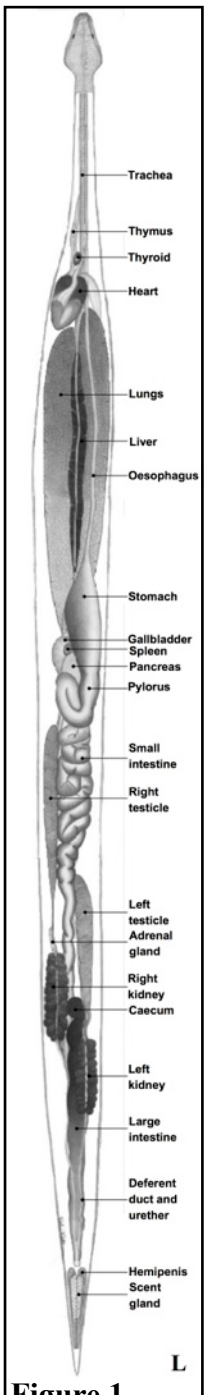

Figure 1

A schematic drawing of the topographic anatomy of the coelomic organs was made on the basis of findings **(Figure 1)**.

Scent glands and hemipenes

Paired scent glands were identified in all snakes examined **(Figure 2)**. In male snakes, paired scent glands were visible ventral to the caudal vertebrae; paired hemipenes were located immediately ventral to the scent glands. In females, the scent glands were more prominent and occupied most of the cranial portion of the tail. The scent glands had a rough and nonhomogeneous echotexture and a poor echogenicity. These glands had a lower echogenicity than the surrounding muscles. They appeared circular and surrounded by an echoic ring (the capsule) in transverse ultrasonographic scan and elongated and bordered by a well-defined capsule in longitudinal scan. An echoic muscular line was visible between the 2 scent glands in males and females. In males, the scent glands had a lower echogenicity and a rougher echotexture than did the hemipenes. Dimensions of the scent glands as measured just caudal to the vent in transverse images were summarized **(Table 1)**. A significant positive correlation was detected between body weight and scent gland thickness ($\rho = 0.29$; $P = 0.003$) and between body length and scent gland thickness ($\rho = 0.24$; $P = 0.003$). The hemipenes were easily identifiable in longitudinal scans of all male snakes but were less evident in

transverse scans because of poorer contact between the body and the transducer consequent to the circular section and the small diameter of the tail. The hemipenes were visible in longitudinal scans as 2 echoic lines (the hemipenes) within 2 parallel anechoic lines (Figure 1). In transverse scan, the hemipenes appeared as 2 echoic circular structures positioned ventrally or laterally to the scent glands. The hemipenes consistently appeared considerably smaller than the scent glands.

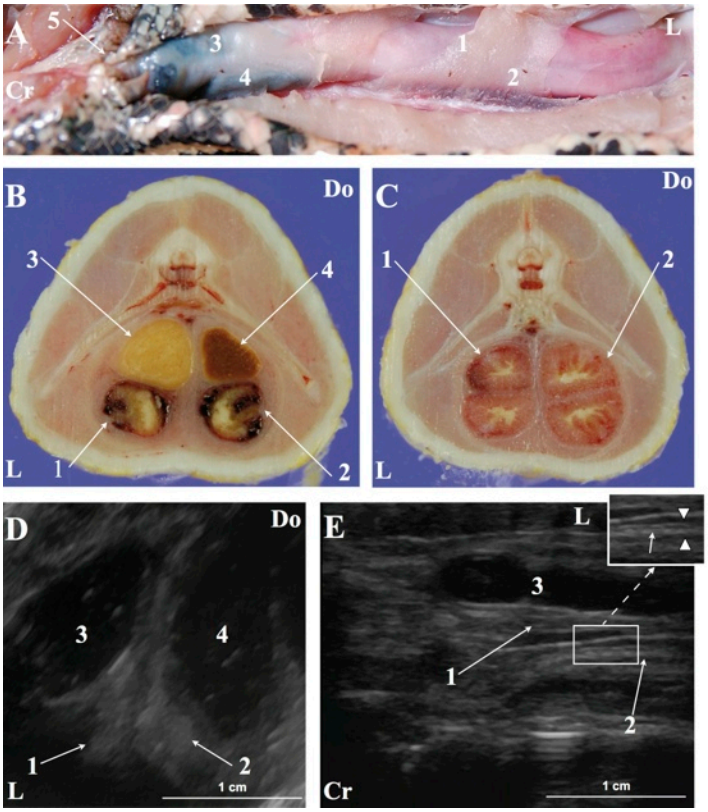

Figure 2—Representative photographs (A–C) and ultrasonographic images (D and E) of the internal organs of boid snakes. A—Grossly dissected tail of a male boa constrictor. B and C—Cross-sections (B is cranial to C) of the tail of a male Indian rock python (*Python molurus molurus*). D—Transverse ultrasonographic image of the tail of a male boa constrictor. E—Longitudinal ultrasonographic image of the tail of a male *Python curtus*. Inset—Muscles surrounding the hemipenes (arrowheads) and the hemipenis (arrow) are indicated. In all dissection photographs, the cranial aspect of snake is to the left of the image and the left side of snake is oriented toward the top. In all cross-section photographs, the left side of snake is to the left; dorsal is oriented toward the top. In all transverse ultrasonographic images, the left side of snake is to the left and dorsal is toward the top. In all longitudinal ultrasonographic images, cranial is to the left and the left side of the snake is toward the top. 1 = Left hemipenis. 2 = Right hemipenis. 3 = Left scent gland. 4 = Right scent gland. 5 = Vent. Cr = Cranial. Do = Dorsal. L = Left. Bar = 1 cm in ultrasonographic images.

Ureters, cloaca, and vagina

The cloaca was identified in all snakes immediately cranial to the vent **(Figure 3)**. The cloacal wall was composed of 3 layers: an external hyperechoic layer, an anechoic or poorly echoic middle layer, and an internal hyperechoic layer. In transverse scans, the shape and the overall appearance of the cloacal wall varied with the cloacal content. In snakes in which it was full of urine and feces, the cloaca appeared round with a thin smooth wall, whereas in snakes with a cloaca containing a limited amount of fluid, its wall appeared thicker and irregular. In longitudinal scans, the almost constant presence of fluids in the cloaca provided optimal organ

visibility. The ureters were identified in their cloacal tract in 2 male Ball pythons and 4 Indian rock pythons (2 males and 2 females) only through transverse scans; peristaltic activity was always evident (Figure 3). The vagina was identified ventral to the cloaca in 4 female Ball pythons, 3 female *P curtus*, and 1 female boa constrictor. The vagina was seen only through transverse scans. The ultrasonographic appearance of the vagina was a figure-8-shaped, thick-walled hollow organ

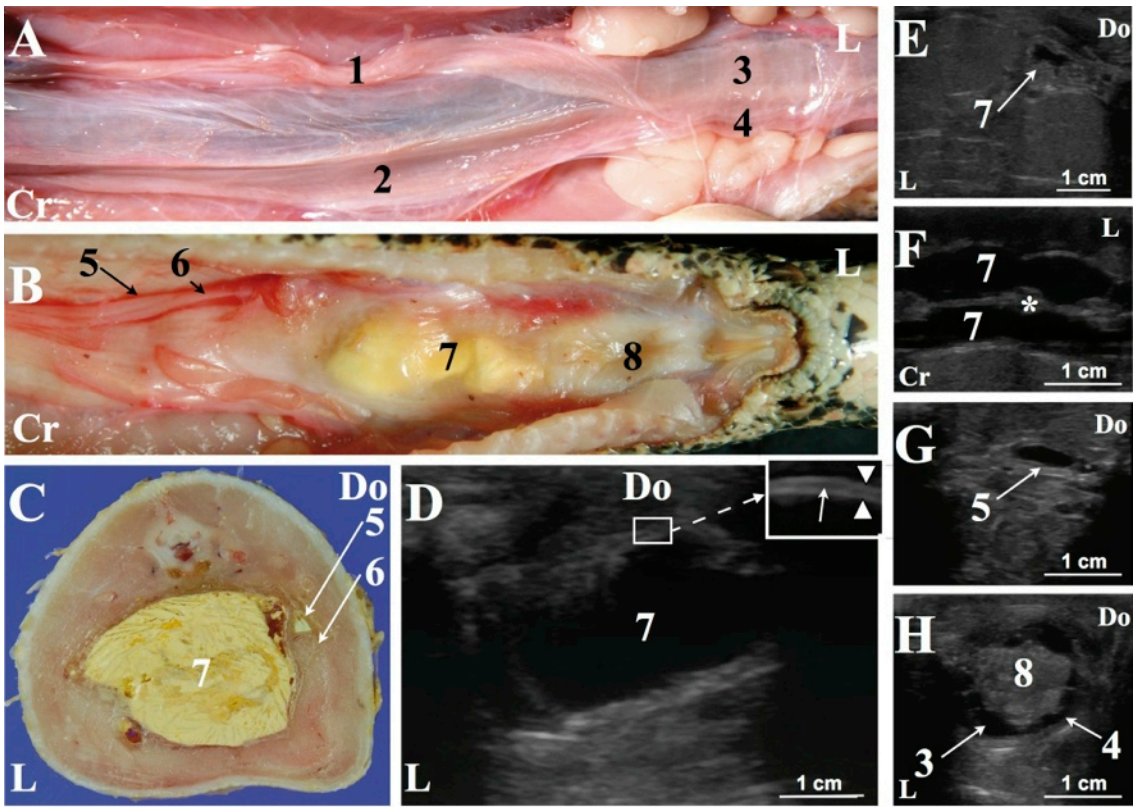

Figure 3—Representative photographs (A–C) and ultrasonographic images (D–H) of the internal organs of boid snakes. A—Grossly dissected female Ball python (*Python regius*) after removal of the fat bodies of the cloaca. B—Gross anatomic dissection after removal of the fat bodies of the cloaca of a male boa constrictor. C—Cross-section of the cloaca of a male Indian rock python. D—Transverse ultrasonographic image of the cloaca (distended with urine) of a female Indian rock python. Inset—External hyperechoic layers (arrowheads) and internal hypoechoic layer (arrow) of the cloacal wall. E—Transverse ultrasonographic image of the cloaca (empty) of a female Ball python. F—Longitudinal ultrasonographic image of the cloaca of a male Ball python. Feces are evident in this snake (asterisk). G—Detail of the ureter. H—Transverse ultrasonographic image of the cloaca and vagina of a female Ball python. 1 = Left oviduct. 2 = Right oviduct. 3 = Left vagina. 4 = Right vagina. 5 = Ureter. 6 = Deferent duct. 7 = Urodeum. 8 = Coprodeum. *See* Figure 2 for remainder of key.

immediately ventral to the colon. No interspecies differences were evident in the ultrasonographic appearance of the cloaca.

Colon and caecum

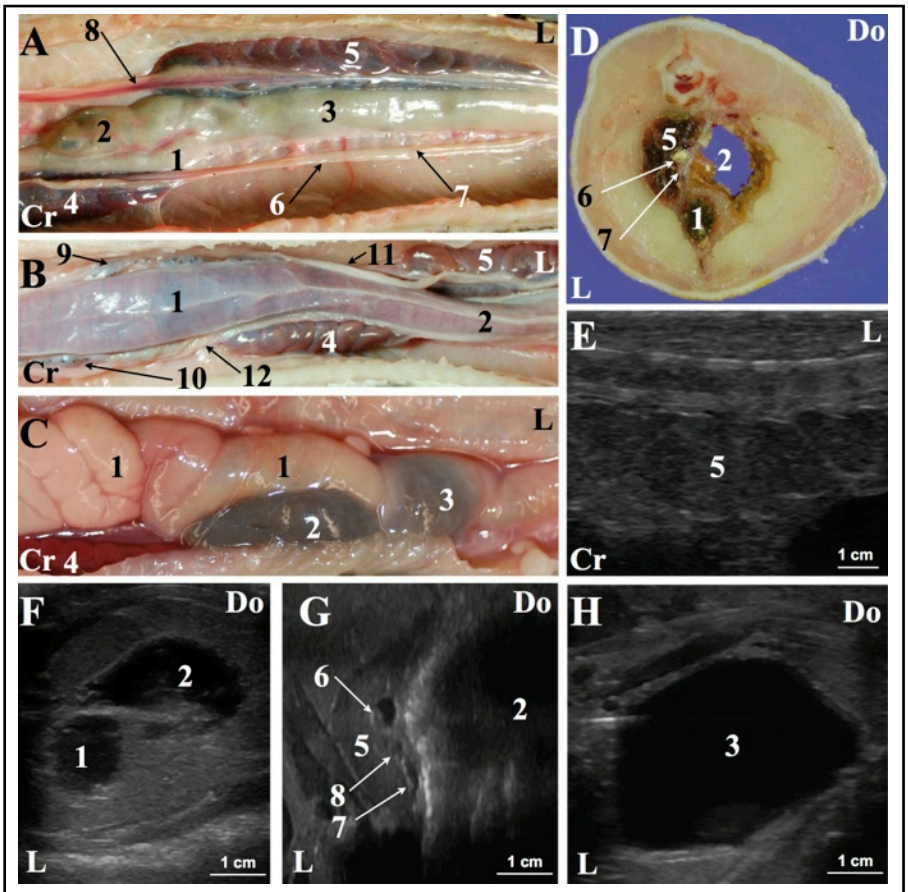

Figure 4—Representative photographs (A–D) and ultrasonographic images (E–H) of the internal organs of boid snakes. A, B, and C—Gross anatomic dissection after removal of the fat bodies at the junction between small and large intestine of a male boa constrictor (A), female Ball python (B), and female *P curtus* (C). D—Cross-section of the small-large intestine junction of a male Indian rock python. E—Longitudinal ultrasonographic image of the left kidney of a male Indian rock python. F—Transverse ultrasonographic image of the small-large intestine junction of a male Indian rock python. G—Transverse ultrasonographic image of the left kidney and colon of a male Ball python from which food had been withheld. H—Transverse ultrasonographic image of the large intestine of a recently fed female boa constrictor. 1 = Small intestine. 2 = Caecum. 3 = Large intestine. 4 = Right kidney. 5 = Left kidney. 6 = Right ureter. 7 = Right deferent duct. 8 = Renal efferent vein. 9 = Left ovary. 10 = Right ovary. 11 = Left oviduct. 12 = Right oviduct. *See* Figure 2 for remainder of key.

The junction between small and large intestine was easily identified in all *P curtus*, Indian rock pythons, and boa constrictors because of the presence of a well-developed caecum that was located beside the terminal portion of the small intestine **(Figure 4)**. No transition in intestinal wall thickness was observed at the junction between small and large intestine. The wall of the colon and caecum appeared similar to that of the cloaca. Only small portions of that wall were clearly visible in most snakes because of the constant presence of gas within the lumen. The amount of gas and fluid appeared to be related to digestive status; snakes fed during the week preceding the examination had a higher fluid content in the colon, whereas snakes from which food had been withheld for more than a week previously had a higher presence of gas. The distinction between the small and large intestine was less evident in Ball pythons than in the other species because of the absence of the caecum and the straight aspect of the intestinal tract. A significant

positive correlation was evident between body weight and colonic wall thickness ($\rho = 0.20$; $P = 0.035$) as well as between body length and colonic wall thickness ($\rho = 0.23$; $P = 0.018$).

Kidneys

The kidneys were identified in all snakes examined. In all snakes, the left kidney was seen just cranial to the cloaca, whereas the right kidney was located cranial to the left kidney (Figure 4). In some snakes, the cranial pole of the left kidney and the caudal pole of the right were visible in the same transverse scan. The echogenicity of the kidneys was similar to that of the fat bodies (particularly in Ball pythons and Indian rock pythons), making the identification of the kidneys challenging. In transverse scans, the kidneys ranged in appearance from triangular to nearly oval, with a fine echotexture similar to that of mammalian renal cortex. The ureter could be traced starting from the cranial pole of the kidney and running medially to the ventral surface of the organ; it was often visible as a round structure with a hyperechoic wall. The renal efferent vein was also visible sometimes lateral and sometimes medial to the ureter. In longitudinal scans, the renal lobules were sometimes visible as multiple hyperechoic lines, whereas all the other renal structures were difficult to identify.

Gonads

Snakes evaluated between July and September had fewer and smaller follicles than those evaluated between October and November **(Figures 5 and 6)**. In the snakes evaluated in the summer, follicle identification was sometimes challenging. Snakes evaluated during October and November had well-developed follicles in the dorsal portion of the coelomic cavity just cranial to or at the same level of the corresponding kidney, depending on the stage of the ovarian cycle. The follicles appeared as multiple round anechoic structures surrounded by a 2-layered wall; the inner layer

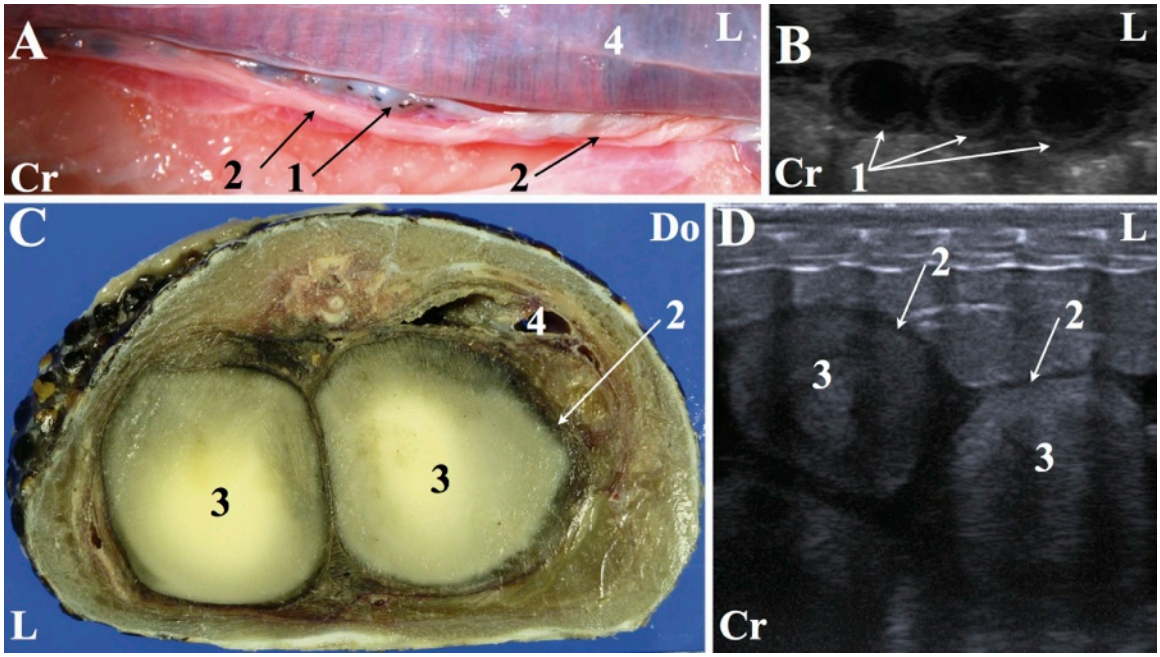

Figure 5—Representative photographs (A and B) and ultrasonographic images (C and D) of the internal organs of boid snakes. A—Detail of the right ovary (fat bodies removed) of a grossly dissected femal Ball python that died in July (sexual resting season). C—Cross section of the oviduct of a gravid female boa constrictor. D—Transverse ultrasonographic image of the oviduct of a gravid female boa constrictor. 1 = Ovary. 2 = Oviduct. 3 = Eggs. 4 = Small intestine. Cr = Cranial. Do = Dorsal. *See* Figure 2 for remainder of key.

appeared as echoic, whereas the outer layer was anechoic. The ovarian parenchyma was not visible. The ovaries appeared loosely connected to the coelomic cavity; for this reason, they appeared sometimes medial and sometimes lateral to the kidneys. In ovulating snakes, the left ovary extended from the stomach to the caudal pole of the left kidney, whereas the right extended from the pylorus to the caudal pole of the right kidney. The right ovary was cranial to the left. Different intermediate phases of ovulation were visible in scanned animals, but an accurate description of the ultrasonographic appearance of the ovarian cycle of the boid snakes is beyond the purpose of this study. The deferent duct in males and the oviduct in females was visible lateral to the ureter and as a small tubular structure with a highly echoic wall. The ultrasonographic characteristics of the oviducts varied widely as a function of reproductive status. In all nonpregnant snakes, the oviducts were visible only in the tract medial to the kidneys. The remaining portion of the oviducts was visible only in gravid snakes. Paired testicles, lying on the dorsal aspect of the coelomic cavity just cranial to the cranial pole of the kidneys, were identified in all sexually mature male snakes (Figure 6). Those evaluated in October and November had noticeably larger testicles than those evaluated

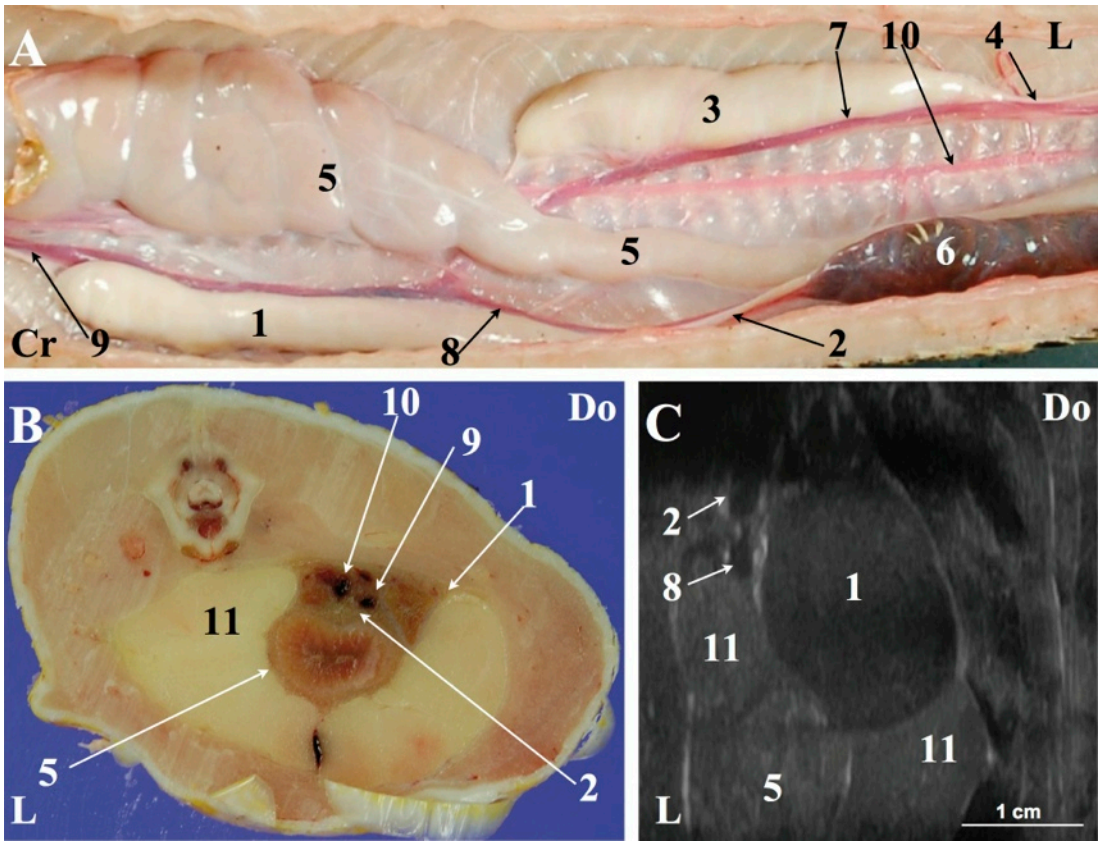

Figure 6—Representative photographs (A and B) and ultrasonographic image (C) of the internal organs of boid snakes. A—Detail of the testicles (fat bodies removed) of a grossly dissected male boa constrictor that died in June (sexual resting season). B—Cross-section of the small intestine and right testicle of a Indian rock python , died in July (sexual resting season). C—Transverse ultrasonographic image (acquired in November [mating season]) of the right testicle and small intestine of a Indian rock python 1 = Right testicle. 2 = Right deferent duct. 3 = Left testicle. 4 = Left deferent duct. 5 = Small intestine. 6 = Right kidney. 7 = Left renal efferent vein. 8 = Right renal efferent vein. 9 = Posterior vena cava. 10 = Dorsal aorta. 11 = Fat body. *See* Figure 2 for remainder of key.

between July and September. In snakes evaluated in the summer, the cranial pole of the right testicle extended to the stomach, whereas the caudal pole overlapped the cranial pole of the left testicle. In transverse scans, the testicles appeared oval to round; in longitudinal scans, they appeared elongated. The testicles had a fine echotexture similar to that of the fat bodies but with a lower echogenicity. In transverse scans, the deferent duct and the renal efferent vein were visible medial to the testicle (the deferent duct was lateral and the vein was medial). Color Doppler ultrasonography was used for the differentiation of the renal efferent vein from the deferent duct; no flow was observed in the deferent duct. In snakes evaluated in October and November, the deferent duct and the renal efferent vein were dorsal to the testicle, presumably as a result of testicle enlargement.

Small intestine

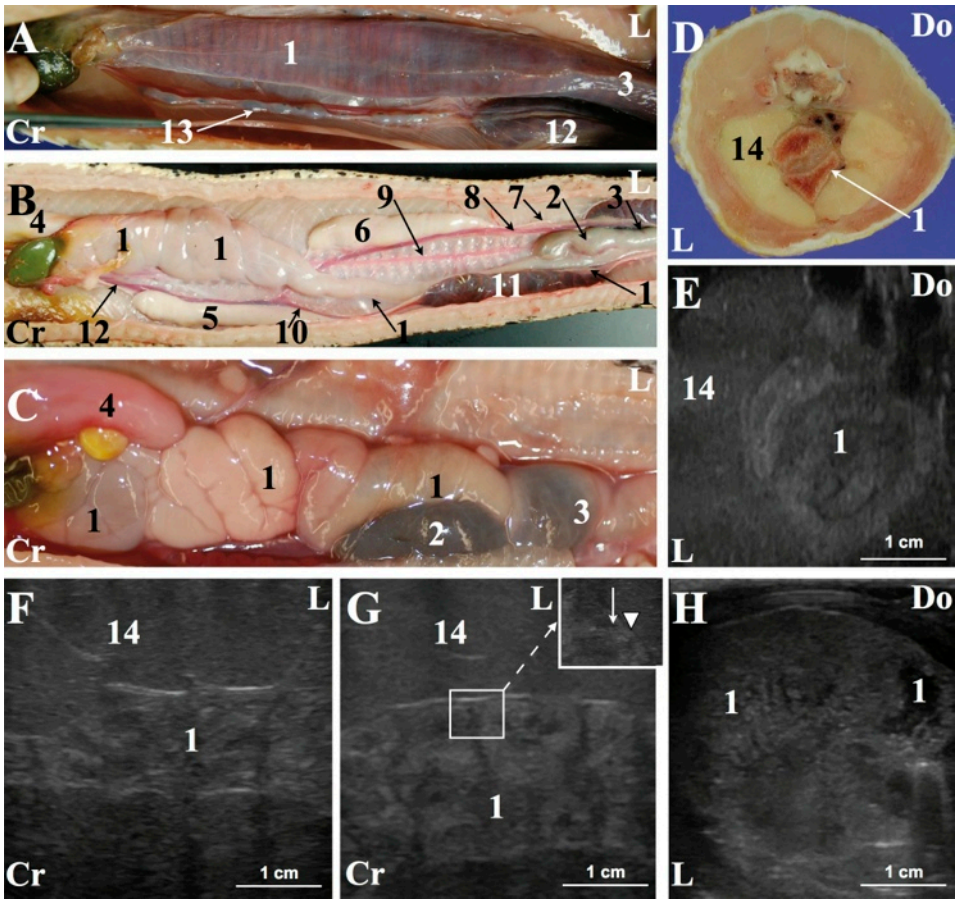

Figure 7—Representative photographs (A–D) and ultrasonographic images (E–H) of the internal organs of boid snakes. A, B, and C—Grossly dissected female Ball python (A), male boa constrictor (B), and male *P curtus* (C), with fat bodies removed to show the small intestine. D—Cross-section of the small intestine of a male Indian rock python. E—Transverse ultrasonographic image of the intestine of a female boa constrictor from which food had been withheld. F—Longitudinal ultrasonographic image of the intestine of a male boa constrictor from which food had been withheld. G—Longitudinal ultrasonographic image of the intestine of a recently fed female boa constrictor. Inset—External hypoechoic layer (arrowhead) and internal nonhomogeneous layer (arrow) of the small intestine wall. H—Transverse ultrasonographic image of the intestine of a recently fed male boa constrictor. 1 = Small intestine. 2 = Caecum. 3 = Large intestine. 4 = Stomach. 5 = Right testicle. 6 = Left testicle. 7 = Left deferent duct. 8 = Right renal efferent vein. 9 = Aorta. 10 = Left renal efferent vein. 11 = Right kidney. 12 = Hepatic vein. 13 = Right ovary. 14 = Fat body. *See* Figure 2 for remainder of key.

The small intestine was identified in all snakes. The small intestine in snakes from which food had been withheld ranged from completely rectilinear (Ball pythons; **Figure 7**) to highly convoluted in the proximal portion of the tract and rectilinear in the distal portion (boa constrictors and Indian rock pythons). The small intestine had few similarities to that of mammals; the typical stratification recognized in mammalians was not appreciable. Only 2 layers could be identified: a thin, external anechoic-hypoechoic layer (the tunica muscularis) and a thick, nonhomogeneous, internal echoic layer (the mucosa). In longitudinal scans, the structures of the intestine became more evident than in transverse scans and the loops could be easily identified. Although an accurate description of the ultrasonographic intestinal changes related to feeding and food withholding were

beyond the scope of the present study, it was apparent that the intestinal mucosa of recently fed snakes was thicker than that of snakes from which food had been withheld.

Pancreas-Spleen-Gallbladder

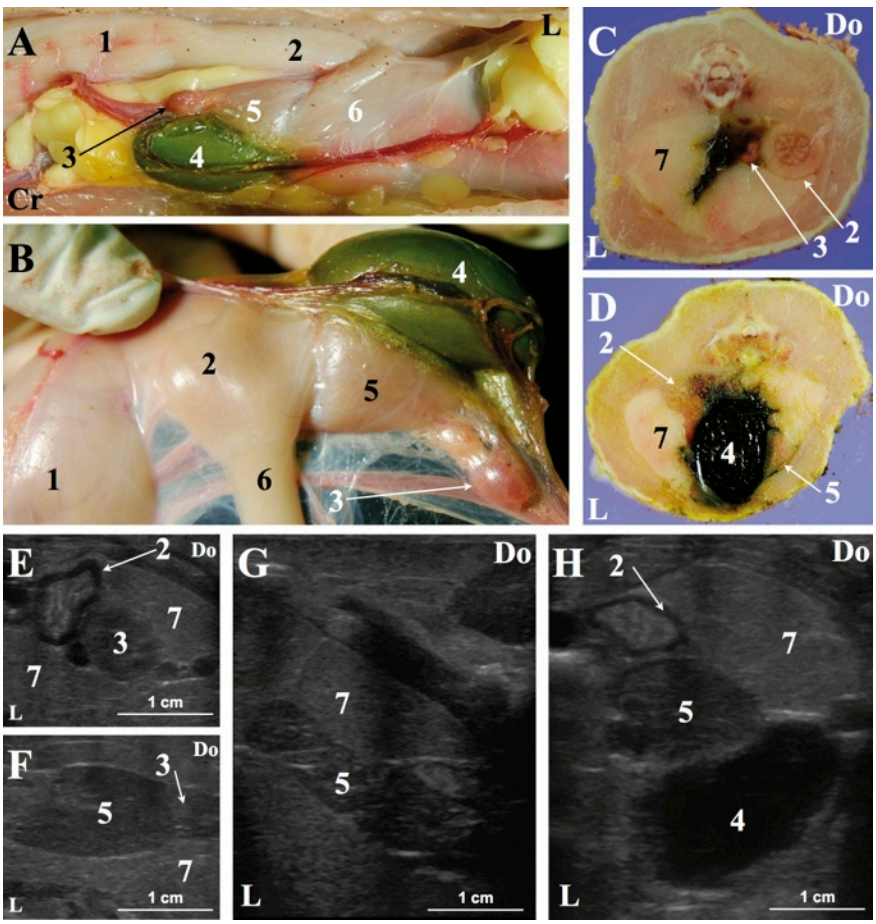

Figure 8— Representative photographs (A–D) and ultrasonographic image (E–H) of the internal organs of boid snakes. A—Grossly dissected male boa constrictor (fat bodies partially removed) showing the pyloric region. B—Detail of the pylorus, spleen, pancreas, and gallbladder of a grossly dissected male boa constrictor. C—Cross-section at spleen level of a male Indian rock python. D—Cross-section at gallbladder-pancreas level of a male Indian rock python. E—Transverse ultrasonographic image of the spleen of a female boa constrictor. F—Transverse ultrasonographic image of the pancreas of a female boa constrictor. G—Transverse ultrasonographic image of the pancreas of a female Indian rock python. H—Transverse ultrasonographic image of the pancreas, gallbladder, and pylorus of a male boa constrictor. 1 = Stomach. 2 = Pylorus. 3 = Spleen. 4 = Gallbladder. 5 = Pancreas. 6 = Small intestine. 7 = Fat body. *See* Figure 2 for remainder of key.

The gallbladder was visible in all snakes when a left lateral approach to probe placement was used to overcome the distal shadowing artifact caused by the caudal portion of the right lung **(Figure 8)**. The gallbladder was separated from the liver and located ventrolateral to the pylorus, pancreas, and spleen. It appeared oval in shape, with its long axis parallel to the midline in all snakes examined. Small amounts of echogenic, non-shadowing, suspended material were present in 36 of the 46 snakes; no interspecies differences were evident. The pancreas was identified medial to the gallbladder and caudal to the spleen in all snakes (Figure 8). The echotexture of the parenchyma was coarse and more hypoechoic than the surrounding structures (fat bodies). No

interspecies differences were detected in the pancreatic echogenicity and echotexture. In Ball pythons, *P curtus*, and boa constrictors, the shape of the pancreas was almost round in longitudinal and transverse scans. It was elongated in transverse scans and round in longitudinal scans involving Indian rock pythons. No differences between fed snakes and snakes from which food had been withheld were noticed. The spleen could be identified in only 2 Indian rock pythons (1 male and 1 female) and 2 female boa constrictors (Figure 8). Identification of the spleen was challenging; gas inside the stomach or the small size of the organ limited visibility. In our experience, the spleen was identified in transverse scans when moving the transducer craniolaterally, starting from the pancreas. The resulting echogenicity of the spleen was lower than that of the pancreas. Splenic echotexture resembled that of a mammalian lymph node except for the presence of multiple hyperechoic lines (the perilymphoid fibrous zone), giving the organ a honeycomb appearance. The spleen appeared round and firmly secured to the pancreas in transverse and longitudinal scans.

Stomach, pylorus, and oesophagus

The stomach was visible in all snakes when a left lateral approach was used (Figures 8–**10**). The pylorus was easily identifiable medial and dorsal to the gallbladder. Remarkable interspecies differences were noticed in the shape of the stomach; in Ball pythons, Indian rock pythons, and boa constrictors, the stomach was saccular, located within the left side of the coelomic cavity and with its long axis parallel to body midline. On the other hand, in *P curtus*, the stomach had a more convoluted shape than in the other species. The distinction between stomach and pylorus was more evident in *P curtus* as well. The stomach and pyloric wall had only 2 layers: a thin external echoic layer and a thick internal anechoic layer. Gastric folds were quite evident both in longitudinal and transverse scan. Snakes lack cardias. Significant positive correlations were detected between body weight and gastric wall thickness ($r = 0.31$; $P = 0.002$) and body length and gastric wall thickness ($r = 0.32$; $P < 0.001$). Moreover, a significant positive correlation was detected between body weight

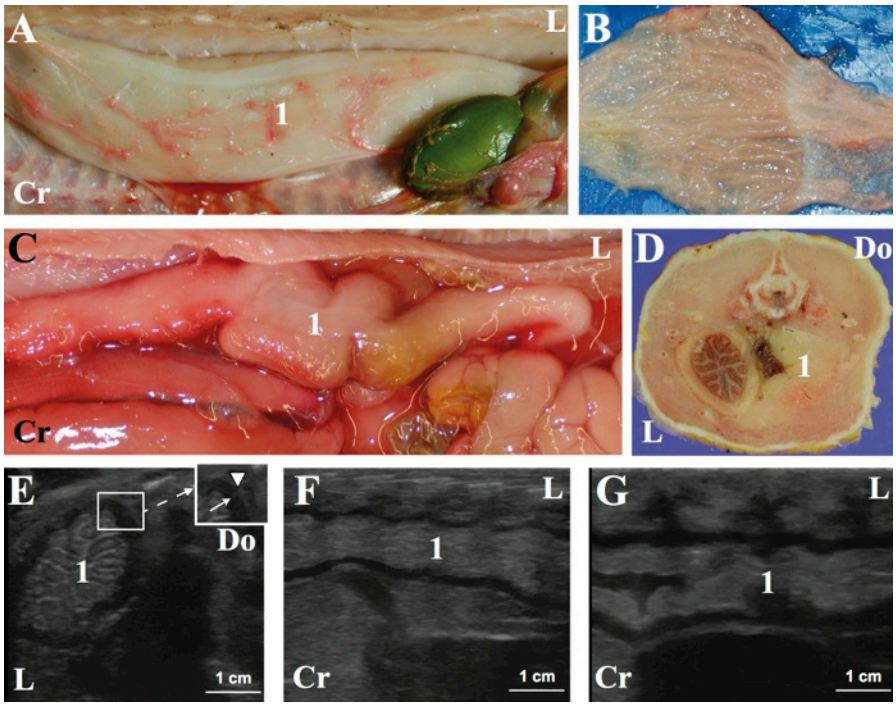

Figure 9—Representative photographs (A–D) and ultrasonographic image (E and F) of the internal organs of boid snakes. A—Grossly dissected male boa constrictor (fat bodies removed) . B—Internal aspect of the stomach of the same snake as in panel A. C—Grossly dissected (fat bodies removed) female *P curtus*. D—Cross-section of the stomach of a male Indian rock python. E—Transverse ultrasonographic image of the stomach of a male *P curtus*. Inset—External echoic layer (arrowhead) and internal anechoic layer (arrow) of the stomach. F—Longitudinal ultrasonographic image of the stomach of a female boa constrictor. G—Longitudinal ultrasonographic image of the stomach of a male *P curtus*. 1 = Stomach. *See* Figure 2 for remainder of key.

and pyloric wall thickness (*r* = 0.17; *P* = 0.024) and body length and pyloric wall thickness (*r* = 0.22; *P* = 0.091). The esophagus (Figure 9) was visible only in transverse scans in 3 Ball pythons (1 male and 2 females), 3 female *P curtus*, 4 Indian rock pythons (3 males and 1 female), and 1 male boa constrictor. The precardiac tract of the esophagus was difficult to see, likely because of the thin wall and the absence of internal material in healthy animals. The postcardiac tract of the esophagus could be identified in some snakes, but the concurrent presence of the lungs and the intrinsic mobility of the organs made its identification somewhat difficult. The esophagus appeared round with its wall comprised of 2 concentric layers: an external echoic and internal anechoic layer.

Liver

In most snakes, the liver was identified in the second third of the snake body when a ventral approach to probe placement was used (Figure 9). The liver had a mammalian-like echotexture but echogenicity could not be compared with that in mammals because neither fat bodies nor parenchymal organs were present in this region. Small round structures with hyperechoic walls,

resembling mammalian portal vessels, were often visible in the parenchyma. Both the posterior vena cava running on the ventral surface of the liver and the hepatic vein on the dorsal surface were visible in all snakes. In transverse scans, the liver appeared oval in shape; a hyperechoic line was visible on the medial surface of the liver at the interface between liver and lungs. In longitudinal scans, the liver appeared as a straight parenchymal organ with an even border in all snakes.

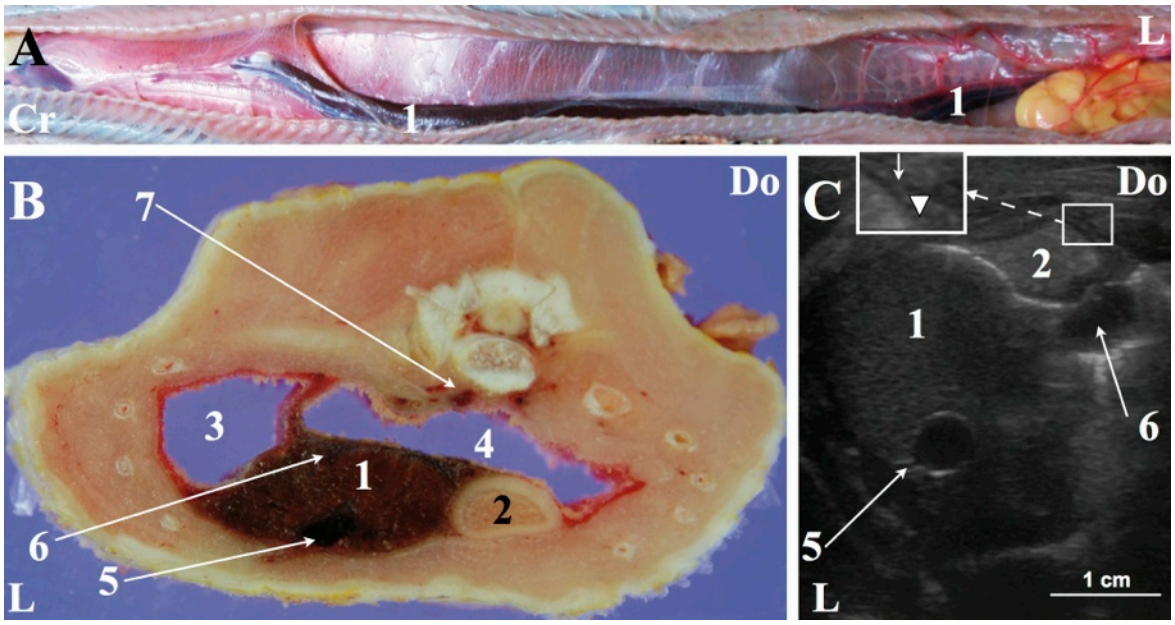

Figure 10—Representative photographs (A and B) and ultrasonographic image (C) of the internal organs of boid snakes. A—Grossly dissected male boa constrictor showing the lungs and liver. B—Cross-section of the lungs and liver of a male Indian rock python. C—Transverse ultrasonographic image of the liver and esophagus of a male *P curtus*. Inset—External echoic layer and internal anechoic layer (arrowhead) of the esophagus. 1 = Liver. 2 = Esophagus. 3 = Left lung. 4 = Right lung. 5 = Hepatic vein. 6 = Posterior vena cava. 7 = Aorta. *See* Figure 2 for remainder of key.

Coelomic cavity and fat bodies

Fat bodies occupying the ventral part of the coelomic cavity except for the lung and neck regions were visible in all snakes, with a constant distribution throughout the body of the species examined (Figure 5–7). Fat bodies had a higher echogenicity than the surrounding parenchyma and a fine echotexture. All *P curtus* had large fat bodies, compared with fat bodies in the other species examined. Small amounts of free fluid within the coelomic cavity were identified in 1 male Ball python, 3 female *P curtus*, 1 male boa constrictor, and 1 female boa constrictor.

Table 1— Scent gland diameter, colonic wall thickness, gastric wall thickness, and pyloric wall thickness of 16 Ball pythons (*Python regius*), 10 Indian rock pythons (*Python molurus molurus*), 12 *Python curtus*, and 8 boa constrictors (*Boa constrictor imperator*).

	Scent glands diameter (cm)		Colonic wall thickness (cm)		Gastric wall thickness (cm)		Pyloric wall thickness (cm)	
Species	Mean ± SD	Range	Mean ± SD	Range	Mean ± SD	Range	Mean ± SD	Range
Ball python	0.27 ± 0.09	0.22–0.33	0.13 ± 0.40	0.11–0.16	0.17 ± 0.07	0.14–0.30	0.21 ± 0.09	0.16–0.28
Indian rock python	1.2 ± 0.35	1.2–0.30	0.19 ± 0.07	0.14–0.24	0.28 ± 0.1	0.24–0.35	0.25 ± 0.09	0.17–0.33
Python curtus	0.44 ± 0.18	0.24–0.63	0.20 ± 0.07	0.15–0.23	0.28 ± 0.09	0.23–0.35	0.24 ± 0.08	0.20–0.32
Boa constrictor	0.40 ± 0.17	0.25–0.59	0.16 ± 0.06	0.12–0.22	0.25 ± 0.09	0.20–0.32	0.24 ± 0.09	0.18–0.30
All species)n = 46)	0.43 ± 0.21	0.14–1.20	0.17 ± 0.05	0.10–0.30	0.24 ± 0.07	0.11–0.35	0.25 ± 0.06	0.17–0.35

Discussion

The existing literature on ultrasonographic examination of boa constrictors describes a ventral approach to overcome shadowing artifact produced by the ribs.[5] In the study reported here, a dorsolateral approach to probe placement was used to scan most coelomic organs (only the liver and the vagina required a ventral approach because of shadowing produced by the lungs for the liver and by the colon for the vagina). In our opinion, a ventral approach leads to 2 problems. For one thing, such an approach is uncomfortable for snakes and so chemical restraint becomes necessary. For another, the fat bodies present, mostly in the ventral aspect of the coelomic cavity, reduce image quality (particularly in large snakes). The heart was not evaluated because comprehensive reports[19,20] of echocardiographic findings in snakes already exist. The results of the present study suggested that a complete ultrasonographic examination of the coelomic cavity of boa constrictors, *P curtus*, Ball pythons, and Indian rock pythons can be easily performed and that ultrasonography can be used as a routine diagnostic tool in these species. Although the ability to use ultrasonography in the evaluation of reptilian species is considered important,[21,22] the large number of these species and the lack of references hinder provision of high-quality veterinary services in reptile medicine. We believe the diagnosis of many diseases of snakes, such as egg retention, abscesses, tumors,

gastroenteritis, renal diseases, and intestinal occlusions, could be improved by the standardization of an ultrasonographic technique. Statistical analysis revealed significant positive correlations between the diameters and thickness of scent glands, gastric and pyloric walls, and colonic wall with body weight and body length in the present study. Moreover, as a consequence of the small intraspecific variation (SD) in the thickness of the colonic, gastric, and pyloric walls among examined snakes, we propose that the values reported here (Table 2) can be used as reference values for those species.

Comparison of the present findings with existing literature[2] on typical ultrasonographic findings in green iguanas reveals some similarities. Seasonal changes exist in the aspect and topography of the gonads, particularly the interposition of the testicles and ovaries between the pylorus and the coelomic wall during the breeding season, and in pyloric and gastric wall layering. The seasonal changes of the dimensions of the gonads described here pertain to captive snakes. For most reptiles (particularly temperate species), reproductive behavior commences in spring after a seasonal cooling.[23] Tropical boid snakes such as boas and pythons usually breed during the cooler seasons.[24] It is so possible that the seasonal changes of the gonads could differ from that described at different latitudes. For captive snakes, environmental conditions are largely controlled by the owners and the breeding season can be modified by controlling the environmental temperature.[22] The findings reported here may not pertain to the ultrasonographic features of the coelomic organs of other snake species. These features could also differ from those of snakes that live in the wild as a result of a more varied diet, different habitat, and greater genetic variation.

References

1. Animal Diversity Web. Boa constrictor. Available at: animaldiversity.ummz.umich.edu/site/accounts/information/Boa_constrictor.html. Accessed Jul 6, 2010.
2. Holland MF, Hernandez-Divers S, Frank PM. Ultrasonographic appearance of the coelomic cavity in healthy green iguanas. *J Am Vet Med Assoc* 2008;233:590–596.
3. Valente A, Parga ML, Espada Y, et al. Normal ultrasonographic imaging of the loggerhead sea turtle (*Caretta caretta*). *Vet Rec* 2007;161:226–232.
4. Sainsbury AW, Gili C. Ultrasonographic anatomy and scanning technique of the coelomic structures of the bosc monitor (*Varanus exantematicus*). *J Zoo Wildl Med* 1991:421–433.
5. Isaza R, Ackerman N, Jacobson ER. Ultrasonographic imaging of the coelomic structures in the Boa constrictor. *Vet Radiol Ultrasound* 1993;34:445–450.
6. O'Malley B. *Clinical anatomy and physiology of exotic species: structure and function of mammals, birds, reptiles and amphibians*. Philadelphia: Saunders Ltd, 2005.
7. Zippel KC, Lillywhite HB, Mlanidich CRJ. New vascular system in reptiles: anatomy and postural hemodynamics of the vertebral venus plexus in snakes. *J Morphol* 2001;250:173–184.
8. Van Bourgondien TM, Bothner RC. A comparative study of the arterial system of some New World Crotalinae (Reptilia: Ophidia). *Am Midl Nat* 1969;81:107–147.
9. Blackburn GD. Structure, function and evolution of the oviducts of squamate reptiles, with special reference to viviparity and placentation. *J Exp Zool* 1998;81:560–617.
10. Van Onderwijs M, En Wetenschappen K. Some notes upon the anatomy of *Tropidophis* and *Trachyboa* (Serpentes). *Zool Meded* 1951;331:108–124.
11. Divers SJ, Lawton MP, Wyneken J. Surgical anatomy of the Serpentine (Colubridae and Boidae) kidney with particular regard to surgical nephrectomy, in *Proceedings*. Assoc Reptil Amphib Vet 1999;175–178.
12. Tanaka Y. Structure of the reptilian spleen. In: Gans C, Abbot S, eds. *Biology of the reptilia*. Vol 19. Ithaca, NY: Society for the Study of Amphibians and Reptiles, 1998;533–580.
13. Miller RM, Lagios MD. The pancreas. In: Gans C, Parson S, eds. *Biology of the reptilia*. Vol 3. London: Academic Press, 1970;319–324.
14. Gardner LW. The thyroid. In: Gans C, Parsons, Thomas TS, eds. In: *Biology of the reptilia*. Vol 3. London: Academic Press, 1970;201–234.
15. Fox H. The urinogenital system of reptiles. In: Gans C, Parsons TS, eds. In: *Biology of the reptilia*. Vol 6. London: Academic Press, 1977;24–109.
16. Parsons TS, Cameron JE. Internal relief of the digestive tract. In: Gans C, Parsons TS, eds. In: *Biology of the reptilia*. Vol 6. London: Academic Press, 1977;159–224.

17. Ottaviani G, Tazzi A. The lymphatic system. In: Gans C, Parsons TS, eds. *Biology of the reptilia*. Vol 6. London: Academic Press, 1977;315–322.
18. Young A, Marsit C, Melzer K. Comparative morphology of the cloacal scent glands in snakes (Serpentes: Reptilia). *Anat Rec* 1999;256:127–138.
19. Schillinger L, Tessier D, Pouchelon JL, et al. Proposed standardisation of the two-dimensional echocardiographic examination in snakes. *J Herpet Med Sur* 2006;16:90–102.
20. Snyder PS, Shaw NG, Heard DJ. Two-dimensional echocardiographic anatomy of the snake heart (*Python molurus bivittatus*). *Vet Radiol Ultrasound* 1999;40:66–72.
21. Silverman S. Diagnostic imaging. In: Mader DR, ed. *Reptile medicine and surgery*. 2nd ed. Philadelphia: WB Saunders Co, 2006;487–488.
22. Schumacher J, Toal RL. Advanced radiography and ultrasonography in reptiles, in *Proceedings*. 10th Semin Avian Exot Pet Med 2001;162–168.
23. Seigal RA, Ford NB. Reproductive ecology. In: Seigal RA, Collins IT, Novak SS, eds. *Snakes: ecology and evolutionary biology*. New York: MC Graw Hill, 1987.
24. Denaro D. Reproductive biology. In: Mader DR, ed. *Reptile medicine and surgery*. 2nd ed. Philadelphia: WB Saunders Co, 2006;378–379.

CHAPTER VII

GASTROINTESTINAL CONTRAST STUDIES IN THE BALL PYTHON

This chapter was adapted from: Banzato T, Russo E, Finotti L, Zotti A. Development of a technique for contrast radiographic examination of the gastrointestinal tract in ball pythons(Python regius). *American Journal of Veterinary Research* 2012;73:997-1001.

Abstract

The objective of this paper is to develop a technique for radiographic evaluation of the of the gastrointestinal tract in ball pythons (*Python regius*). 10 ball python cadavers (5 males and 5 females) and 18 healthy adult ball pythons (10 males and 8 females) have been used. Snakes were allocated to 3 groups (A, B, and C). A dose (25 mL/kg) of barium sulfate suspension at 3 concentrations (25%, 35%, and 45% [wt/vol]) was administered through an esophageal probe to groups A, B, and C, respectively. Each evaluation ended when all the contrast medium had reached the large intestine. Transit times through the esophagus, stomach, and small intestine were recorded. Imaging quality was evaluated by 3 investigators who assigned a grading score on the basis of predetermined criteria. Statistical analysis was conducted to evaluate differences in quality among the study groups. The esophagus and stomach had a consistent distribution pattern of contrast medium, whereas 3 distribution patterns of contrast medium were identified in the small intestine, regardless of barium concentration. Significant differences in imaging quality were detected among the 3 groups. Radiographic procedures were tolerated well by all snakes. The 35% concentration of contrast medium yielded the best imaging quality. Use of contrast medium for evaluation of the cranial portion of the gastrointestinal tract could be a reliable technique for the diagnosis of gastrointestinal diseases in ball pythons. However, results of this study may not translate to other snake species because of variables identified in this group of snakes.

Introduction

Snakes, similar to other animals that feed at irregular prolonged intervals, have a complex digestive physiologic process. However, in contrast to other animals, they have pronounced physiologic and morphological gastrointestinal responses to feeding. Comprehensive studies[1–3] have been conducted on the digestive physiology of snakes. However, to our knowledge, no detailed studies have been performed to evaluate the use of contrast radiography to examine gastrointestinal transit in snakes.

Many gastrointestinal diseases can affect snakes. Most common pathologic conditions are the consequence of husbandry-related problems (temperature too high or too low, unsuitable humidity, or inappropriate cage substrate); stress (loud noises or a paucity of hiding places in a cage); gastrointestinal parasitism; gastroenteritis from viral, fungal or bacterial infections; or intestinal occlusions caused by foreign bodies (pieces of cage substrate [eg, bark, wood chips, gravel, or towels] or impaction, tumors[4,5]). Ileocolic intussusception has also been reported.[6] Similar to these conditions in other nonreptilian species, the signs of gastrointestinal tract disease are nonspecific and include anorexia, emesis, regurgitation, diarrhea, and abdominal distention.[4]

Contrast radiography is a standard procedure for the evaluation of gastrointestinal transit in dogs and cats with vomiting, palpable abdominal masses, signs of acute abdominal pain, or suspected intestinal foreign body.[7] Furthermore, analysis of the literature[8–10] suggests that contrast radiography could also be a useful tool for the diagnosis of disorders of the gastrointestinal tract in reptiles.

The purpose of the study reported here was to develop a technique for radiographic evaluation of the cranial portion of the gastrointestinal tract in ball pythons by the use of contrast medium. In particular, our objectives were to determine the concentration of contrast medium for optimum results and time at which radiographic images should be obtained after administration of contrast medium and to describe radiographic features in this species.

Materials and Methods

Samples

Two evaluations were conducted during the study. The first evaluation involved 10 cadavers of ball pythons, and the second involved 18 live adult ball pythons. Informed consent was obtained from all clients for use of their snakes in the study. The study was conducted under the Approval of the Padua University Ethical Committee.

Anatomic evaluation

The cadavers of 10 ball pythons (5 males and 5 females) with a mean ± SD body weight of 0.9 ± 0.5 kg and mean body length (snout to vent) of 89.4 ± 17.6 cm were used in this experiment. Snakes had died as a result of various causes. Cadavers were stored at –20^{o}C for a mean of 1 month and were dissected prior to the beginning of the experiment. The objective of these dissections was to provide an unambiguous description of the gastrointestinal tract of ball pythons. The gastrointestinal tract of each of the 10 cadavers was carefully analyzed to characterize the anatomic structures, topography, and individual variations.

Radiographic evaluation

Eighteen client-owned healthy ball pythons (10 males and 8 females) were included in the evaluation. Mean ± SD body weight was 1.3 ± 0.4 kg, and mean body length (snout to vent) was 97.2 ± 27.4 cm. Snakes were considered healthy on the basis of medical history and results of a complete physical examination. The study period lasted from June to September 2010.

Radiographic procedures began within 4 hours after each snake was admitted at the Department of Veterinary Clinical Sciences of the University of Padua, Italy. During the radiographic procedures, snakes were housed in plastic cages at a steady environmental temperature of 28°C, which was maintained via air conditioning. All snakes were not fed for at least 7 days (range, 7 to 14 days) before examination. Chemical restraint for the snakes was not needed. The snakes were allocated into 3 groups (groups A, B, and C; 6 snakes/group). A barium sulfate (Barium Sulfate 400gr, Caesar &Lorenz Gmbh, Hilden, Germany) suspension was orally administered (25 mL/kg) as a contrast medium. The suspension was administered at a concentration of 25%, 35%, and 45% (wt/vol) for groups A, B, and C. respectively. Contrast medium was administered through an esophageal probe by manually restraining each snake and gently opening its mouth. A gauze pad was placed over the operator's hand to prevent injury to both the snake and the operator. To obtain comparable results among snakes and to obtain images in which the body of each snake was as straight as possible, each snake was placed in a 6.3-cm-diameter radiolucent pipe; the pipe had been sectioned along its longitudinal axis to enable it to be rapidly opened for insertion of each snake and removal of each snake immediately after the radiographic procedure. Radiographic images were all obtained by use of the same computed radiography device(Kodak point-of-care CR-360 system, Carestream Health Inc, Rochester, NY). Dorsoventral radiographic images were obtained by use of the following settings: 52 to 58 KV (depending on the size of the snake), 300 mA, and 0.02 seconds. No grid was used. An initial snake (included in group A) was used to verify the feasibility of the procedures and to establish an indicative time course for the procedures. We considered the radiographic procedures concluded when all of the contrast medium had reached the large intestine. The initial animal was radiographed at 5, 10, 20, and 30 minutes and 1, 2, 3, 6, 9, 12, 24, 48, and 72 hours after administration of contrast medium. On the basis of results for this initial snake, it was decided that images of all snakes should be obtained at 5 minutes and 1, 2, 3, 6, 9, 12, 24, 48, and 72 hours after administration of contrast medium.

Imaging data analysis

To assess transit time, the radiographic variables ETT, OGF, GET, OSIT, OLIT, and SITT were evaluated. The ETT was defined as the first radiographic time point at which no residual contrast medium was seen in the esophagus. The OGF was defined as the first radiographic time point at which contrast medium could be seen inside the stomach. The GET was defined as the first radiographic time point at which contrast medium was detected leaving the stomach; GET was considered complete when the contrast medium in the stomach consisted of only contrast medium that remained adhered to the gastric folds. The OSIT was defined as the first radiographic time point at which contrast medium could be seen in the small intestine. The OLIT was defined as the first radiographic time point at which contrast medium could be seen in the large intestine. The SITT was defined as the first radiographic time point at which no residual contrast medium was visible in the small intestine; the SITT corresponded to the end of the evaluation. To determine the concentration of contrast medium that provided the best radiographic imaging quality, images were evaluated by 3 investigators (TB, ER, and AZ). Images were assessed on the basis of general distribution of contrast medium (flocculation and segmentation in the small intestine), which were each graded on a scale from 1 to 4 (grade 1 = extremely evident and grade 4 = not detected). Images were also assessed for visibility of esophageal folds, gastric folds, intestinal villi, the pylorus, and superimposed loops of small intestine (when present); these were graded on a scale from 1 to 4 (1 = poor, 2 = fair, 3 = good; and 4 = excellent). When the interpretations of the 3 investigators were not unanimous, a consensus was reached, and that value was used as the final grade. The number of snakes that regurgitated immediately after administration of the contrast medium was recorded as part of the assessment.

Statistical analysis

Because of the small quantity of data, statistical analysis could not be performed to determine whether the transit time was related to barium concentration. Mean ± SD values of transit time for each radiographic variable for each group as well as the entire sample population were reported. Variations in quality of images among the groups were tested with both the Kruskal-Wallis test for the 3 groups and Dunn multiple comparison test to compare the groups in pairs. Mean ± SD for each group and the entire sample population were reported. All analyses were performed by use of commercially available software(GraphPad Prism, version 4.00 for Windows, GraphPad Software Inc, San Diego, Calif). Values of $P < 0.05$ were considered significant.

Results

Anatomic evaluation

Gross anatomic findings related to the esophagus and stomach were consistent among all the cadavers. However, both the gross appearance and topography of the small intestine differed among the cadavers. The esophagus appeared as a long structure starting at the base of the head and ending at the caudal lobe of the left lung **(Figure 1)**. The stomach appeared as a saccular structure starting at the caudal lobe of the left lung and extending beyond the caudal lobe of the right lung **(Figure 2)**. Gross anatomic variability was detected in the small intestine **(Figure 3)**. Aspects of intestinal loops and villi visible in some cadavers differed from an almost straight small intestine with less evident villi detected in other cadavers.

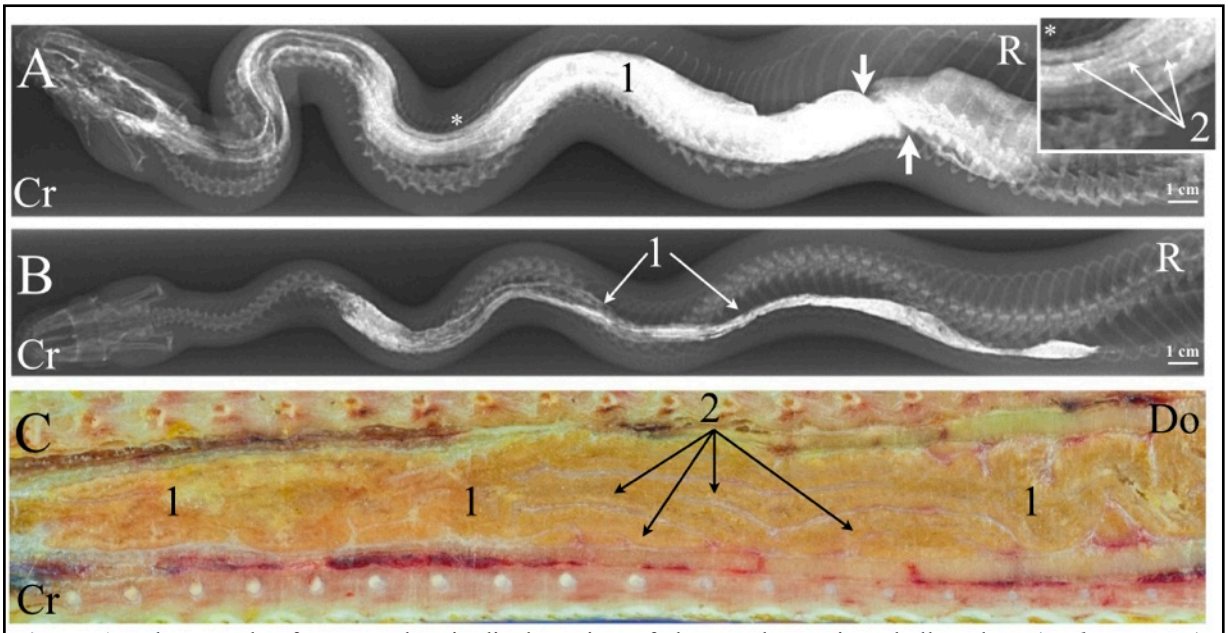

Figure 1—Photograph of a gross longitudinal section of the esophagus in a ball python (*Python regius*) cadaver (A) and dorsoventral radiographic views of the esophagus of a live ball python 5 minutes (B) and 1 hour (C) after oral administration of contrast medium. Notice the appearance of the esophagus (1) and the esophageal folds (2). At 5 minutes after administration of the contrast medium, there is normal dilation of the esophagus (large white arrows). In the inset, there is a larger view of the normal-appearing esophageal folds. Cr = Cranial. Do = Dorsal. R = Right. In panels B and C, bar = 1 cm.

Radiographic evaluation

The esophagus, stomach, and small and large intestines were easily identified, regardless of the concentration of contrast medium. Distribution patterns of contrast medium in the esophagus and stomach were consistent among all snakes, whereas the radiographic patterns differed in the small intestine, regardless of the concentration of contrast medium. Long longitudinal esophageal folds were often visible as thin, parallel, undulated filling defects within the organ. Dilation of the esophagus was visible in all snakes at the first radiographic time point (5 minutes after administration of contrast medium). Segmentation in the esophagus was a consistent finding and likely was a result of peristaltic activity associated with a long ETT (Figure 1). However, flocculation was not evident in the esophagus, despite a long ETT. Peristaltic activity of the stomach was evident in 15 of 18 snakes. The gastric folds were visible as thick longitudinal filling defects within the stomach (Figure 2). Reflux from the stomach to the esophagus was not observed; moreover, the gastric folds appeared to be extremely tight in the cranial portion of the stomach. The pylorus was identified in all snakes as the terminal part of the stomach. The pylorus appeared oval

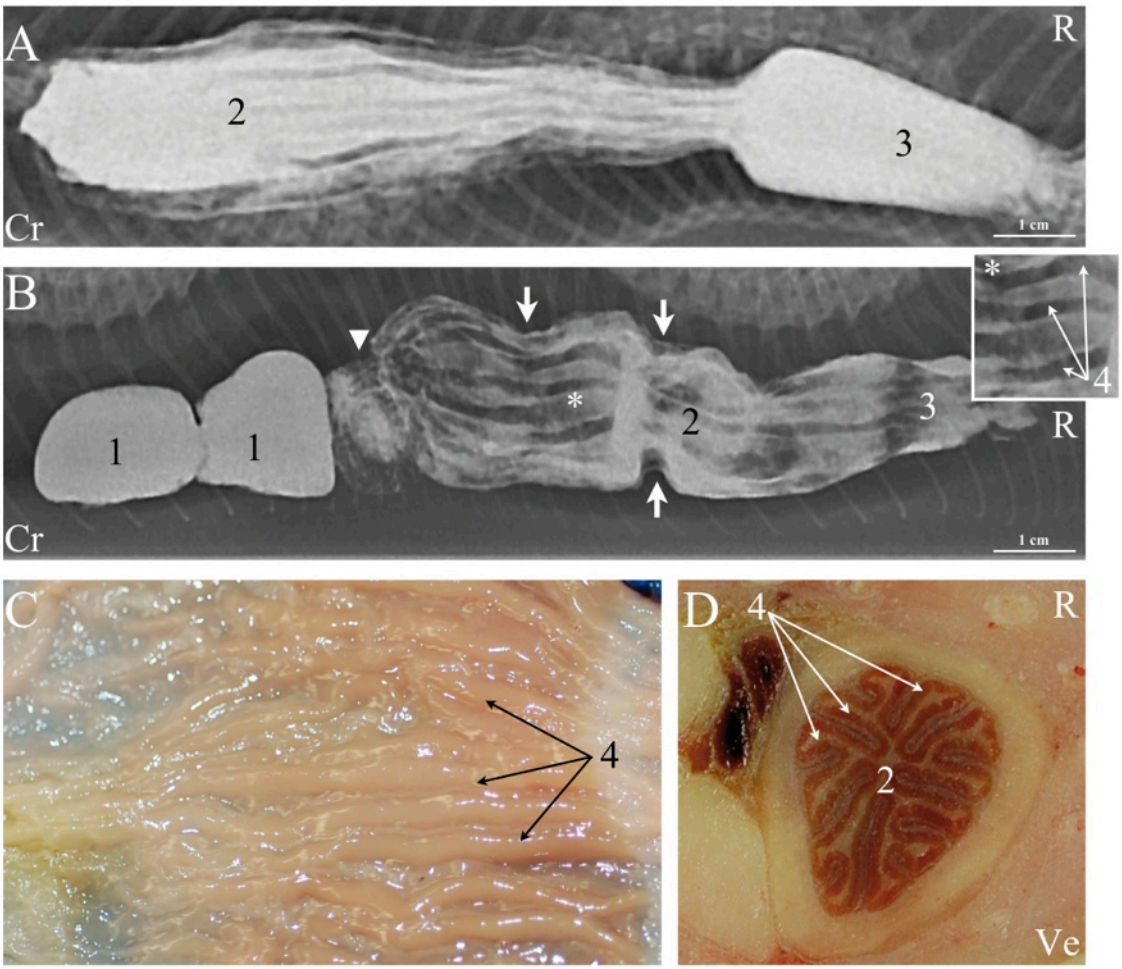

Figure 2—Photographs of the gross appearance of the internal surface of the stomach (A) and a transverse cross section of the stomach (B) in the cadaver of a ball python and dorsoventral radiographic views of the stomach of a live python 1 hour after oral administration of contrast medium (C and D). In the cadaver, Nnotice the esophagus gastric folds (1), stomach stomach (2), stomach pylorus (3), and gastric foldsesophagus (4). In panel C, the pylorus appears round. In panel D, the pylorus appears elongated and there is evidence of peristaltic waves (large white arrows) and an unusual pattern of gastric folds in the proximal portion of the stomach (white arrowheads). In the inset, there is an enlarged view of the normal-appearing gastric folds. The pylorus appears elongated. Ve = Ventral.

shaped in some snakes, whereas it was more elongated in other snakes. Similar to the gross anatomic findings, the distribution pattern for contrast medium in the small intestine was rather inconsistent among the live snakes, regardless of the concentration of contrast medium administered. Nevertheless, image analysis allowed the identification and description of 3 distribution patterns for the contrast medium, with each pattern characterized by common radiographic features. Distribution pattern 1 was observed in 4 snakes (1 snake in group A, 2 snakes in group B, and 1 snake in group C **[Figure 4]**). The OSIT started during the first radiographic time point (5 minutes after administration of contrast medium). The intestinal loops and the villi were

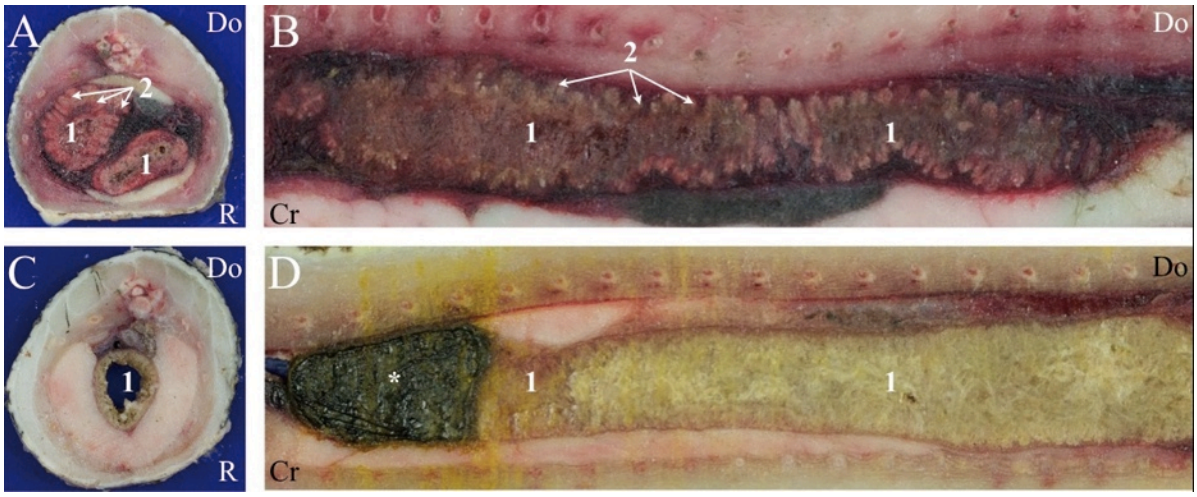

Figure 3—Photographs of a transverse section (A and C) and longitudinal section (B and D) of the small intestine (1) of the cadaver of a ball python. In panels A and B, notice the intestinal loops and evident villi (2). In panels C and D, notice that the villi are less evidentce and the small intestine has a rectilinear appearance. The gallbladder is indicated (asterisk).
See Figure 1 for remainder of key.

evident during the entire transit through the small intestine. There was a clear distinction between the small and large intestine.

Distribution pattern 2 was observed in 6 snakes (3 snakes in group A, 1 snake in group B, and 2 snakes in group C **[Figure 5]**). The OSIT started during the first radiographic time point. The contrast medium outlined less evident intestinal loops in addition to an overall more rectilinear appearance of the small intestine. Villi were clearly evident until 24 hours after administration of contrast medium). There was a clear distinction between the small and large intestine. Distribution pattern 3 was observed in 8 snakes (2 snakes in group A, 3 snakes in group B, and 3 snakes in group C **[Figure 6]**). The OSIT started during later radiographic time points (3 to 6 hours after administration of contrast medium). Furthermore, the contrast medium did not outline any recognizable intestinal structures (ie, intestinal loops or villi). The contrast medium was completely segmented and there was diffuse flocculation. The distinction between the small and large intestine could only be detected on the basis of thickness and amount of contrast medium. Mean ± SD values of the transit time were determined for each radiographic variable **(Table 1)**. To provide a more graphic representation of transit of contrast medium in relation to time, the number of snakes in which contrast medium was detected in the esophagus, stomach, small intestine, and large intestine

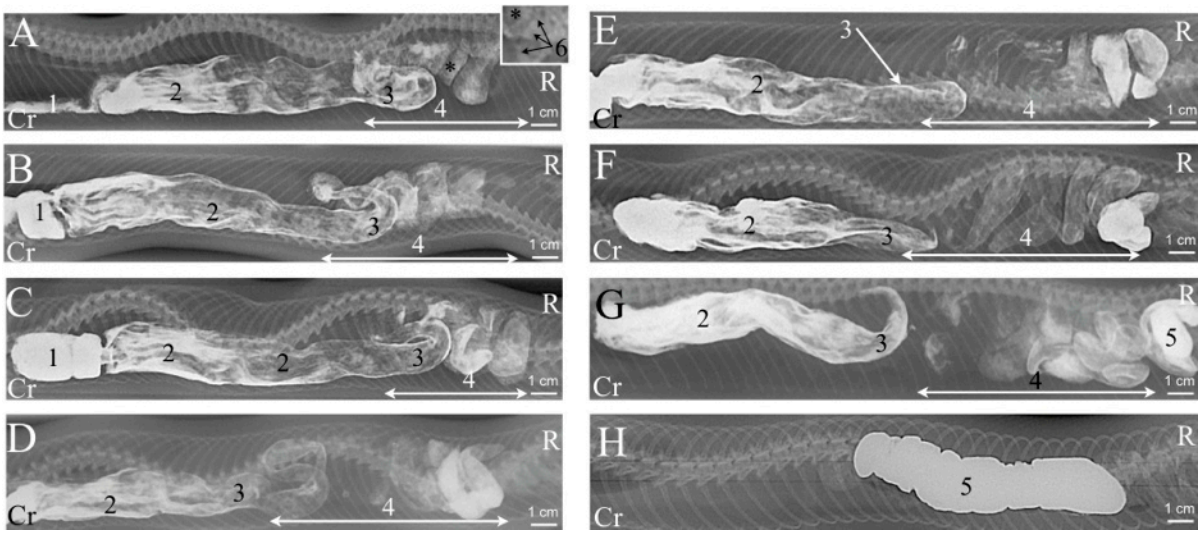

Figure 4—Dorsoventral radiographic views of the small intestine of a python in group A at 5 minutes and 3, 6, 9, 12, 24, 48, and 72 hours (A through H, respectively) after oral administration of contrast medium at a concentration of 25% (wt/vol). Distribution of the contrast medium was defined as distribution pattern 1 (evident villi and intestinal loops). The inset provides an enlarged view of the normal-appearing intestinal villi. Notice the esophagus (1), stomach (2), pylorus (3), small intestine (4), large intestine (5), and intestinal villi (6). Bar = 1 cm.
See Figure 1 for remainder of key.

at each radiographic time point were plotted **(Figure 7)**. The mean ± SD values for the assessments performed by the investigators and differences among the 3 groups were summarized **(Table 2)**. Flocculation was detected in all 3 groups; however, values did not differ significantly among groups. Segmentation appeared to decrease as the concentration of barium increased. Group A had a significantly higher segmentation pattern than did the other 2 groups. Esophageal and gastric folds were similarly visible in group A and group B but became less evident in group C. The pylorus was clearly visible in all 3 groups. Visibility of small intestinal villi did not differ significantly among the 3 groups. Visibility of the superimposed intestinal loops was good and did not differ significantly among the 3 groups.

Regurgitation of contrast medium

One snake in group A, 2 snakes in group B, and 1 snake in group C regurgitated a small amount of contrast medium immediately after administration. None of the snakes regurgitated contrast medium later during the study.

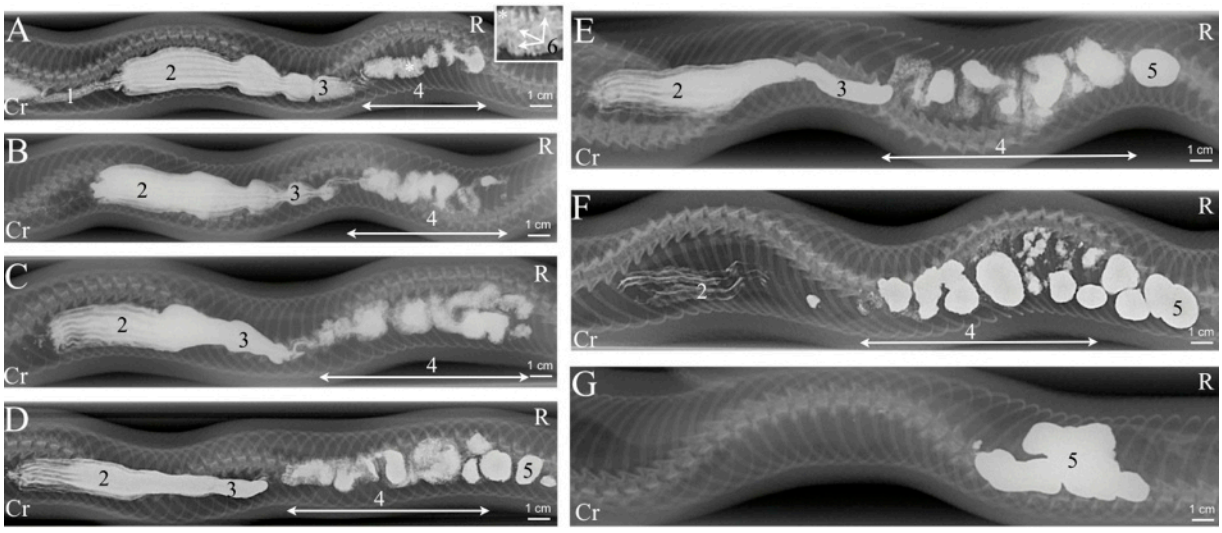

Figure 5—Dorsoventral radiographic views of the small intestine of a python in group B at 5 minutes and 3, 6, 9, 12, 24, and 48 hours (A through G, respectively) after oral administration of contrast medium at a concentration of 35% (wt/vol). Distribution of the contrast medium was defined as distribution pattern 2 (evident villi and less-evident intestinal loops with an overall rectilinear appearance of the small intestine). Bar = 1 cm.
See Figure 5 for remainder of key.

Discussion

The radiographic procedure described in the study reported here was tolerated well by all snakes. Administration of contrast medium was easy to perform and a relatively safe procedure, although it must be mentioned that all the snakes in the study were client-owned animals and were used to manipulation. Furthermore, the use of a radiolucent pipe allowed comparable images to be obtained without the need for chemical restraint of the snakes. All snakes had not been fed for at least 7 days, which has been reported as the time necessary for the gastrointestinal tract of pythons to return to a resting phase after feeding.[1] The minimum 1-week period of not feeding was required to obtain comparable results and to reduce the stress of the snakes; snakes are particularly vulnerable to stress during the immediate postfeeding period. The dose of contrast medium administered to the snakes in the present study was the dose used in green iguanas in another study[8]; other authors[10] reported a lower dose for gastrointestinal tract evaluation in reptiles. It is the authors' opinion that the dose used in the study reported here is the most suitable because of the unique capacity for distention of the gastrointestinal tract in snakes.[1–3] The anatomic outline of some gastrointestinal tract organs within the snakes of the present study was extremely good and enabled investigators to view

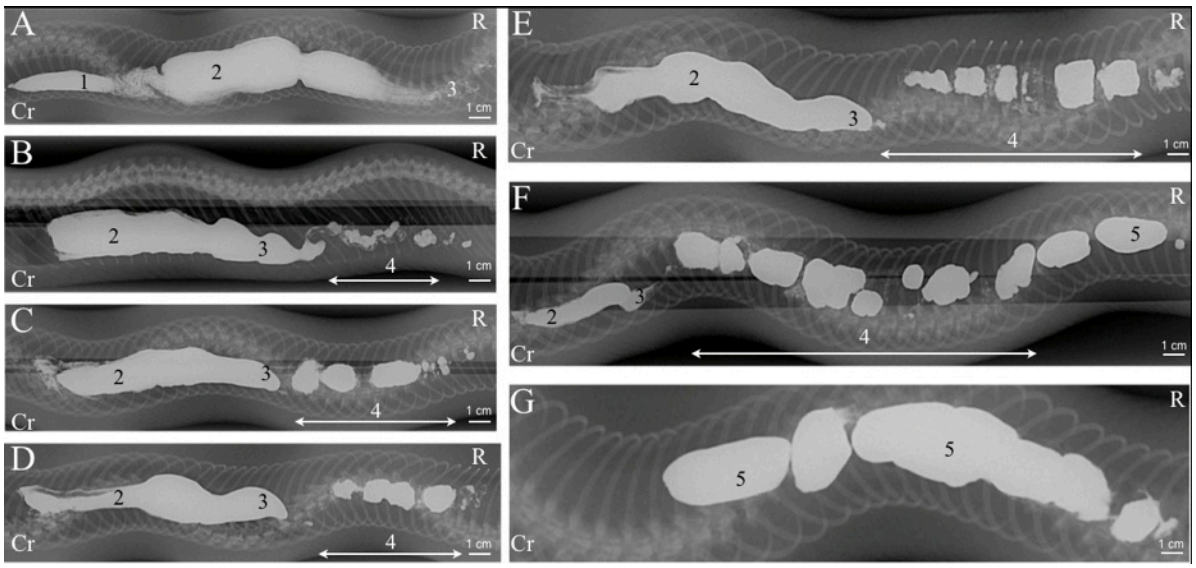

Figure 6—Dorsoventral radiographic views of the small intestine of a python in group B at 5 minutes and 3, 6, 9, 12, 24, and 48 hours (A through G, respectively) after oral administration of contrast medium. Distribution of the contrast medium was defined as distribution pattern 3 (no recognizable structures evident). Radiolucent bands visible in panels B and F are attributable to the presence of free air within a 6.3-cm-diameter radiolucent pipe that was used to help immobilize the snake during the radiographic procedures. Bar = 1 cm. *See* Figure 5 for remainder of key.

structures that typically cannot be visualized in survey radiographs. The consistent appearance of the esophagus and stomach should help veterinary practitioners in detecting anomalies in these organs. Despite the mean ± SD values of the various radiographic variables (Table 1), it is important to notice that the last radiographic time point at which contrast medium was visible inside the stomach of all snaked, except for 1, was 24 hours after administration of contrast medium (Figure 7). Furthermore, the last radiographic time point at which contrast medium was detected within the small intestine was 48 hours after administration of contrast medium.

Snakes are described as not having a cardia portion of the stomach.[11] However, despite the lack of a recognizable specific anatomic structure, the lack of reflux of contrast medium from the stomach to the esophagus suggested the existence of an effective physiologic mechanism that separated the stomach and esophagus. Gross anatomic differences in the small intestine were detected. Three distribution patterns of contrast medium in the cranial portion of the gastrointestinal tract were identified within the snakes of the present study. The 3 radiographic patterns detected in the study may have been related to the gross anatomic findings observed in snakes (snakes have high intraspecific anatomic differences, some of which even involve the lungs[12]). Another possible

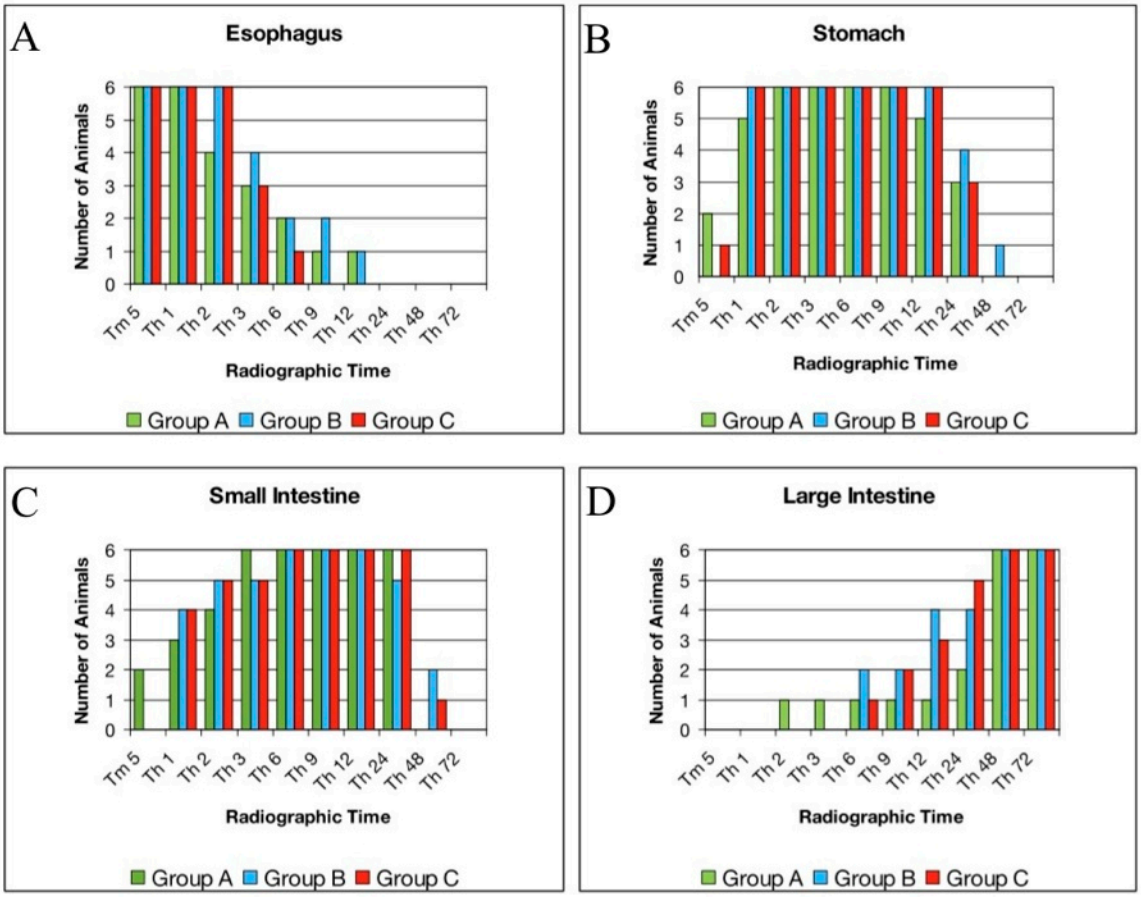

Figure 7—Number of snakes in each of 3 groups (A [black bars], B [gray bars], and C [white bars]) that had contrast medium in the esophagus (A), stomach (B), small intestine (C), and large intestine (D) at various time points after oral administration of contrast medium. A dose (25 mL/kg) of barium sulfate suspension at 3 concentrations (25%, 35%, and 45% [wt/vol]) was administered through an esophageal probe to groups A, B, and C, respectively.

explanation is that they may have been the expression of various gastrointestinal digestive phases or morphological changes attributable to each snake's captivity conditions, regardless of the similar period of no feeding. Snakes are poikilothermic animals, and gastrointestinal transit time and morphological adaptation depend on the species of snake, environmental temperature, seasonal changes, diet, and interval since the last meal.[1–3,10] The present study was conducted under standardized conditions; however, the environmental and nutritional conditions of each snake before entrance into the study could not be controlled and standardized. It was beyond the scope of the present study to determine the nature of the aforementioned gastrointestinal variability. Nevertheless, we believe that the radiographic findings reported may be considered comprehensive of the multiple aspects of clinically normal snakes that should be examined in clinical practice. The imaging data analysis did not reveal significant differences between groups A and B with regard to

visibility of the internal topography of the gastrointestinal tract, whereas the use of a high concentration of contrast medium, as in group C (45% [wt/vol]), reduced visibility of both esophageal and gastric folds. Group A (concentration of contrast medium, 25% [wt/vol]) had a significantly higher value for segmentation than did the other 2 groups. Flocculation was detected in all 3 groups, and this most likely was related to the slow transit from the stomach to the small intestine identified in some snakes, rather than to the concentration of contrast medium administered. On the basis of analysis of the data, the best imaging quality was obtained for group B (concentration of contrast medium, 35% [wt/vol]). Analysis of results of the present study suggested that contrast radiography could be a reliable tool for use in assessing the anatomic and functional aspects of the cranial portion of the gastrointestinal tract in ball pythons. However, the great variability among snakes observed in the study and the differences among snake species[13,14] do not permit the results to be used as a reference for species other than ball pythons, unless the anatomic and physiologic differences are known.

References

1. Secor MS, Diamond J. Adaptative responses to feeding in Burmese pythons: pay before pumping. *J Exp Biol* 1995;198:1313–1325.

2. Stark MJ, Wimmer C. Patterns of blood flow during the postprandial response in ball pythons, *Python regius*. *J Exp Biol* 2005;208:881–889.

3. Cox LC, Secor SM. Matched regulation of gastrointestinal performance in the Burmese python, *Python molurus*. *J Exp Biol* 2008;211:1131–1140.

4. Funk RS. Differential diagnoses divided by symptoms (snakes). In: Mader DR, ed. *Reptile medicine and surgery*. 2nd ed. Philadelphia: WB Saunders Co, 2006;675–677.

5. Latimer KS, Rich GA. Colonic adenocarcinoma in a corn snake (*Elaphe guttata guttata*). *J Zoo Wildl Med* 1998;29:344–346.

6. Wosar MA, Lewbart, GA, Ileocolic intussusception in a pine snake (*Pituophis melanoleucus*). *Vet Rec* 2006;158:698–699.

7. Bradley K. The small intestine. In: O'Brien R, Barr F, eds. BSAVA manual of canine and feline abdominal imaging. New York: Wiley & Sons, 2009;110–131.

8. Smith D, Dobson H, Spence E. Gastrointestinal studies in green iguana: technique and reference values. *Vet Radiol Ultrasound* 2001;42:515–520.

9. Di Bello A, Valastro C, Staffieri F, et al. Contrast radiography of the gastrointestinal tract in sea turtles. *Vet Radiol Ultrasound* 2006;47:351–354.

10. Schumacher J, Toal RL. Advanced radiography and ultrasonography in reptiles, in *Proceedings*. 10th Semin Avian Exot Pet Med 2001;162–168.

11. Parsons TS, Cameron JE. Internal relief of the digestive tract. In: Gans C, Parsons TS, eds. *Biology of the reptilia*. Vol 6. London: Academic Press, 1977;192–212.

12. Van Wallach. The pulmonary system: the lungs of snakes. In: Gans C, Gaunt AS, eds. *Biology of the reptilia*. Vol 19. Ithaca, NY: Society for the Study of Amphibians and Reptiles, 1998;117–126.

13. Holmberg A, Kaim J, Persson A, et al. Effects of the digestive status on the reptilian gut. *Comp Biochem Physiol A* 2003;133:499–518.

14. Xantos X, Llorente GA. Gastrointestinal responses to feeding in a frequently feeding colubrid snake (*Natrix maura*). *Comp Biochem Physiol A* 2008;150:75–79.

GENERAL DISCUSSION

Snakes and lizards include respectively 3378 and 5634 different species[1] and are the most conspicuous reptile taxa, including altogether approximately 95% of all living reptiles species. Great anatomical and physiological differences occur between snakes and lizards and among the different snakes and lizards species.

Lizards are the most widely distributed and the most diverse among reptiles. Great differences occur among the different lizard species regarding the size (the largest living lizard is the Komodo dragon which can be up to three meters long and weigh up to 140 kg, although 80% of lizards weigh less than 20g), alimentary habits (some are almost exclusively carnivorous, some are omnivorous whereas several species are insectivorous), habitat and external conformation[2].

Snakes are a more homogeneous taxon; all snakes lack limbs and all snake species are strictly carnivorous. The dimensions of snake species vary enormously, from the giant species, as for example the green anaconda, to some very small blind snakes, as for example the *Leptotyphlops carlae,* which is the smallest living snake species [3].

The snakes' species object of our experimental works belong to the Pythonidae (*Python regius*, *Python molurus* and *Python curtus*) and Boidae (*Boa constrictor*) families. The main difference between these two families is that the snakes belonging to the Pytonidae family are oviparous whereas the snakes belonging to the Boidae family are ovoviviparous.

For the diagnostic imaging studies in lizards we have chosen the green iguana (*Iguana iguana*; infraorder Iguania, family Iguanidae), the bearded dragon (*Pogona vitticeps*; infraorder Iguania, family Agamidae) and the black and white tegu (*Tupinambis merianae*; infraorder Scincomorpha, family Teiidae). These species are intended to represent an herbivorous, an insectivorous and an omnivorous lizard respectively.

Although some excellent references regarding the anatomy and the physiology[4-8] of reptiles are available, no comprehensive description of the anatomy of the species object of our experimental investigations are available. Therefore, cadavers for each species have been collected for the anatomical studies before performing the diagnostic imaging studies. Some cadavers for each considered species have been dissectioned in order to characterise the normal anatomy. Individual organs have been recognised, with the aid of available references, during the necropsies; in author's experience, this first step is mandatory for a correct interpretation both of the anatomical cross sections and the diagnostic images. Often the existing anatomical references describe similar species to those considered in our experimental studies and a careful anatomical comparison between the species described in literature and the species object of the experimental investigation was done. Moreover, different anatomical references use different terms to describe the same structures; in order to overcome this problem we have decided to use the terminology proposed by the most recent references on every topic.

The radiographic studies performed on the head both of snakes and lizards retrieved high quality images, especially of the bony structures. Nevertheless, some remarkable differences were evident in the visualisation of the soft tissues between snakes and lizards. In the boa constrictors' head only the masticatory muscles and the trachea were evident whereas in the head of the different lizards species several different soft tissues (the masticatory muscles, the trachea, the larynx, the oesophagus, the nasal glands) have been identified. The lack of detail of soft tissues encountered on the boa constrictors' head is likely due to the fact that the radiographic studies have been performed on cadavers. Another possible explanation is that the different conformation of the head of snakes and lizards could lead to a different possibility to visualise the soft tissues by means of radiology.

CT scans of the head of snakes and lizards also retrieved different quality images. In the CT scans of the boa constrictors' head the detail of the soft tissues is low and it is impossible to distinguish the different soft tissues. In the CT scans of the head of lizards, especially in those of the green iguana and the black and white tegu, the soft tissues are well visualised. It is author's opinion that such differences are likely to be related both to the different dimensions of the study subjects and to the fact that by using live animals contrast medium could be used in lizards. Although the usual venous sites for the administration of drugs in lizards are the cephalic or the jugular vein [9], we decided to administer the contrast medium through the caudal vein. To date, the dose of intravenous contrast medium administration in reptiles has been reported only for the descending urography[10-11] (and is actually the same dose of contrast medium indicated in mammals). It is author's opinion that both the dose and the route administration of contrast medium were adequate to produce an acceptable contrast enhancement of the soft tissues. Moreover, the administration of contrast medium through the caudal vein is less traumatic than the administration through the cephalic or jugular vein which require a surgical approach to be catheterised. On the other hand, if using a automated power injector for the administration of contrast medium an intra-venous catheter would become necessary[12]. The high field MRI anatomy of the head of the gartner snake has been described[13]; in comparison with the CT images reported in chapter III, a better resolution of the soft tissues, especially of the brain, is evident in the diagnostic images presented in this paper. To date, the availability of such technology is limited to some specialised research centres. With newer CT devices, with a lower slice thickness and an adjustable field of view it should be possible to obtain better imaging results. In such a scenario, it is the author's belief that the gross and cross sectional anatomical images proposed in chapter 2-3 could be greatly useful for diagnostic imaging purposes.

Due to the paucity of fat interposed to the coelomic organs of snakes and lizards the inner radiographic contrast of the coelomic cavity is low, for this reson only few organs can be evaluated

by means of plain radiographs [5,14]. Other diagnostic imaging modalities, alike US, CT and MRI may play a fundamental role[15-18]. The descriptions of the ultrasonographic anatomy of the green iguana[19], the bosc monitor[20] and the boa constrictor[21] were already present in literature at the beginning of our experimental studies. The normal ultrasonographic features of the coelomic cavity of some snake species, together with the reference values of the dimensions of some selected coelomic structures are reported in Chapter VI. To the best of authors' knowledge no other ultrasonographic reference values in snakes species are reported in literature. To date no comprehensive description of the CT or MRI anatomy of the coelomic cavity of snakes is available so that a comparison between these diagnostic imaging techniques is impossible.

Following the description of the ultrasonographic anatomy of the green iguana[15] and the bosc monitor[16] resulted clear that the peculiar anatomy of this lizards (the large intestine occupies a large part of the coelomic cavity) hindered the visualisation of several coelomic organs suggesting that other diagnostic imaging modalities (such as CT) might provide better imaging results. From this starting point we decided to describe the CT anatomy of three lizards species meaning to represent an herbivorous (the green iguana), an omnivorous (the black and white tegu) and an insectivorous (the bearded dragon) alimentary habit. The CT description of the coelomic cavity retrieved very good imaging results (specially in the green iguana) and allowed a thorough visualisation of most of the coelomic structures thus overcoming the major limitations encontered both with radiology and ultrasonography. While the stomach, the small intestine, the pancreas and the cloaca are reported to be impossible to evaluate through ultrasonography[15] in the present study all the coelomic organs were thoroughly observed in all the study subjects by means of CT. Moreover, the use of intravenous contrast medium enhanced significantly the visualisation of the major vessels and the intestinal wall thus allowing a thorough interpretation of the CT images.

Gastro-intestinal contrast studies are often reported to be useful in the diagnosis of several different gastro-intestinal diseases in reptiles[13]; nevertheless the interpretation of such studies requires a broad knowledge of the anatomy, physiology and pathology of the species object of the clinical investigation. Numerous studies describing the unique gastrointestinal physiology of snakes are present in literature[22-25]. This complex digestive physiology derives from their unique way of feeding; snakes are the only vertebrates known to be able to ingest a prey that can exceed their body weight. Therefore, a comparison between the normal features of the normal upper gastro-intestinal examination in snakes and other reptile species is very difficult. Gastro-intestinal impaction secondary to the administration of barium enema is reported[13]; in our work no animal experienced such side effects. All animals included in the study were healthy and is beyond our knowledge if an abnormal gastro-intestinal transit could predispose to desiccation of contrast medium and cause iatrogenic obstruction. Some authors[13] report noniodinated contrast media to be the contrast media of choice for the upper gastro-intestinal examination in reptiles. To date, no comparison between these different contrast media has been reported.

As a general conclusion, results of the reported studies provide a useful basis for the interpretation of different diagnostic imaging modalities in snakes and lizards. A limitation of studies reported in this PhD thesis is the restricted number of species considered. The very large number of snake and lizard species commonly kept as pets, together with the high intra- and inter-specific anatomical differences peculiar of these animals, do not enable to extend the results of these studies to species different from those described. Further studies, considering a larger number of species and placing the anatomical variation in an intra-genus and intra-species phylogenetic contest might be helpful to achieve a full standardisation of diagnostic imaging in snakes and lizards.

References

1. Uetz P. http://www.reptile-database.org/db-info/SpeciesStat.html, Accessed 2 January 2013.
2. O'Malley. Lizards. In: Ed O'Malley Clinical Anatomy and Physiology of the Exotic Species: Structure and Function of Mammals, Birds, Reptiles and Amphibians. Philadelphia: WB Saunders Co, 2005;57-74
3. O'Malley. Snakes. In: Ed O'Malley Clinical Anatomy and Physiology of the Exotic Species: Structure and Function of Mammals, Birds, Reptiles and Amphibians. Philadelphia: WB Saunders Co, 2005;75-90.
4. Eds Gans, C., Bellairs, A.A., Parsons, T.S., Dawson, W.R., Tinkle, D.W., Kyoko, A., Gans, R., Northcutt, G., Ulinski, P.S., Harvey Pough, F., Billett, F., Maderson, P.F., Huey, R.B., Crews, D., Gaunt, A.S., Adler, K., Liner, E.A. (1970 – 2010) Biology of the Reptilia. Society for the study of Amphibians and Reptiles. Vol. 1-24
5. Ed O'MALLEY (2005) Clinical Anatomy and Physiology of the Exotic Species: Structure and Function of Mammals, Birds, Reptiles and Amphibians. W.B. Saunders Co. pp 1-270
6. Edgeworth FH. *The cranial muscles of vertebrates*. Cambridge: Cambridge University Press, 1935;405–430.
7. Grassè P. Traité de zoologie. Vol 14. 2nd ed. Paris: Masson et Cie, 1970;360–375.
8. Taub AM. Ophidian cephalic glands. *J Morphol* 1966;118:529–542.
9. Mitchell, MA. Therapeutics. In: Mader DR, ed. *Reptile medicine and surgery*. 2nd ed. Philadelphia: WB Saunders Co, 2006;631-670.
10. Selleri P, Hernadez-Divers SJ. Renal diseases of reptiles. *Veterinary Clinics of North America: Exotic Animal Practice,* 2006;9, 161-174.
11. Hernadez-Divers SJ. (2003) Green iguana nephrology: a review of diagnostic techniques. *Veterinary Clinics of North America: Exotic Animal Practice,* 2006; 6, 233-250
12. Pollard R, Puchalsky S. CT contrast media and applications. In: Schwarz T, Saunders S eds. Veterinary Computed Tomography. Iowa: Wiley-Blackwell, 2011; 57-66.
13. Silverman S. Diagnostic Imaging. In: Reptile Medicine and Surgery. Ed Mader DR 2nd ed. W.B. Saunders Co, 2005;471-489
14. Anderson CL, Kabalka GW, Layne DG, Dyke JP, Burgardt G. Noninvasive high field MRI brain imaging of the garter snake (Tamnhophis sirtalis). *Copeia,* 2000;1:265-269
15. Pees M (2010a) Radiographic investigation. In Diagnostic Imaging of Exotic Pets: Birds, Small Mammals, Reptiles. Eds M.E. Krautwald-Junghanns, M. Pees, S. Reese, T. Tully. Schluetersche Verlagsgesellschaft mbH & Co. pp 310-333

16. Pees M. Ultrasonography. In: Diagnostic Imaging of Exotic Pets: Birds, Small Mammals, Reptiles (Vet S). Schluetersche; 2010.

17. Kiefer I, Pees M. Computed Tomography. In: Diagnostic Imaging of Exotic Pets: Birds, Small Mammals, Reptiles (Vet S). Schluetersche; 2010:358–367.

18. Ludewig EW, Pees M. Magnetic Resonance Imaging. In: Diagnostic Imaging of Exotic Pets: Birds, Small Mammals, Reptiles (Vet S). Schluetersche; 2010:368–377.

19. Holland MF, Hernandez-Divers S, Frank PM. Ultrasonographic appearance of the coelomic cavity in healthy green iguanas. *J Am Vet Med Assoc* 2008;233:590–596.4.

20. Sainsbury AW, Gili C. Ultrasonographic anatomy and scanning technique of the coelomic structures of the bosc monitor (*Varanus exantematicus*). *J Zoo Wildl Med* 1991:421–433.

21. Isaza R, Ackerman N, Jacobson ER. Ultrasonographic imaging of the coelomic structures in the Boa constrictor. *Vet Radiol Ultrasound* 1993;34:445–450.

22. Secor MS, Diamond J. Adaptative responses to feeding in Burmese pythons: pay before pumping. *J Exp Biol* 1995;198:1313–1325.

23. Stark MJ, Wimmer C. Patterns of blood flow during the postprandial response in ball pythons, *Python regius*. *J Exp Biol* 2005;208:881–889.

24. Cox LC, Secor SM. Matched regulation of gastrointestinal performance in the Burmese python, *Python molurus*. *J Exp Biol* 2008;211:1131–1140.

25. Xantos X, Llorente GA. Gastrointestinal responses to feeding in a frequently feeding colubrid snake (*Natrix maura*). *Comp Biochem Physiol A* 2008;150:75–79.

SUMMARY

The increasing popularity of snakes and lizards as pets has led to an increasing demand of specialised veterinary duties in these animals. Diagnostic imaging is often a fundamental step of the clinical investigation. The interpretation of diagnostic images is complex and requires a broad knowledge of anatomy, physiology and pathology of the species object of the clinical investigation. Moreover, in order to achieve a correct diagnosis, the comparison between normal and abnormal diagnostic images, for all the diagnostic imaging modalities, is mandatory. In this PhD thesis the diagnostic imaging features of some snake and lizard species are described. The aim of all the works presented is to provide some normal atlases matching the normal gross and cross-sectional anatomy with the normal radiographic, ultrasonographic, CT features of some of the most popular pet lizard and snake specie.

In **Chapter I** a review of literature regarding snakes and lizards is presented. The aim of this chapter is to review the most commonly used diagnostic imaging modalities as well as to make an updated collection of the available international references describing the normal and pathological imaging features in snakes and lizards. Most of papers describing radiography, ultrasonography, computed tomography, magnetic resonance imaging and other imaging modalities have been collected in order to overcome the lack of a unique reference regarding diagnostic imaging in snakes and lizards.

The scientific aims and the outline of this thesis are presented in **Chapter II.** The general aim of this PhD thesis is to provide some useful anatomical and diagnostic imaging references in snakes and lizards. The first part of this work (Chapters III and IV) is focused on the description of

the normal radiographic and computed tomographic features of the head of some snakes and lizards species. The second part (Chapters V to VII) is focused on the diagnostic imaging of the coelomic cavity; the description of the normal contrast enhanced computed tomographic features of the coelomic cavity of some lizards, the normal ultrasonographic features of the coelomic cavity of some snake species and the normal upper gastro-intestinal examination in the ball python are presented.

In **Chapter III** the normal stratigraphic and cross sectional anatomy is matched with the normal radiographic and computed tomographic features of the head of the *Boa constrictor*. 4 boa constrictor's cadavers head where used in this study. Radiographs of the head were taken in LL and DV projections using a high detail screen-film combination. CT scans scans of the head where performed in a CC and a LL direction with a slice thickness of 1,5mm and displayed in a bone window. 2 heads where dissected following a stratigraphic approach and 2 heads frozen for 24h (-20°C) and then sectioned into 3mm slices respecting the imaging protocol. All anatomical structures have been identified and labelled with the aid of available literature in the anatomical images and then matched on the corresponding radiographic and computed tomographic images. Radiographic and CT images provided a high detail for the visualisation of bony structures; soft tissues were not easily identified on radiographic and CT images.

In **Chapter IV** the normal radiographic and contrast enhanced computed tomographic features of the head of the green iguana, common tegu and bearded dragon are described. The study included 4 cadavers for each considered species and 6 adult green iguanas, 4 tegus, 3 bearded dragons. Prior to the beginning of the radiographic and computed tomographic studies 2 cadavers were dissected following a stratigraphic approach and 2 cadavers were cross-sectioned for each species. Anatomical studies were performed following the same approach described in Chapter III.

Both the radiographic and the computed tomographic studies were performed only in live animals. Radiographic studies included a LL and a DV projection. Pre- and post- contrast computed tomographic studies of the head were performed in a CC direction. CT images were displayed in both bone and soft tissue windows. Individual anatomical structures were first recognised and labelled on the anatomic images and then matched on radiographs and CT images. Radiographic studies provided a good detail both of the soft tissues (especially in the green iguana) and of the bony structures. CT images provided an excellent detail of the bony structures in all the considered species. The soft tissues were clearly outlined only in the green iguana. In the common tegu and the bearded dragon only the eyes were clearly outlined from the remaining soft tissues.

In **Chapter V** the normal contrast enhanced computed tomographic features of the coelomic cavity of the green iguana, black and white tegu and the bearded dragon are described. 4 cadavers and 4 live animals for each considered species were object of this study. The cadavers were frozen for 24 hours and then cross sectioned at 5mm intervals. The slices have been cleaned with water and photographed on both sides. In order to reduce the duration of the procedure only contrast enhanced CT scans have been performed. The CT scans have been performed in a CC direction. The CT scans have been displayed in a soft tissue and, when appropriate, in a lung window. Individual organs have been recognised and labelled on the anatomical images and then matched on the corresponding CT images. Most of the coelomic organs have been identified in all the considered species. Results provide an atlas of the normal cross sectional and CT features of the coelomic cavity of lizards.

In **Chapter VI** the normal ultrasonographic features of the coelomic cavity of the *Boa constrictor*, *Python molurus*, *Python curtus* and *Python regius* are described. Moreover, normal reference ultrasonographic measurements of the scent glans, the colonic, gastric and pyloric wall

thickness are reported. 46 live snakes (16 *Python regius*, 10 *Python molurus*, 12 *Python curtus* and 8 *Boa constrictor*) and 23 cadavers (6 *Python regius*, 4 *Python molurus*, 10 *Python curtus*, 3 *Boa constrictor*) where object of this study. Anatomical studies where performed prior to the beginning of the ultrasonographic studies in order to characterise the normal anatomical features of the above mentioned species. In previous ultrasonographic studies of the coelomic cavity of the *Boa constrictor* studies a ventral approach on sedated animals was proposed. We have decided to use a lateral approach on unsedated animals. Although, especially in larger animals, the shadowing effect produced by the ribs was evident in some images, most of the coelomic organs (scent glands, hemipenes, cloaca, ureters, colon, small intestine, pylorus, stomach, pancreas, liver, gallbladder and oesophagus) have been recognised. The rate of ultrasonographic recognition of individual organs is reported. Results provide a description of the normal ultrasonographic features of coelomic cavity of boid snakes along with a series of tables matching the gross and cross sectional anatomy with corresponding normal ultrasonographic images.

In **Chapter VII** the technique and the normal features of upper gastro-intestinal examination in ball pythons are described. 10 ball python's cadavers have been dissected and cross sectioned prior to the the beginning of the study in order to characterise the normal features of the intestine in this species.18 healthy ball pythons where object of this study. All animals where not fed for at least 7 days before the beginning of the study. The animals have been divided into three groups (A, B, C). Contrast medium (barium sulphate) at the dose of 25 ml/kg has been administered through an esophageal probe at an increasing concentration (25%, 35% and 45 wt/vol) to three groups. An initial animal (Group A , 25% wt/vol) was used to verify the feasibility and establish a time course for the procedure. Imaging quality was evaluated by 3 investigators who assigned a grading score on the basis of predetermined criteria. Results of present study revealed that the 35% wt/vol concentration of contrast medium provided the best imaging quality. Moreover, three pattern of

distribution of the contrast medium in the small intestine, independent from the concentration, have been described.

SOMMARIO

Negli ultimi anni ofidi e sauri sono diventati sempre più diffusi come animali da compagnia. Questa crescente diffusione ha comportato un aumento della richiesta di servizi veterinari specializzati in questi animali. L'imaging diagnostico spesso è una parte fondamentale dell'indagine clinica. La corretta interpretazione delle immagini diagnostiche implica una conoscenza approfondita dell'anatomia, fisiologia e patologia della specie oggetto dell'indagine clinica. Il confronto tra immagini normali e immagini patologiche spesso è di vitale importanza per una corretta interpretazione delle immagini diagnostiche. Lo scopo di questa tesi di dottorato è quella di fornire degli atlanti che mettano in relazione l'anatomia normale e per sezioni con le corrispondenti immagini radiografiche, tomografiche e ecografiche di alcune delle specie più popolari di ofidi e sauri.

Il **Capitolo I** è riportata una revisione della letteratura corrente sull'imaging in ofidi e sauri. Al momento manca un riferimento univoco su questo argomento e la letteratura presente è spesso frammentaria a volte difficile da reperire. L'obiettivo di questo capitolo, quindi, è quello di fare il punto sullo stato dell'arte della diagnostica per immagini in ofidi e sauri. Molti articoli internazionali riguardanti la radiologia, l'ecografia, la tomografia computerizzata, la risonanza magnetica e altre tecniche di imaging sono stati citati in modo da creare un riferimento utile ai clinici che si occupano di animali esotici.

Nel **Capitolo II** vengono presentati gli obiettivi scientifici e la struttura di questa tesi. L'obiettivo generale è quello di fornire una descrizione dell'anatomia e dell'imaging normale in ofidi e sauri. La prima parte (Capitoli III e IV) è incentrata sul confronto tra la l'anatomia normale e per sezioni della testa alcune specie di ofidi e sauri con i normali aspetti radiografici e tomografici.

La seconda parte (Capitoli dal V al VII) è incentrata sull'imaging della cavità celomatica. In questi capitoli sono descritti: gli aspetti normali valutati in tomografia computerizzata della cavità celomatica di alcune specie di sauri, l'ecografia normale in alcune specie di ofidi e il

Nel **Capitolo III** sono descritti i normali aspetti anatomici, radiografici e tomografici della testa del *Boa constrictor*. Per questo studio sono stati impiegate le teste di 4 cadaveri di *Boa constrictor*. Utilizzando una combinazione pellicola-casetta ad alta definizione sono state ottenute proiezioni latero-laterali e dorso-ventrali di tutte le teste. L'esame tomografico è stato eseguito in direzione cranio-caudale e latero-laterale con uno spessore di fetta di 1,5mm. Le immagini sono state visualizzate in una finestra da osso. 2 teste sono state dissezionate con un approccio stratigrafico. 2 teste invece sono state congelate per 24 ore a -20°C e poi sezionate in fette di 3mm rispettando il protocollo utilizzato in tomografia computerizzata. Le strutture anatomiche sono state identificate nelle immagini anatomiche e poi accoppiate con le corrispondenti immagini radiografiche e tomografiche. I tessuti ossei sono ben definiti sia nelle immagini radiografiche che tomografiche; i tessuti molli risultano poco definiti in entrambe.

Nel **Capitolo IV** l'anatomia stratigrafica e per sezioni della testa dell'iguana, del tegu e del drago barbuto vengono messi in relazione con il loro normale aspetto radiografico e tomografico. Per realizzare questo studio sono stati usati 4 cadaveri per specie e 6 iguane, 4 tegu e 3 draghi barbuti adulti. Prima di iniziare gli studi di imaging 2 cadaveri per specie sono stati dissezionati con un approccio stratigrafico e 2 sono stati sezionati. Gli studi anatomici sono stati eseguiti con la stessa metodica riportata nel Capitolo III. Gli studi radiografici e tomografici sono stati eseguiti solo sugli animali vivi. Le radiografie sono stata scattate in proiezione latero-laterale e dorso-ventrale. Le scansioni tomografiche sono state effettuate pre e post contrasto scansionando gli animali in direzione cranio-caudale. Le immagini tomografiche sono state quindi visualizzate sia in finestra da

tessuti molli che da osso. Le strutture anatomiche sono state individuate prima nelle immagini anatomiche e poi correlate con le corrispondenti immagini radiografiche e tomografiche. Gli studi radiografici hanno permesso di visualizzare in maniera ottimale sia i tessuti duri che i tessuti molli (specialmente nell'iguana). Negli studi tomografici le strutture ossee sono state visualizzate in modo ottimale in tutte le specie. I tessuti molli sono chiaramente delineati solo nell'iguana; nel tegu e nel drago barbuto si riescono a distinguere chiaramente solo gli occhi.

Nel **Capitolo V** i normali aspetti anatomici della cavità celomatica dell'iguana verde, del tegu bianco e nero e del drago barbuto sono messi in relazione con i normali aspetti tomografici di queste specie. Per questo studio sono stati usati 4 cadaveri e 4 animali vivi per specie. I cadaveri sono stati congelati per 24 ore e poi sezionati a intervalli di 5mm. Le fette così ottenute sono state lavate da entrambi i lati e poi fotografate. Per ridurre la durata delle procedure diagnostiche sono state effettuate solo procedure post-contrasto. Le scansioni tomografiche sono state effettuate in direzione cranio-caudale. Le immagini tomografiche sono state visualizzate in finestra da tessuti molli e da polmoni. La maggior parte degli organi celomatici sono stati individuati sia nelle immagini anatomiche che nelle immagini tomografiche. Il risultato di questo lavoro è un atlante degli aspetti anatomici e tomografici normali della cavità celomatica di queste specie di sauri.

Nel **Capitolo VI** vengono descritti gli aspetti ultrasonografici normali della cavità celomatica del *Boa constrictor, Python molurus, Python curtus e Python regius*. Inoltre vengono fornite le misure ecografiche di riferimento delle scent glands e delle mucose gastica, pilorica e del colon nelle suddette specie. Per questo lavoro sono stati utilizzati 46 serpenti vivi (16 *Python regius*, 10 *Python molurus*, 12 *Python curtus* and 8 *Boa constrictor*) and 23 cadaveri (6 *Python regius*, 4 *Python molurus*, 10 *Python curtus*, 3 *Boa constrictor*). Gli studi anatomici sono stati effettuati prima di iniziare gli studi ecografici in modo da caratterizzare i normali aspetti anatomici

di queste specie. In un lavoro precedente, nel quale vengono descritti i normali aspetti ecografici del *Boa constrictor*, viene proposto un approccio ventrale al paziente. In questo studio proponiamo un approccio laterale. In alcune immagini ecografiche i coni d'ombra prodotti dalle coste di questi animali, specialmente nei soggetti di maggiori dimensioni, degradavano leggermente la qualità dell'esame. Nonostante ciò è stato possibile riconoscere la maggior parte degli organi celomatici (scent glands, emipeni, cloaca, ureteri, colon, piccolo e grosso intestino, piloro, stomaco, pancreas, fegato, cistifellea ed esofago). Il numero di animali nei quali i singoli organi sono stati visualizzati è stato riportato. Questo lavoro ha prodotto una descrizione completa degli aspetti ecografici normali in alcune specie di boidi oltre a una serie di tavole che mettono in relazione l'anatomia normale e per sezioni con le corrispondenti immagini ecografiche.

Nel **Capitolo VII** è riportata la tecnica e gli aspetti normali dello studio radiografico dell'esofago, stomaco e piccolo intestino nel *Python regius.* Per caratterizzare l'aspetto normale del piccolo intestino di questa specie i cadaveri di 10 *Python regius* sono stati dissezionati prima dei iniziare procedure diagnostiche. Per questo lavoro sono stati utilizzati 18 *Python regius.* Tutti gli animali utilizzati non sono stati nutriti nella settimana precedente lo studio. Gli animali sono stati divisi in 3 gruppi (A, B, C). Il mezzo di contrasto (bario solfato) è stato somministrato alla dose di 25ml/kg tramite una sonda esofagea a concentrazione crescente (25%, 35%, 45% p/v) nei tre gruppi. Un soggetto appartenente al gruppo A (25% p/v) è stato usato per verificare la fattibilità della procedura e per stabilire una timeline radiografica approssimativa per gli studi successivi. La qualità delle immagini diagnostiche è stata valutata da tre autori in basi a criteri pre-definiti. I risultati di questo studio suggeriscono che la concentrazione ideale di mezzo contrasto per questo tipo di indagine diagnostica è del 35%. Inoltre, sono stati descritti tre pattern di distribuzione del mezzo di contrasto nel piccolo intestino, indipendenti dalla concentrazione.

BIBLIOGRAFIA DELL'AUTORE

1. Zotti A, **Banzato T**, Cozzi B. Cross-sectional anatomy of the rabbit neck and trunk: Comparison of computed tomography and cadaver anatomy. 2009, *Research in Veterinary Science* 87, 171–176.
2. **Banzato T**, Russo E, Di Toma A, Palmisano G, Zotti A. Evaluation of radiographic, computed tomographic, and cadaveric anatomy of the head of boa constrictors. 2011, *American Journal of Veterinary Research* 72, 1592-1599.
3. **Banzato T**, Russo E, Milan MC, Gianesella M, Finotti L, Zotti T. Ultrasonographic anatomy of the coelomic organs of the boid snakes (Boa constrictor, Python regius, Python molurus, Python curtus). 2012. *American Journal of Veterinary Research* 73, 634-345.
4. **Banzato T**, Selleri P, Veladiano IA, Martin A, Zanetti E, Zotti A. Comparative evaluation of the cadaveric, radiographic and computed tomographic anatomy of the heads of green iguana (*Iguana iguana*), common tegu (*Tupinambis merianae*) and bearded dragon (*Pogona vitticeps*). *BMC Veterinary Research* 2012, 8.
5. **Banzato T**, Russo E, Finotti L, Zotti A. Development of a technique for contrast radiographic examination of the gastrointestinal tract in ball pythons (*Python regius*). 2012. *American Journal of Veterinary Research* 73, 997-1001.
6. Zotti A, **Banzato T**, Mandara MT, Bernava A, Bernardini M. What Is Your Diagnosis? Idiopathic atlanto-axial calcinosis circumscripta causing spinal cord compression in a dog. *Journal of the American Veterinary Medical Association. Accepted for publication* (Ref.: JAVMA-11-12-0692)
7. **Banzato T**, Selleri P, Veladiano IA, Zotti, A. Comparative evaluation of the cadaveric and computed tomographic features of the coelomic cavity in the green iguana (*Iguana iguana*), black and white tegu (*Tupinambis merianae*) and bearded dragon (*Pogona vitticeps*). *Anatomia, Histologia, Embryologia. Corrected proofs, in press* (doi: 10.1111/ahe.12037)
8. **Banzato T**, Hellebuick T, Van Calenberg A, Saunders J, Zotti A. Diagnostic imaging of Snakes and Lizards: State of the Art. *Veterinary Record* 2012. *Submitted for publication*.